ISBN 978-82-326-2476-8 (printed version)
ISBN 978-82-326-2477-5 (electronic version)
ISSN 1503-8181

NTNU
Norwegian University of
Science and Technology

Doctoral Thesis
Peter Joachim Gogstad

Doctoral theses at NTNU, 2017:202

Peter Joachim Gogstad

Experimental investigation and mitigation of pressure pulsations in Francis turbines

Doctoral theses at NTNU, 2017:202
NTNU

NTNU
Norwegian University of
Science and Technology
Faculty of Engineering
Science and Technology
Department of Energy andProcess Engineering

NTNU
Norwegian University of
Science and Technology

Peter Joachim Gogstad

Experimental investigation and mitigation of pressure pulsations in Francis turbines

Thesis for the degree of Philosophiae Doctor

Trondheim, August 2017

Norwegian University of Science and Technology
Faculty of Engineering
Science and Technology
Department of Energy andProcess Engineering

NTNU
Norwegian University of
Science and Technology

NTNU
Norwegian University of Science and Technology

Thesis for the degree of Philosophiae Doctor

Faculty of Engineering
Science and Technology
Department of Energy andProcess Engineering

© Peter Joachim Gogstad

ISBN 978-82-326-2476-8 (printed version)
ISBN 978-82-326-2477-5 (electronic version)
ISSN 1503-8181

Doctoral theses at NTNU, 2017:202

Printed by Skipnes Kommunikasjon as

Preface

This work has been conducted at the Waterpower Laboratory, Department of Energy and Process Engineering at the Norwegian University of Science and Technology(NTNU) in Trondheim. The project was funded by Statkraft, Norway's leading hydro power company.

Abstract

Hydraulic turbomachines, such as Francis turbines, have been utilized for more than a century to generate renewable energy. Research and development has led to an outstanding level of efficiency and reliability, with the Francis turbine at the top end with almost 96% efficiency. To achieve such levels of efficiency, the turbine has to be design for a specific operating point. The development of a continental transmission grid and introduction of intermittent renewables such as wind and solar has led to a fundamental change in the energy market. The hydraulic turbomachines in hydro power has now become one of the stabilizing force of an energy market demanding flexibility. Amongst other reasons, this has led to operation of hydraulic turbines outside the design point.

Operating turbines outside the design point may lead to heavy vibrations and potentially mechanical failure. In addition, modern design is focused on increasing efficiency, possibly at the expense of the runner characteristics outside the design load. The vibrations are a consequence of the turbine, which generates pressure pulsations. The pressure pulsations propagates into the water conduit. In case of resonance, the pressure pulsations will increase in amplitude and induce further vibrations. However, they can be reduced.

The main objective of this thesis has been to investigate and possibly reduced the pressure pulsations occurring at part load operation. An experimental investigation of different methods to reduce pressure pulsation in Francis turbines has been carried out. Air injection was investigated at La Higuera Hydro Power Plant (HPP) in Chile. A free rotating runner cone extension (FRUCE) was developed and investigated at the Waterpower Laboratory and in Leirfossene HPP.

The air injection through the runner cone and draft tube wall was tested in La Higuera HPP. Both options gave a significant dampening of pressure

pulsations at part load by reducing the maximum value of the peak-to-peak values by 60%. However, an increase in the vortex rope frequency was observed when air was injected.

At the Waterpower Laboratory, the free rotating runner cone extension was tested with different lengths. The developed FRUCE is an extension of the runner cone where the outer shell is mounted on bearings allowing it to rotate independently from the turbine. It was concluded that the FRUCE had some dampening effect, but that the diameter was too small to achieve a significant dampening effect of the pressure pulsations.

Three FRUCEs with different length and diameter were designed and tested at Leirfossene HPP. A dampening in pressure pulsations was achieved at part load operation. However, different FRUCEs worked best at different loads. The FRUCE also reduced pressure pulsations at full load, but the drawback is reduced efficiency at full load. An adjustment of the FRUCE length and diameter is necessary to achieve the maximum dampening.

The FRUCE had development potential and may be possible solution to reduce pressure pulsations in Francis turbines. However, it will require numeric simulations, further prototype testing and possibly implementation of technology to actively control the FRUCE length and possibly the rotational speed.

Acknowledgements

A long period of my life has suddenly come to an end. I would not gotten where I am today without help. The contributors to this work in one way or another are enumerable, but not forgotten.

First of all, I would like to thank my supervisor, Professor Ole Gunnar Dahlhaug, for luring me into starting on this thesis. And secondly, for helping me finish it. I hated it and I have loved it and now I am finished with it. There have been many good discussions and positive pushes through the years. My co-supervisor, Professor Torbjørn Nielsen also deserves his praise for taken his time to help and listen.

In many ways, Statkraft has been a large contributor. Statkraft provided founding for the project and allowed me to use their hydro power stations in Leirfossen to conduct prototype experiments. I would especially thank Jens Davidsen believing in me and the project. I know you have worked hard to help me through. I also have to mention Børge Nilssen Stafne, who have been my go-to-guy in Statkraft. Always positive and with good ideas and good advice. The technicians in Statkraft Midt-Norge have also been of great help in the execution of the physical tasks at hand.

The work would not have been done without the Waterpower Laboratory, the 100 years old building with all the amazing people. The technical staff in the lab with Joar Grilstad, Halvor Haukevik and Trygve Opland have been invaluable. You all have your expertise, which I exploited with the best intensions. In addition, Wenche Johansen has always been there with time for a chat and to fix the administrative problems.

All the students and Ph.D. candidates of the lab have also played an important, if more social, role in my years at the lab. The social environment at the lab was one of the reasons I stayed. It has not only been beers and gatherings in the sofa, but also good discussion and valuable input to the

final product. Thanks for sharing some of your time with me.

I would also thank Stjørdal maskinering AS, A/S Delprodukt, Strømmen dreieverksted and the Statkraft guys in Tydal for producing the parts to my new invention known as the FRUCE.

All though I have spent countless hours at my desk and in different hydro power plant there have been many people outside the lab who deserves praise for keeping me sane. Thanks for dragging me off to the mountains in the weekends so I could recharge. A special thanks to Kristine and Lars, and Magni and Jo for giving me guidance and a place to stay in time of need. I am forever grateful for the support everyone has given.

Contents

List of Figures

List of Tables

Nomenclature

Symbols

Symbol	Description	Unit
A	Area	m^2
b	Relative torque	$-$
c	Absolute velocity	m/s
c_p	Heat capacity	$kJ/(kg{\cdot}K$
d	Diameter	m
D	Diameter	m
E	Specific hydraulic energy	J/kg
F	Force	N
f	Frequency	Hz
f_N	Nyquist frequency	Hz
g	Acceleration of gravity	m/s^2
h	Relative head	$-$
Δh	Height difference	m
H_e	Head	m
K	Loss coefficient	$-$
k	Conduction factor	$-$
L	Length	m
m	Mass	kg
N	Number of measurements	m
n_{ED}	Speed factor	$-$
n	Rotational speed	rpm
o	Relative rotational speed	m
p	Pressure	Pa
Δp	Pressure difference	Pa
P	Power	W

q	Relative volume flow	$-$
Q	Flow rate	m^3/s
r	Radius	m
R	Radius	m
Re	Reynolds number	$-$
S	Swirl number	$-$
T	Temperature	$°C$
$t_{\alpha/2}$	Student t-value for confidence interval 1 - α	$-$
V	Volume	m^3
u	Peripheral velocity	m/s
w	Relative velocity	m/s
X	Aritmetic mean of measurements	$-$
Z	Height	m

Greek Symbols

Symbol	Description	Unit
α	Confidence level, 1-α	$-$
β	Blade angle	$^{\circ}$
η	Efficiency	$-$
λ	Turbine coefficient	$-$
π	Constant	$-$
μ	Kinematic viscosity	$kg/(m{\cdot}m)$
ρ	Density	kg/m^3
ω	Angular velocity	rad/s

Sub-symbols

$*$	Refers to best efficiency point of turbine
amb	Refers to ambient
$asyn$	Refers to asynchronous
c	Refers to FRUCE
dyn	Refers to dynamic
e	Refers to effective
f	Refers to friction
h	Refers to hydraulic
loc	Refers to local
m	Refers to measured static pressure
R	Refers to rated
SE	Refers to sudden expansion
$stat$	Refers to static
n	Refers to nominal
m	Refers to meridional direction
$loss$	Refers to losses
s	Refers to isentropic
s	Refers to FRUCE
$sync$	Refers to synchronous
u	Refers to peripheral direction
1	Refers to inlet of turbine runner
2	Refers to outlet of turbine runner

Abbreviations

BEP	Best Efficiency Point
CFD	Computational Fluid Dynamics
DFT	Discrete Fourrier Transform
DO	Dissolved Oxygen
DT	Draft Tube
FFM	Flow-feedback method
FFT	Fast Fourrier Transform
FRUCE	Free Rotating Runner Cone Extension
HPP	Hydropower Plant
IEC	International Electrotechnical Commission
LDV	Laser Doppler Velocimetry
NPSH	Net Positive Suction Head
NTNU	Norwegian University of Science and Technology
PIV	Particle Image Velocimetry
PLS	Programmable Logic Controller
PSD	Power Spectrum Density
rpm	Revolutions per minute
RVR	Rotating Vortex Rope
SST	Shear Stress Transport

Part I

Main part

Chapter 1

Introduction

1.1 Structure of thesis

1.2 Background

Hydro power has been used for more than a century and is today a well-known technology with high efficiency, high reliability and a good regulating capacity, which has made it a superior renewable energy resource. These factors combined with reversible pump turbine technology and large storage capacity gives hydro power an important position, particularly for the European energy marked in the coming years. This is because Europe is expanding investments in intermittent renewable energy resources, such as wind and solar, which requires flexible energy resources to balance the power supply.

Hydropower is an energy resource well suited for balancing intermittent resources. In Norway, the storage capacity is 86 TWh in combination with 29 600 MW available power [66], where Francis turbines above 10 MW stands for approximately 60% of the available power. In addition, hydro power turbines have a wide operating range, i.e. 40%-120% of the nominal power output. However, the market requires more start and stops, large load variations and more operation time outside best efficiency point. In reaction turbines with a wide operating range, such as Francis and Kaplan, the load variations cause significant changes in the flow regime in the draft tube. For Kaplan turbines, which has runners with adjustable runner blades, the flow regime can be controlled to a certain extent. While fixed blade runners,

e.g. Francis turbines, pressure pulsation problems and related problems may occur. In Norway, several Francis runners have suffered failure due to fatigue loads, with material cracks in Francis runners [56][18]. As a consequence of the increased demand for flexibility, more runners may suffer failure due to fatigue.

1.3 Motivation

The vortex breakdown occurring in the draft tube is considered to be the main cause of severe flow instabilities and pressure pulsations. The consequences are heavy vibrations and noise, which may cause high fatigue load and ultimately lead to mechanical failure [22]. Mitigation of pressure pulsations is considered an imported task since it will increase the life time of the turbine.

Leirfossene Hydro Power Plant (HPP) experienced heavy vibrations during part load operation after the start-up in 2008. Norway's leading hydro power company, Statkraft, initiated a project to investigate methods to reduce the vibrations. Norwegian University of Science and Technology (NTNU) was contacted and became a research partner. This opened an opportunity to do prototype measurements with different methods to mitigate pressure pulsations.

1.4 Objectives and scope

The overall objective of the work presented in this thesis is to reduce pressure pulsations in Francis turbines at part load in order to improve part load operation and increase the turbine lifetime. Leirfossene HPP and La Higuera HPP have been used as prototype cases. To approach this objective two secondary objectives have been defined. First, to develop an understanding of the Rotating Vortex Rope (RVR) and pressure pulsations at part load operation. The second part of the work is to propose an efficient way to manipulate the flow in the draft tube to reduce the pressure pulsation amplitudes.

The first secondary objective includes an investigation different methods to mitigate pressure pulsations, focusing on the influence of a runner cone extension and air injection. The second part includes design and test a

runner cone extension on a model Francis runner and to design and test a runner cone extension in the prototype runner at Leirfossene HPP.

1.5 Contributions

There have been carried out a series of prototype measurements which are included in this thesis. Two sets of measurements was carried out at La Higuera Hydro Power Plant (HPP) in Chile as a part of the recommissioning. Tinguiririca Energia is the owner the La Higuera HPP and allowed the Waterpower Laboratory to design and test two different air injection options for the power plant. First, pressure measurements of two different air injection options was carried out together with Ole Gunnar Dahlhaug. The second set also included efficiency measurements and was carried out with Ole Gunnar Dahlhaug and Jim Abregu from SN Power Peru.

The opportunity to do measurements at Statkraft's Øvre Leirfoss HPP and Nedre Leirfoss HPP came as a part of a course in head loss in tunnels. The pressure measurements was carried out as a separate part outside the course with help from Chirag Trivedi.

As a direct part of the project, measurements were carried out in Leirfossene HPP. The first set of efficiency and pressure measurements was carried out together with master student Stian Solvik. The second set of measurements with free rotating runner cone extension (FRUCE) was carried out by the author. Great help provided by Statkraft and NTNU for installation of the FRUCE.

1.6 Publication of work

Paper 1

Gogstad PJ, Dahlhaug OG. Evaluation of runner cone extension to dampen pressure pulsations in a Francis model turbine. IOP Conference Series: Earth and Environmental Science 2016, (1), 082019
Relevance to this thesis: Experiments on a model Francis runner with a fixed runner cone extension and a free rotating runner cone extension (FRUCE) was carried out. In this paper the results are presented. The experiments gave the base for the design of the FRUCE tested at Leirfossene Hydro Power Plant.

My contribution: I prepared and carried out the experiments at the Waterpower Laboratory as well as the post-processing of the data.

Paper 2

Trivedi C, Gogstad PJ, Dahlhaug OG. Investigation of the Unsteady Pressure Pulsations in the Francis Turbine Prototypes-Part 1: Steady State Operating Conditions. Submitted to Mechanical Systems and Signal Processing 2016
Relevance to this thesis: The pressure measurements was carried out to investigate pressure pulsations at low head Francis prototypes. The measurements gave an understanding of pressure pulsations in low head Francis turbine operating at steady state operation.
My contribution: I was in charge of the measurements at the power plant. I contributed in the analysis and editing the paper. I also contributed to the discussion and conclusion.

Paper 3

Trivedi C, Gogstad PJ, Dahlhaug OG. Investigation of the Unsteady Pressure Pulsations in the Francis Turbine Prototypes-Part 2: Transient Operating Conditions. Submitted to Mechanical Systems and Signal Processing 2016
Relevance to this thesis: The pressure measurements was carried out to investigate pressure pulsations at low head Francis prototypes. The measurements gave an understanding of transient pressure pulsations in low head Francis turbine.
My contribution: I was in charge of the measurements at the power plant. I contributed in the analysis and editing the paper. I also contributed to the discussion and conclusion.

Paper 4

Gogstad PJ, Dahlhaug OG. Experimental investigation of air injection in high head Francis turbine. Submitted to Hydropower and dams 2017
Relevance to this thesis: The measurements was carried out to investigate the dampening effect of different air injection options for a Francis turbine.
My contribution: I prepared and carried out the pressure measurements at the La Higuera Hydro Power Plant as well as the post-processing of the data.

1.7 Previous work at NTNU

The velocity profile in the draft tube is assumed to have an impact on the pressure pulsations. In 1997, Dahlhaug [11] published his study on swirl flow in draft tube. Dahlhaug investigated different draft tube shapes experimentally and numerically. Measurements were carried out with pitot and Laser Doppler Velocimetry (LDV) to chart how the flow developed through a conical diffusor and bend. Further tests were carried out on model and prototype turbines. The vortex rope was observed and visually measured at different sections. The results show a decreasing vortex diameter as the swirl number increases. The diameter also increased as it moved through the conical diffusor. Observations with a bend showed that the vortex rope collapsed in the bend.

Kobro [35] focused his work on pressure pulsations with onboard measurements on a model Francis runner. Pressure sensors and strain gauges where flush mounted on the suction side and pressure side of the runner blade. In addition pressure sensors where mounted on the vaneless space and draft tube cone. The analysis show that the wake leaving the guide vane is the most severe source of dynamic pressure in the runner, both for prototype and model runner. In the model runner, the draft tube vortex rope pulsations propagates upstream into the runner, almost undampened. The strain amplitudes measured associated with the vortex rope pulsations are only at a moderate level. Due to the relatively low number of cycles and moderate amplitudes, Kobro [35] suggests that the vortex rope frequency itself should not be a threat regarding fatigue. However, if in resonance with other system frequencies, large system fluctuations and power swings may occur.

Runner cone extensions in a Francis model runner was investigated by Vekve [74] in 2004. The medium head Francis runner was tested with extensions of different lengths and diameters. Pressure measurements were performed in two planes in the draft tube cone in addition to LDV measurements. The runner cone extension with the largest diameter, $0.41D_2$, where D_2 is the runner outlet diameter, resulted in the largest reduction in pressure pulsation amplitude. The results also showed that the runner cone extension could have a positive effect on the efficiency. Prototype measurements were also carried out at Litjfossen Hydro Power Plant and Oksla Hydro Power Plant. The measurements revealed that the runner cone diameter is important to achieve damping of the pressure pulsations.

Chapter 2

Theoretical background

Francis runners are known to cause swirling flow in the draft tube at off-design operation [22]. Swirling flows are natural flows observed in phenomena such as tornadoes and typhoons and have many technical applications in different fields. However, the presence of a swirl flow in a Francis turbine draft tube is often the cause of separations and pressure fluctuations. At best efficiency point (BEP), a minimum of swirl is entering the draft tube and no flow separation occurs. At off-design operation, both part load and high load, a significant swirling component is present in the draft tube flow. The concept of swirling flow is closely linked to phenomena such as boundary layers, flow separation, vorticity and vortex breakdown. The occurrence of one phenomenon may often be the result of an other.

This chapter further describes the physical mechanisms that influences the pressure fluctuations in the draft tube. Their occurrence and impact is dependent on the flow rate, local pressure, velocity field, runner design, draft tube shape and the system dynamic response [13]. Some parameters can be modified and controlled to a certain extent, while others, such as runner design is often out of reach for an independent researcher. The focus of the second part is on different methods of reducing pressure pulsations in the draft tube. The methods can be divided into active methods such as water injection, and passive methods, such as fins.

2.1 Swirling flow concepts and vortex breakdown

The flow regime in the draft tube of a Francis runner is generally described by two velocity components: axial and tangential. The tangential velocity component changes depending on the turbine operation point as visualized in the runner outlet velocity diagrams in Figure 2.1. The swirl number S is a non-dimensional ratio between swirl momentum and axial momentum of the flow [13].

$$S = \frac{\int_0^{R_i} c_m c_u r^2 dr}{R_i \int_0^{R_i} c_m^2 r dr} \tag{2.1}$$

R_i represent the pipe radius, c_m and c_u are the axial and tangential velocity components, respectively.

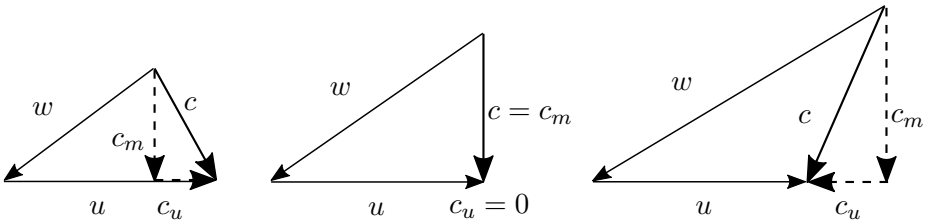

(a) Part load (b) Zero swirl (c) High load

Figure 2.1: Runner outlet velocity triangles. The velocity components c_m and c_u are the axial and tangential component of c which is the absolute velocity, while w is the relative velocity and u is the peripheral velocity.

The swirl number ranges from 0, where 0 is no swirl, and 1 equals zero axial velocity in the draft tube center. There is usually always a small tangential velocity component present which will cause axial circulation around the flow axis. At low swirl number (S<0.6), there may be high radial pressure gradients, but this will not increase the longitudinal pressure gradient enough to cause longitudinal circulation along the flow axis. Meaning there is a pressure difference along the axis is not strong enough to create a circulation zone along the axis. As the driving pressure is not strong enough, the coupling between the axial and tangential velocity components is not established [43].

With an increasing swirl number, a strong coupling between axial and tangential velocity components is established [43]. At a certain point the pressure along the axis becomes unfavourable. The kinetic energy of the fluid flowing in the axial direction cannot overcome the unfavourable pressure gradient and the central part of the flow will then start a longitudal circulation. The fluid transport will now occur in the outer region of the pipe and a stagnation zone may develop in the center region [9][13]. If the swirl increases, reverse flow may occur in central stalled region as shown in Figure 2.2a.

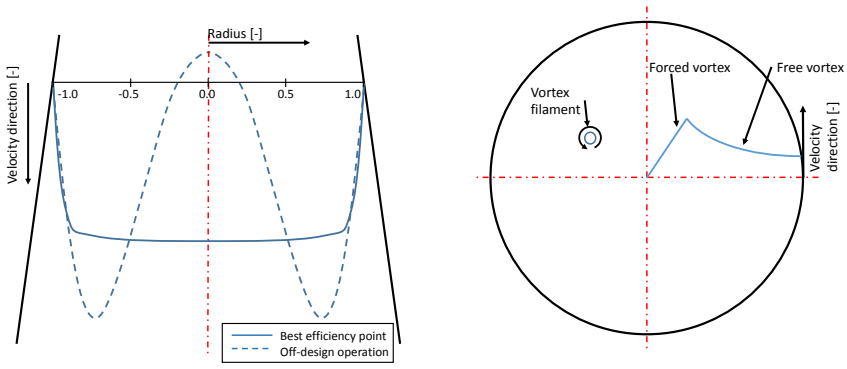

(a) Axial velocity profile

(b) Tangential velociy profile with vortex filament

Figure 2.2: Theoretical velocity profiles in a turbine draft tube

The tangential velocity profile is generally assumed to be a combination of a forced and free vortex known as a Rankine vortex, as shown in Figure 2.2b [32][15]. For swirl numbers larger than 0.10, a Rankine vortex is present [11][62].

2.2 Early research

One of the first major works on dynamic instabilities, presented in 1940, was 'Power swings in hydroelectric plants' by Rheingans [55]. Rheingans concluded that power swings are caused by draft tube surges. A draft tube surge is defined as a violent pressure fluctuation having a quasi-synchronous nature caused by resonance [49]. The draft tube surges are often approximately periodic in the frequency order of 1 Hz and may therefore produce

significant eletrical power swings [13].

Initially, Squire [63] has presented an analytical study of swirl flow and vortex breakdown. Both Squire [63] and Benjamin [4] developed independent theories for an axisymmetric, inviscid and steady vortex. Both used the terms subcritical and supercritical flow states and a critical state with separated the two flow states. Subcritical flow allows for propagation both upstream and downstream while the supercritical only support downstream propagation. Benjamin [4] defined vortex breakdown as the point when the swirl number equals one (i.e., S=1), and noted that it can often be the cause of reverse flow in the draft tube. Harvey [26] worked with aerodynamics and performed experiments to determine under what conditions vortex breakdown occurred in a straight tube. His observations confirmed Squire's analytical work. Both Harvey and Benjamin agreed that vortex breakdown is a transition between conjugate flow states. Benjamin's definition further implied that vortex breakdown is a wave, and he proposed that the transition is analogous to the hydraulic jump in open channel flow.

Several authors have suggested a similar definition of vortex breakdown. Leibovich [41] also compared the vortex breakdown with a hydraulic jump and describes it as a change in structure of a vortex initiated by a variation in the characteristic ratio of tangential to axial velocity components known as the swirl number. Faler and Leibovich [17] defined the vortex breakdown as the abrupt occurrence of an internal stagnation point on the axis of a concentrated vortex with an axial flow. Sarpkaya [59][60] argued that a vortex breakdown is an abrupt change in the structure of the core of a swirling flow.

Leibovich [40] related the vortex breakdown to the instability of axisymmetric waves on the vortex core due to the influence of an adverse pressure gradient. The adverse pressure gradient have been highlighted by several authors [40][39][61]. For an expanding axisymmetric tube, such as a draft tube, the resulting adverse pressure affects the position of the vortex breakdown [61]. Sarpkaya [61] argued that the adverse pressure gradient influenced the position where vortex breakdown would occur. An increase in the adverse pressure gradient would shift the vortex breakdown position upstream, the same way increased swirl also would move the vortex breakdown point upstream.

Cassidy and Falvey [9] related the work of Squire and Harvey to flow in draft tubes. They used a stationary swirl generating apparatus to investigate frequency and amplitudes at different flow rates and with different

geometries. Experiments showed that the frequencies and amplitudes were dependent on geometry and flow rate, but independent of viscosity for high Reynolds numbers (Re $>$ 80,000). Further, it was found that the central stalled region would not develop before the swirl number reached a rather low threshold. A stagnation point would then form at the draft tube exit and a separated flow core would form downstream. With increased swirl number, the stagnation point moved upstream and eventually merged with the runner hub. The stagnation point is also the starting point of the helical vortex rope forming downstream of the vortex breakdown. Cassidy and Falvey [9] argued that draft tube surges are an unsteady form of flow occurring after vortex breakdowns.

2.3 Vortex breakdown and vortex rope

Vortex breakdown has been classified in the literature in terms of four main topologies: bubble, spiral, double helix and later also conical [17, 59]. Faler and Leibovich [16] showed that vortex breakdown can occur in six different forms, primarly dependent on the Reynolds number. In most cases the different forms can be considered either bubble or spiral form. For a given runner, the occurrence of the different topologies is dependent on the turbine's operating point. Sarpkaya [59] carried out experiments with various swirl numbers and Reynolds numbers. With increasing Reynolds number and swirl number, he found that the vortex breakdown shape changed from helical shapes into an axisymmetric or conical shape [59, 60].

A Francis turbine at part load is prone to make a relatively strong swirling flow in the draft tube. The flow contains a number of travelling vortices or vortex filaments, which may orignate from flow separation at the leading or trailing edges of the blades. The vortex filament within swirl flow was described analytically by Hardin [24] and Alekseenko and Kuibin [1]. If the swirl is sufficiently strong, the vortex filaments may easily roll up into a single vortex core [50]. This type of filament is also found in draft tubes, where it is observed as a helix or spiral rotating around the draft tube center [13, 50] as shown in Figure 2.3. In the field of hydro power, the spiral vortex filament is known as a rotating vortex rope (RVR) [31] as it rotates about the axis of the draft tube. If the static pressure drops to reach the vapor pressure of the fluid, the RVR is visible. The size of the vortex rope is dependent on the submergence. Less submergence will result in a larger RVR.

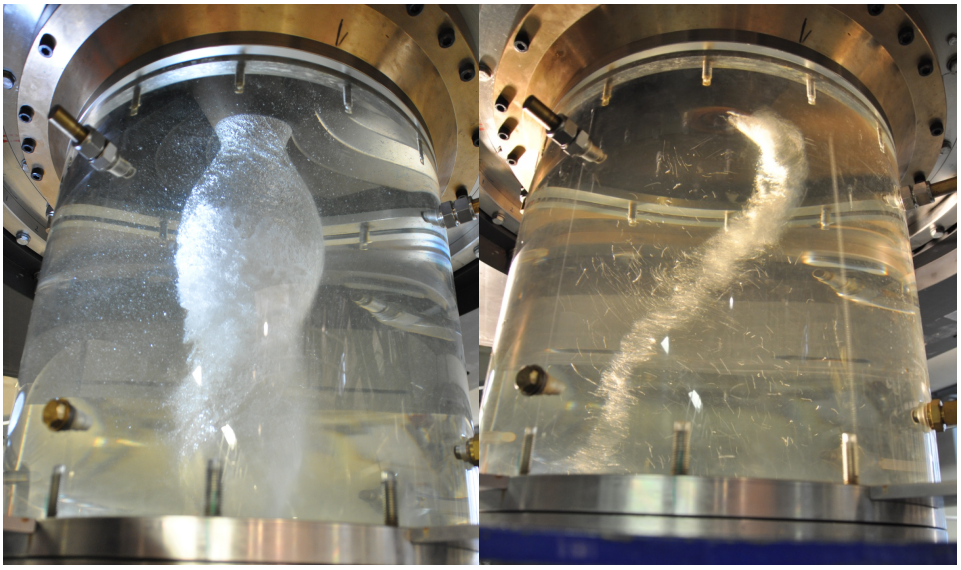

(a) (b)

Figure 2.3: Vortex breakdown in a model turbine. A full load vortex breakdown(a), and part load rotating vortex rope (b) in a model runner in the Waterpower Laboratory. Photo: Bjørn Winther Solemslie

Visual observations by Alekseenko and Kuibin [1] show that the vortex rope is formed in the area where the axial flow changes direction. Nishi and Liu [50] later showed that the vortex rope is located in the shear layer between the central stalled region and the swirling main-flow with a low pressure zone in the center of the vortex rope. Particle Image Velocimetry (PIV) measurements performed by Ciocan and Iliescu [10] demonstrated the movement of the rotating vortex rope. The movement of the vortex rope was also documented with Laser Doppler Vibrometer (LDV) by Vekve [74].

A visible vortex rope is caused by development of vapor- or gas-filled cavities which leads to a change in the vibration behavior and flow stability. The collapse of bubbles creates noise and can be seen in a wide band of frequencies power spectrum. The amplitude will of course be a lot smaller than of the vortex rope. The dynamic transmission behavior of the fluid conduit is affected by the occurrence of vapor as it is compressible, in addition the collapse of the vapor bubbles will typically reduce the natural frequency. Hydraulic instability may occur due to the collapse of large cavities and the resulting strong pressure shocks [13].

2.4 Pressure pulsations

The swirling flow in the draft tube often cause vortex breakdown which is recognized as the primary cause of severe flow instabilities and pressure pulsations [3]. Pressure pulsations are an area of great interest because they may produce heavy vibration, power swings and other undesirable effects [23, 12], which may cause high fatigue loads and ultimately lead to mechanical failure. Mitigation of pressure pulsations is considered an important task because it increases the lifetime of the turbine.

The main focus of pressure pulsations have been the draft tube pressure pulsations (DTPP), and in particular the pressure pulsations occurring at part load. The rotating vortex rope pulsation is composed of two different components with the same frequency, an asynchronous and a synchronous component [48]. The pressure pulsations are usually measured at the draft tube wall. To understand the distribution and phase measured, it is necessary to decompose the pressure pulsation into a synchronous and asynchronous component.

The synchronous component has equal phase and amplitude for all locations

in same cross section of the draft tube. It may be seen as an axisymetric pressure wave propagating through the draft tube. The asynchronous component is also known as the rotating component as this refers to a pressure pattern rotating around the axis of the draft tube. Each natural frequency an object produces, has its own vibration mode. The lowest resonant frequency of a vibrating object is called the fundamental frequency. Most vibrating objects have more than one resonant frequency which are know as harmonics. A harmonic is defined as an integer multiple of the fundamental frequency. Harmonics may be significant, but the fundamental component is the most important as this will have the highest amplitude. Both components are a consequence of the rotating vortex rope and the frequency is the same as the precession frequency of the vortex rope. The distinction between the two components are interesting as their mechanical effects are different [12].

The rotation of the flow makes the low pressure zone move around in the draft tube. Pressure measurements have shown that under certain loads and under the influence of flow controlling methods (e.g., the injection of water and air), the pressure pulsation can become synchronous. A synchronous vortex rope pressure pulsation is known as a synchronous or plunging component [31].

The synchronous and asynchronous component of the pressure pulsations with a single rotating vortex rope can be found using equations 2.2 and 2.3, where DT1 and DT2 are at 180 degree circumferentially apart from each other [12, 7]

$$p_{sync} = \frac{DT1 + DT2}{2} \tag{2.2}$$

$$p_{asyn} = \frac{DT1 - DT2}{2} \tag{2.3}$$

Where DT1 and DT2 are pressure signals from the same plane, but opposite side of the draft tube.

2.5 Methods to mitigate draft tube pressure pulsations

Various methods have been used to mitigate pressure pulsations. Active methods include the techniques of air and water injection. Passive methods such as fins, shaft extension and grooves have also been explored.

2.5.1 Overview of Active methods

Air injection

A Central air injection into draft tube center (usually through the upper cover and runner cone)

B Peripheral air injection through the draft tube wall

C Distributed air injection from the trailing edge of the runner blade

D Upstream air injection between the runner and guide vanes

The different alternatives for air injection are illustrated in Figure 2.4.

Water injection

- Axial injection into the draft tube
- Tangential injection into the draft tube

2.5.2 Overview of Passive methods

- Fins
- Shaft extension
- J-grooves

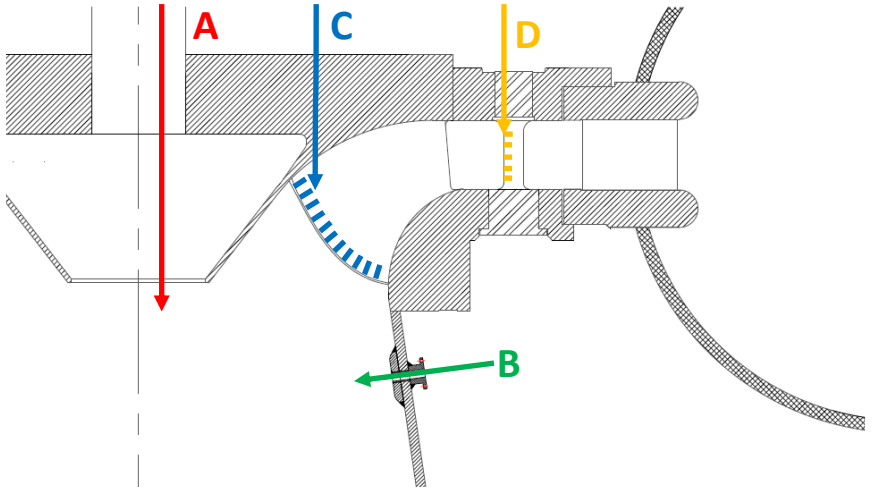

Figure 2.4: Methods of air injection: A - Central, B - Peripheral, C - Distributed and D - Upstream

2.6 Active methods

2.6.1 Air injection

Different methods exist to achieve air injection and air admission. The methods can be beneficial by potentially dampening the high frequency components of noise and vibration [13]. In cases where the average pressure in the draft tube is lower than the atmospheric pressure, the air does not need to be compressed into the draft tube. The most conventional air injection method, the injection of air through the shaft into the draft tube center, is referred to as central air injection and is shown as method A in Figure 2.4. Peripheral air injection through the draft tube wall downstream of the runner, shown as method B in Figure 2.4, is another well-known method. Further distributed air injection from the trailing edge of the runner blade (Method C) and upstream air injection, i.e., admitting air in behind the guide vanes upstream of the runner, Method D), have also been studied. Depending on design, other methods may be used, but these are often intrusive and not further discussed.

Papillon et al. [52] investigated a low head model runner with specific speed of 0.235. Different runner cone shapes for air injection through a discharge ring at the draft tube, shown as method B in Figure 2.4 was tested. The runner cone was modified to increase the airflow by baffles or by a step, as

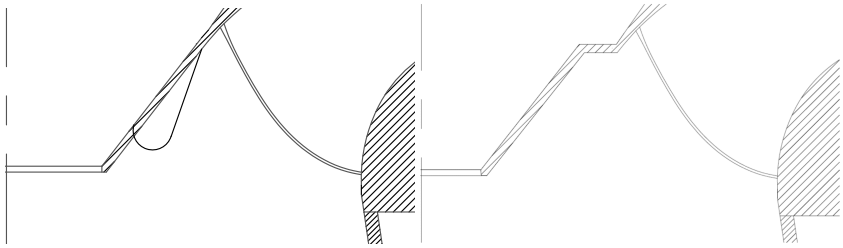

(a) Baffles (b) Step

Figure 2.5: Modified runner cones

shown in Figure 2.5. The modifications of the runner cone for enhancing air flow rate decreased the efficiency by up to 0.5% for the best efficiency point (BEP) when no air was admitted. For partial load operation, the efficiency decreased in average by 0.3%. For small flow rates of air, a significant increase in efficiency was observed at the best efficiency point. Further, the modified runner cones showed a positive effect on operation at $1.15Q_{BEP}$ and higher. Air injection through the discharge ring at the draft tube had a negligible effect on the turbine efficiency. Air admission through the discharge ring created better distributed and smaller bubbles, favouring oxygen transfer. Thus, an even air admission through the runner cone resulted in better air admission capacity at almost every operational point.

The Norris project [44] was a low head prototype runner installed with the following three different air admission options to increase the dissolved oxygen (DO) level in the water for environmental reasons: central air injection through the runner cone, peripheral air injection into the draft tube and distributed air injection through the trailing edge of the runner blades. Typical efficiency losses for the Norris configuration ranged from 0.2% - 4%. Central air injection resulted in the greatest loss, whereas distributed air injection led to negligible losses. Peripheral air injection exhibited smaller values than central air injection, up to 1.2% at 3% relative air content. Typical effects on turbine efficiency from air flows were reported by Foust et al. [21] and indicated significant loss for central air injection, whereas distributed air injection led to negligible losses for relative air content $< 3\%$. Peripheral air injection resulted in similar losses to those reported in the Norris project. The trend was similar for operational points from $0.8Q_{BEP}$ to $1.2Q_{BEP}$.

Muntean et al. [45] investigated a low head Francis prototype with central

air injection. The investigation included six partial load operation points and measurements from five pressure sensors at the draft tube wall. The frequency spectra highlighted the dominating frequency corresponding to flow instabilities (e.g., vortex rope). Further, air injection had a minor influence on operating points with discharge greater than $0.81Q_{BEP}$. For air injection at a discharge of $0.69Q_{BEP}$, the dynamic behaviour, i.e. a larger reduction in pressure amplitudes was measured. However, for lower discharge of 0.53-$0.29Q_{BEP}$ the dynamic behaviour deteriorated when air was injected. The frequency spectra revealed that the highest amplitudes were found at the pressure taps farthest from the runner in the cases without air injection. This finding contradicts results presented by Baya et al. [3], in which the highest value was observed closest to the runner at partial load operation with discharge less than $0.8Q_{BEP}$. Muntean et al. [45] also noted that the highest amplitudes can in some cases be found farther upstream in the draft tube when air is injected.

Casanova García and Mantilla Viveros [8] performed an experimental analysis of vibrations in a Francis prototype with air injection from a single point in front of the runner blades. Air was injected from a pressurized tank with a constant volume. As a result, the flow rate decreased over time. The results indicated a significant decrease in pressure pulsation amplitudes and wall stress at a volume airflow of 0.34% (at 93 kPa) of the water discharge when operating at 60% load. Measurements of the pressure pulsations indicated that the amplitudes were reduced to almost a third when air was injected at a part load operating condition. The measurements also indicated that the highest amplitudes were found at the lower part of the draft tube. Casanova García and Mantilla Viveros [8] also used strain gages along three different directions, vertical, horizontal and 45°-angle. At the wall of the upper cone, stresses were reduced from 2.95 MPa to 0.95 MPa when air was injected at 60% load.

Nakanishi and Ueda [47] investigated peripheral air injection at both models and prototypes. They observed that air injected into the draft tube would create a foam in the low pressure zone in the draft tube center, breaking down the forced vortex core. A small amount of air would not stabilize the center cone or decrease draft tube surging. The center cone may become more unstable and pressure pulsation amplitudes may increase. When reaching the threshold of air supply, the center cone will abruptly become larger and stable, while the draft tube surging sharply decreases. The critical air flow was found to be from 1.5% - 2.5% of the turbine discharge for the different model turbines.

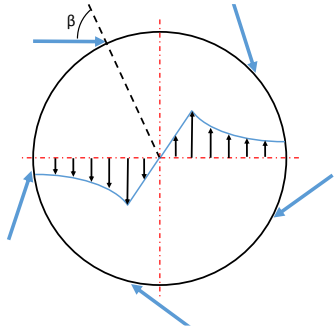

Figure 2.6: Tangential water injection. The water is injected in the opposite direction of the tangential velocity

2.6.2 Water injection

Until recently, experiments were performed with air (rather than water) both as a working fluid and an injection fluid [13, 51]. Currently, simplified models use water as a working fluid. Every turbine has a unique geometry that influences the draft tube flow. Due to lack of prototype geometries, simplified models such as swirl generators, as shown in Figure 2.7 , are used to investigate specific flow phenomena. However, swirl apparatuses can produce sufficient swirl, but the radial distribution of velocity differs from an actual turbine [13]. Therefore, model turbines are preferred.

Tangential water injection

How to use tangential water injection to widen the operating range of a turbine was investigated by Francke [22]. Tangential water injection can increase the operating range to counteract the swirl component and thereby decrease pressure pulsation amplitudes. Water was injected tangentially, in the opposite direction of the swirl component, through 5 - 7 nozzles mounted on the draft tube wall, as shown in Figure 2.6. The injection angle, represented by β in Figure 2.6, was adjustable, as was the horizontal angle. The nozzles were connected to the high pressure side of the turbine to provide pressurized water. This required some of the water to bypass the turbine, which was considered a leakage loss.

Francke [22] carried out model tests on a high head Francis turbine. When water was injected, the tangential velocities and the standard deviation of pressure were reduced. Improved hydraulic efficiency was measured for the

model tests. However, when the loss arising from the leakage loss related to the nozzles was incorporated, the total efficiency was reduced for part load operational points. The measured overall efficiency was reduced by 3.4% for operation at approximately 30% of Q_{BEP}, but only by 0.4 - 0.9% at 40% of Q_{BEP}.

Two measurements at prototypes were also carried out. Measurements at the Skarsfjord HPP indicated a decrease in tangential and axial velocity. When water was injected, the standard deviation of the pressure was significantly reduced at operation between 35% and 50% of nominal load. This indicates a reduction in the amplitude of the pressure pulsations. Frequency analysis showed that the Rheingans frequency amplitude was reduced but not completely removed, indicating that the vortex rope was still rotating inside the draft tube. For operation above 50% load, the amplitude of the pressure pulsations increased with the number of operating nozzles, whereas the mean pressure decreased with increasing load. At partial load operation, an increase in the turbine hydraulic efficiency was measured with increasing nozzle flow rate. However, the efficiency increase of the turbine only compensate for the increased leakage losses so the total efficiency remains more or less constant.

The second prototype measurements were carried out at the Skibotn HPP. The results indicated increased pressure fluctuations with an increasing number of nozzles in use. However, frequency analysis showed a significant decrease in amplitude of the Rheingans frequency for 1 - 3 operating nozzles. The mean pressure was reduced for up to three operating nozzles, but the use of additional nozzles increased the mean pressure. This result is somewhat contradictory to the results from the Skarsfjord HPP. It is expected that increasing velocity will decrease the mean pressure. Francke suggested that the increase in mean pressure is related to overpressure in the draft tube.

Axial water injection into draft tube center

Another method for injection of water is axial injection. Water is injected through the runner cone into the draft tube center, as shown in Figure 2.7. This is similar to air injection method A shown in Figure 2.4. For water injection, the method is referred to as axial water injection. The experiments performed using a swirl rig do not have a specific operating point. They are used to investigate specific flow phenomena such as the vortex rope. The

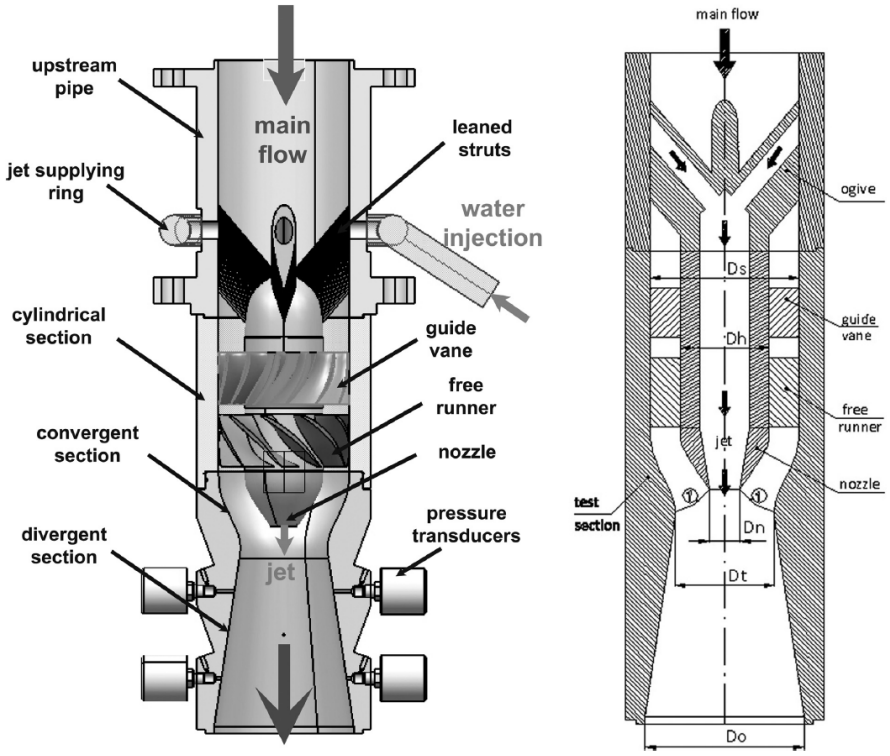

Figure 2.7: Axial water injection in a swirl rig. Source: [6]

experiments presented in this section investigate the visible vortex rope and correspond to a partial load operating point for the turbine. The precise load depends on the turbine design.

Susan-Resiga et al. [68] numerically investigated axial water injection into the draft tube of a low head Francis turbine from the FLINDT project [2]. The study included a variety of different jet diameters and flow rates from 1 - 28% of the turbine discharge. The axially injected water, hereafter referred to as the jet discharge, was supplied from the spiral casing and was therefore considered a leakage loss, as this flow was not available for power generation. The simulations indicated a significant reduction in pressure fluctuations at the draft tube wall. Susan-Resiga et al. [68] concluded that axial water injection changed both the amplitude and the frequency of the pressure fluctuations, though no further quantification was reported. The reduction of pressure fluctuations corresponded to an efficiency increase. At partial load, the water injection improved both the draft tube flow and

runner flow and the overall efficiency losses were only in the order of 0.2%. However, the conditions used to obtain these results were not reported.

This axial water injection method addresses directly the main cause of the flow instability. Susan-Resiga et al. [68] concluded that the jet effectively removes the vortex breakdown at partial load, with minimum effect on overall turbine efficiency. Further, it can be adjusted to the operating point and does not change the runner geometry. Susan-Resiga et al. [67] presented numerical simulations of the swirl rig with conical expansion of approximately 17.2° and an inlet diameter of 100 mm and outlet diameter of 160 mm. The simulations showed that the jet discharge must be as high as 10% of the turbine discharge to efficiently mitigate the vortex breakdown at partial load. This is an impractically large fraction of the turbine discharge. Water from the spiral casing can be used to supply a high velocity jet, but when the jet discharge reaches 10% of the turbine discharge, the losses are no longer acceptable.

The method was further investigated numerically and experimentally by Ruprecht et al. [58]. The experimental study was carried out with a swirl generator similar to the one shown in Figure 2.7. The actual cone had an inlet diameter of 80 mm and outlet diameter of 130 mm giving a conical expansion of 17.2°. The results from PIV measurements showed that the vortex rope was removed when the jet discharge was only 4% of the turbine discharge. A frequency analysis showed that water injection removed the dominant vortex rope frequency when only 2% of the turbine discharge was injected. Further, the amplitudes of the low frequency pressure pulsations were significantly reduced. The numerical results were similar to the experimental results. The vortex rope was not observed in the numerical results for jet discharge values above 5.6% of the turbine discharge. A comparison of the pressure pulsations showed that in both the experimental and numerical cases, the amplitudes decreased towards zero with increasing jet discharge and reached zero when an amount between 4.8% and 5.6% of the turbine discharge was injected. However, there were significant differences between the amplitudes of the pressure pulsations for the experimental and numerical parts. At the draft tube inlet, the amplitudes were 50% higher in the experimental results. At the draft tube outlet, the different turbulence models produced different results. The SST model exhibited higher amplitudes, up to three times the experimental values, whereas the k-e-model undershot at approximately 50%. Further, Ruprecht et al. [58] concluded that the optimal value for water injection is highly dependent on the operating point. Results by Ruprecht et al. [58] show a significant lower jet

discharge is needed than found by Susan-Resiga et al. [67]. The difference in test rig size and the introduced swirl of the swirl rig may explain the different results.

Muntean et al. [46] tested axial injection of water into the draft tube and documented how the frequency spectra changed with increasing jet discharge. The swirl rig is shown in Figure 2.7. The swirl rig had conical expansion of approximately 17.2° and an inlet diameter of 100 mm and outlet diameter of 160 mm which is the same as numerical simulations by Susan-Resiga et al. [67]. The frequency analysis indicated no significant improvement for jet discharge amounts less than 5% of the turbine discharge. At 7% jet discharge, the frequency analysis indicated a significant increase in low frequency amplitudes. When the jet discharge was larger than 8.5% of the turbine discharge, all of the pressure fluctuations were mitigated. The amplitudes of two dominant frequencies at 6 and 20 Hz were effectively reduced with approximately 70% and 60%, respectively. Further, Muntean et al. [46] concluded that a 10% jet discharge is required to operate without pressure fluctuations and with maximum pressure recovery.

Kirschner et al. [33] performed experiments with axial water injection in a model pump turbine with different nozzle diameters and flow rates up to 13.6% of the turbine discharge. Two partial load operational points were investigated; $0.72Q_{BEP}$ and $0.43Q_{BEP}$. At $0.72Q_{BEP}$ the vortex rope was observed. Only a small reduction of pressure fluctuations was measured for a nozzle diameter of 38 mm and jet discharge at 8.0% of the turbine discharge. However, the vortex rope frequency amplitude was decreased by 20% when water was injected. A decrease in nozzle diameter to 30 mm and a jet discharge of 7.4% led to a larger decrease in pressure fluctuations and reduced the amplitude of the vortex rope frequency by 65%. The last test presented for $0.72Q_{BEP}$ combined water and air injection. The jet discharge was reduced to 2.8% of the volume discharge, whereas the mass flow rate of air was 0.023% of the turbine discharge. A slightly larger decrease in pressure fluctuations was observed compared to the nozzle with the smaller diameter, and the vortex rope frequency amplitude was reduced by 60%. In all three tests, the vortex rope frequency was shifted towards a lower frequency.

The results using the second operating point at $0.43Q_{BEP}$ were similar to the two water injection tests [33]. However, the dominating frequency was no longer the vortex rope frequency, but the runner frequency. For the last test, which combined a jet discharge of 4.8% and an air mass flow rate of 0.040% of the turbine discharge, the pressure fluctuations were reduced to

approximately 80%. The frequency analysis showed that only one frequency, at approximately 0.2 of the runner frequency, was detectable. This finding may indicate that water injection is more efficient at partial load operational points at which a vortex rope frequency is dominant. At lower partial load, air injection performs better.

Bosioc et al. [6] used the swirl rig shown in Figure 2.7 to further investigate the vortex rope. They presented similar results as Ruprecht et al. [58] in terms of the ability of water injection to reduce vortex rope related frequencies. The vortex rope generated was similar to that of a Francis turbine operating at 70% of Q_{BEP} [6]. Bosioc et al. [6] injected water at rates of up to 14% of the turbine discharge. The results indicated a steady decrease in pressure pulsation amplitudes until the jet discharge reached 11.5% of the turbine discharge. At this point, the pressure pulsation amplitudes were reduced by 50% compared to the slightly lower jet discharge. A further increase in jet discharge up to 14% of the turbine discharge did not significantly change the amplitudes. Bosioc et al. [6] therefore referred to 11.5% jet discharge as a threshold. An investigation of the pressure pulsations showed that the rotating component of the pressure pulsation dominated until the jet discharge threshold was reached. After the threshold, the amplitudes dropped and the plunging component became the dominating factor. Bosioc et al. [6] concluded that the water jet injection removed the vortex rope and that the swirling flow became axisymmetric as a result.

Investigation of the axial water injection revealed that it is more effective to use a low velocity but high discharge jet than a higher velocity and low discharge jet [67]. For best results, the jet velocity should be on the same order of magnitude as the average axial velocity. Susan-Resiga et al. [67] therefore proposed the flow-feedback method (FFM), which supplies the jet with water from the draft tube instead of the spiral casing. This method thereby effectively removes the losses related to bypassing the turbine and consequently is expected to improve efficiency because losses are reduced in the draft tube. The water is collected at the end of the diffusor cone and is directed to the jet. This system takes advantage of the pressure difference between the jet in the draft tube center and the supply from the draft tube wall.

Tanasa et al. [69] and Tănasă et al. [71] further investigated the proposed FFM by Susan-Resiga et al. [67] experimentally with a swirl rig with conical diffusor by comparing it to the original design with water provided from the spiral casing. They measured the pressure fluctuations at four levels below the swirl rig. The results showed that axial water injection effecti-

vely reduced the amplitude of the dominant frequency by 20-32% in the three levels closest to the jet discharge. There was no significant difference between the FFM and water supplied from the spiral casing. At the level farthest from the turbine, an amplitude increase of approximately 60% was measured. In addition, the dominant frequency changed from 15 Hz when no water was injected to 10.7 Hz and 10.5 Hz for injection from the spiral casing and FFM, respectively. Further, they concluded that the FFM has the potential to mitigate pressure pulsations generated by the vortex rope without any additional energy consumption.

Tănasă et al. [72] further investigated the FFM. As a result of losses in pipes feeding the water back, the actual discharge was lower than first estimated. Therefore, an improved method was tested that used an ejector pump to increase the jet discharge. This is hereafter referred to as the FFM+. Whereas the jet discharge is 10% of the turbine discharge for the FFM, the FFM+ increases it to 12% of the turbine discharge. This allows for the water injection to cross the threshold found by Bosioc et al. [6]. Only a small increase in draft tube pressure was measured, corresponding to the small increase in jet discharge. However, a significant reduction in pressure pulsation amplitudes was measured. By crossing the threshold, the amplitudes of the pressure pulsation were reduced by more than 50% compared with the FFM. In addition, the rotating component of dominating frequency was reduced, and the plunging component became dominant. Tănasă et al. [72] thus achieved the same result as Bosioc et al. [7] without a volumetric loss.

Swirl rig experiments have demonstrated promising results for mitigating pressure pulsations. The swirl rig used by Bosioc et al. [6], Tănasă et al. [72] and Susan-Resiga et al. [67] have a straight draft tube, with no bend causing reflections, possibly reducing the pressure pulsation amplitude measured.

2.7 Passive methods

Different passive installations in model turbines have been investigated by several authors [54][74][38][37][36][70]. The general strategy of passive installations is to change the flow in the draft tube center by physical installations at the runner cone or draft tube wall.

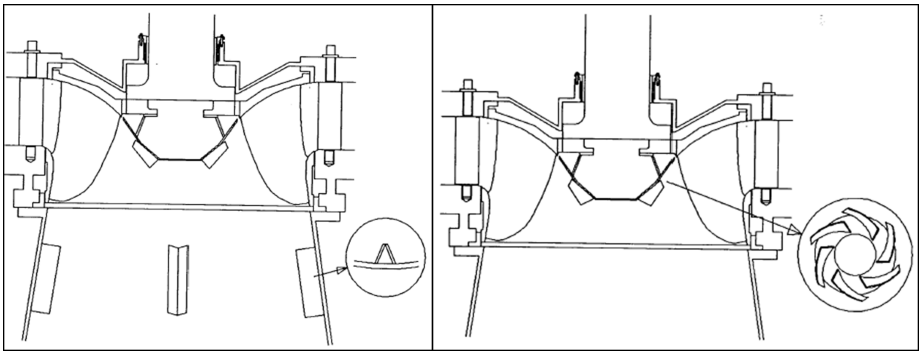

(a) Turbine with fins attached to the wall

(b) Turbine with fins attached to the runner cone

Figure 2.8: Different types of fins

2.7.1 Fins

Thicke [70] reviewed some practical solutions for improving draft tube flow stability. The investigation of different runner cones showed that the runner cone shape plays an important role in controlling the draft tube velocity distribution, which greatly affects the characteristics of the draft tube rope formation and pressure pulsations. The design of the runner cone is extremely important in controlling the velocity profile and pressure in the draft tube [70][5][57]. This is because the shape of the runner cone may change the dominant frequency in the draft tube and influence the vortex rope [54][70]. Thicke [70] recommended that the velocity at the draft tube throat should not exceed 3.5 m/s. Testing and observation of a prototype showed that the partial load pressure pulsations could be reduced with a runner cone extension [70]. A conical extension with a length of approximately 30% of the draft tube inlet diameter reduced power swings of 3-5 MW (i.e., 4-8% of the turbine's nominal load). A reduction in pressure below the runner from 90 kPa to 50 kPa also improved the air injection in this case. Thicke [70] further concluded that for good air injection, the runner cone must extend at least to the bottom of the runner. Model tests indicated that the longest and largest runner cone extensions were most effective in reducing pressure pulsations. The pressure and velocity in the draft tube center were increased by the runner cone. Additionally, Thicke [70] evaluated various stabilizing fins attached to the draft tube wall. The fins were beneficial in mitigating draft tube swirl and reduce pressure pulsations amplitudes in the draft tube. The reduction of pressure pulsation amplitudes are found in the

synchronous component which is related to draft tube resonance and power swings [13]. The fins have less influence on the asynchronous component and is usually ineffective at high load [13]. However, efficiency losses were observed for low- and medium-head units. The fin geometry and configuration have been designed on a trial-and-error basis to minimize the efficiency loss [68].

Nishi et al. [49] further investigated the ability of fins to reduce draft tube surges by analysing wall pressure pulsations at the draft tube wall. Draft tube surges are caused by resonance occurring when the rotating frequency of the cavitating vortex rope at the elbow section coincides with the natural frequency of the draft tube vibration. The trigger is attributed to the oscillation of pressure recovery in the bend downstream the diffusor having the same frequency as the rotating vortex rope. The extensive testing of fins by Nishi et al. [49] enabled the important conclusion that the natural frequency cannot always be changed by installing fins. Fins can also introduce severe resonance in the turbine as a result of the additional cavity volume behind the fins at low cavitation number. This may also lead to increased pressure pulsation amplitudes. However, installation of fins is useful to broaden the partial load operating range. The frequency of the rotating vortex rope increases with increasing fin height.

2.7.2 Runner cone extension

Different runner cone extensions on a medium head Francis model runner were investigated by Vekve [74]. An example of a runner cone extension is shown in Figure 2.9. Pressure measurements were performed in two planes in the draft tube cone in addition to LDV measurements. The runner cone extension with the largest diameter, $0.41D_2$, where D_2 is the runner outlet diameter, resulted in the largest reduction in pressure pulsation amplitude. The runner cone extension with $0.41D_2$ was tested with two lengths: $0.81D_2$ and $2.95D_2$. The longest runner cone extensions resulted in the best performance in regards to pressure pulsations. Only minor differences in amplitude were measured at low load (i.e., $0.58Q_{BEP}$), while as soon as the flow was increased to $0.71Q_{BEP}$, the pressure pulsation amplitudes in the upper plane dropped to the same level as at the BEP. For the lower measuring plane, this did not happen before $0.835Q_{BEP}$. The shorter runner cone extension performed worse, but better than the runner without extension. The model tests showed an improvement of efficiency for $0.58Q_{BEP}$ of approximately 1.5 - 1.8% for the largest runner cones. For

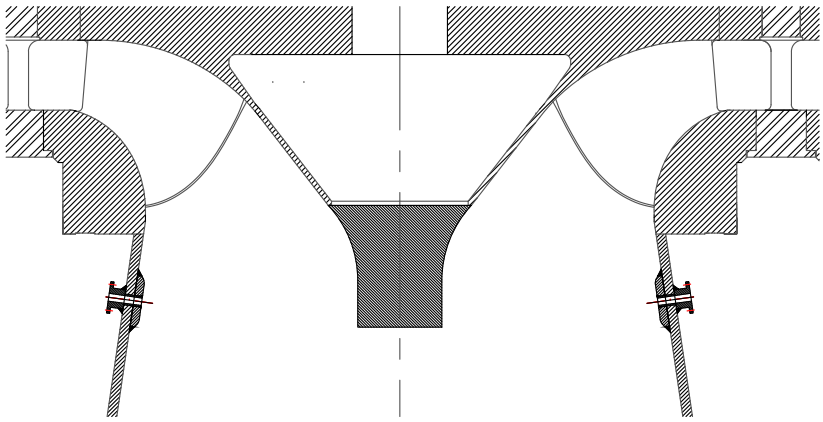

Figure 2.9: Francis runner with runner cone extension

the other operational points, the largest runner cone extension had no or minor positive effect on the efficiency.

Vekve [74] also performed prototype measurements at the Litjfossen HPP. These prototype measurements confirmed that the shaft extension has to be sufficiently large, in this case a diameter 21% of the runner outlet diameter, to properly dampen the pressure fluctuations. A test at 75% load showed dampening in the pressure fluctuations, whereas at 45% load the shaft extension was too small to have a significant effect. At 75% load, the amplitude of the rotating component of the vortex rope pressure pulsation was reduced to approximately 35%. Prototype measurements at Oksla with a runner cone extension showed no significant improvement. The runner cone extension in this case had a diameter 16% of the runner outlet diameter. Vekve concluded that the shaft extension moves the initiation point of the vortex rope further downstream and can reduce the strength of the vortex rope (i.e., the amplitude of the RVR). The further downstream the vortex breakdown occurs, the shorter the distance the RVR has available for longitudinal development.

Qian et al. [54] carried out tests of four different runner cone shapes in a high head runner model. The original shape and the three modified shapes are

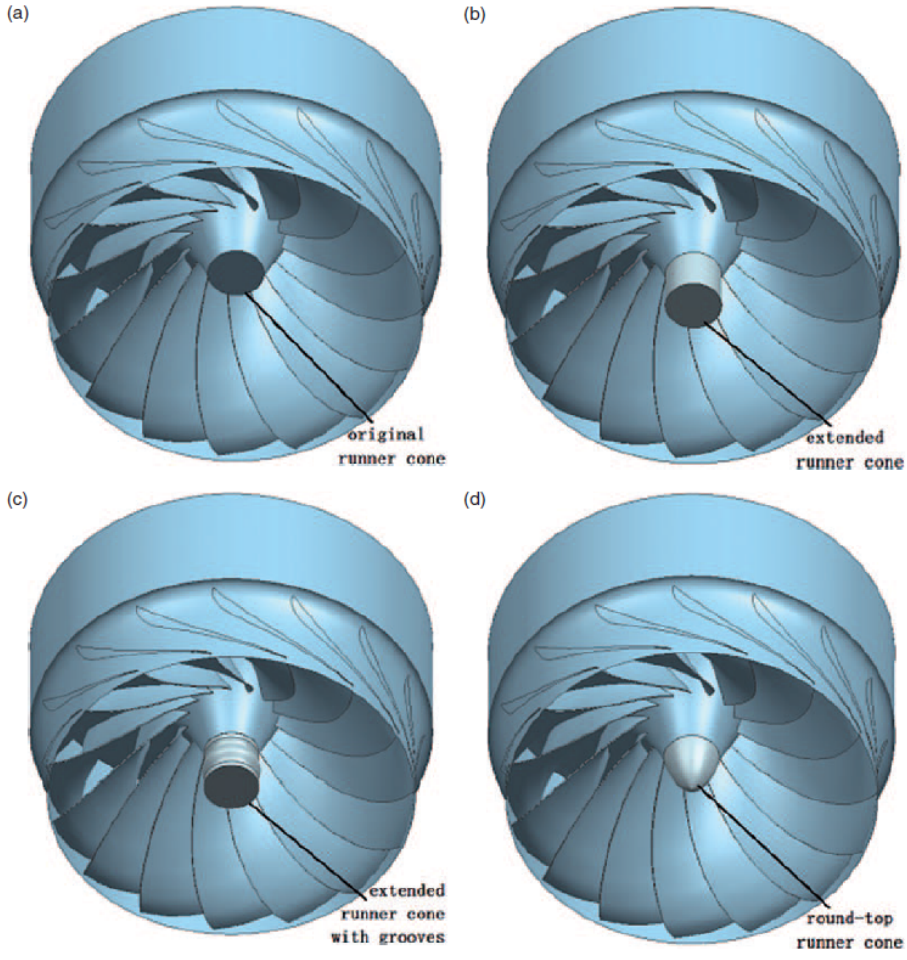

Figure 2.10: Different runner cone extensions. Source: [54]

shown in Figure 2.10. Compared with the work by Vekves [74], these runner cones were smaller and shorter. The pressure was measured at 30 points in the spiral casing and draft tube. Measurements from three locations in the draft tube with different distances from the runner were presented. Five different guide vane openings were tested. With a 16° guide vane opening, the amplitude of the dominating frequency was doubled for cases b and c, whereas the last case did not change the amplitude significantly. At 17° guide vane opening, the dominating frequency was changed from 7.58 Hz to 4.55 Hz and the amplitude almost doubled for all the modified runner cones. With an 18° guide vane opening, the dominating frequency was shifted from 5.24 Hz to 5.13 Hz for cases b and c. However, the amplitude changed by 10 - 20% in the positive and negative directions depending on the distance from runner to the pressure measurement location. Similar results were found for a 19° guide vane opening. With a 20° guide vane opening, the dominating frequency increased the farther away from the runner cone the measurements were taken. The extreme case was runner cone b, which increased the frequency consecutively from 1.7 Hz – 5.49 Hz – 13.74 Hz. The use of runner cone b also resulted in significantly lower amplitudes, reduced by approximately 70% and 40% from original case, in the two measuring levels farthest downstream the runner. A higher dominant frequency was also measured compared to the other cases. It is also worth noting that for 16° and 19° guide vane openings, the pressure pulsation amplitude increased with the distance from the runner, whereas at 18° the highest amplitude was found at the second level downstream of the runner. With a 17° guide vane opening, the amplitudes remained almost constant for the modified runner cones at all levels, whereas the original runner cone exhibited an increased amplitude. The amplitude increased from 20% of the modified runner cone amplitude closest to the runner, to 70% of the modified runner cone amplitude. In general, their conclusion was that the modified runners had a positive effect on the vortex rope induced frequencies.

2.7.3 J-grooves

Kurokawa et al. [37] and Kurokawa [36] turned fins into shallow grooves called J-grooves. By placing shallow grooves in the axial direction downstream a swirl generator, Kurokawa et al. [37] measured velocity profiles and pressure pulsations in a diverging channel. The results showed that the deepest groove at 4 mm, which was diverging from 11.3 - 26.9 mm, significantly decreased the tangential velocity of the water. In the largest swirl case, the

groove reduced the maximum tangential velocity by nearly 60% and significantly reduced the pressure pulsation amplitudes. In contrast to the results report by Thicke [70], Kurokawa et al. [37] reported the hydraulic losses to be negligible. However, the grooves increased reverse flow in the draft tube center and a reverse flow occurred in the latter part of the grooves. Consequently, a higher maximum axial velocity was achieved compared to the configuration without grooves. According to experimental findings and theoretical considerations by Kurokawa et al. [37] and Kurokawa et al. [38], the groove effect is explained by two mechanisms:

- a decrease in tangential velocity at the diffusor inlet leading to increased mixing of the flow
- increase in radial velocity arising from reverse flow in the groove

Chapter 3

Free Rotating Runner Cone Extension

Vekve [74] found that a runner cone extension could move the initiation point of the vortex rope downstream. The runner cone extension will also remove the centre volume beneath the runner and thereby the central stalled region. As a physical object is introduced, the cross section area is also reduced. This would increase the average axial velocity of the flow and thereby reduce the swirl number. Due to friction, the swirl decreases downstream in the draft tube. Thereby the rotating component becomes less dominant. With an ordinary runner cone extension the rotation of the runner cone will be equal to the runner rotation. As this reaches further down in the draft tube, swirl will increase in the center region.

A free rotating runner cone extension (FRUCE) is a runner cone extension connected to the hub with bearings. The bearings allows the outer part of the extension to rotate freely and independent of the runner rotation. The FRUCE will then only be driven by the viscous forces in the water. Essentially, the free vortex in the draft tube will extend all the way from the draft tube wall to the FRUCE surface as the forced vortex is removed as shown in Figure 3.1. When moving downstream in the draft tube, friction will reduce the swirl. As the swirl is reduced, the velocity of the FRUCE is also reduced. This means a reduction in tangential velocity and thereby a reduction in pressure pulsation amplitudes.

Figure 3.2 displays a cross section of one of the FRUCEs tested in the Waterpower Laboratory at NTNU. The rotating part is shown in red beneath

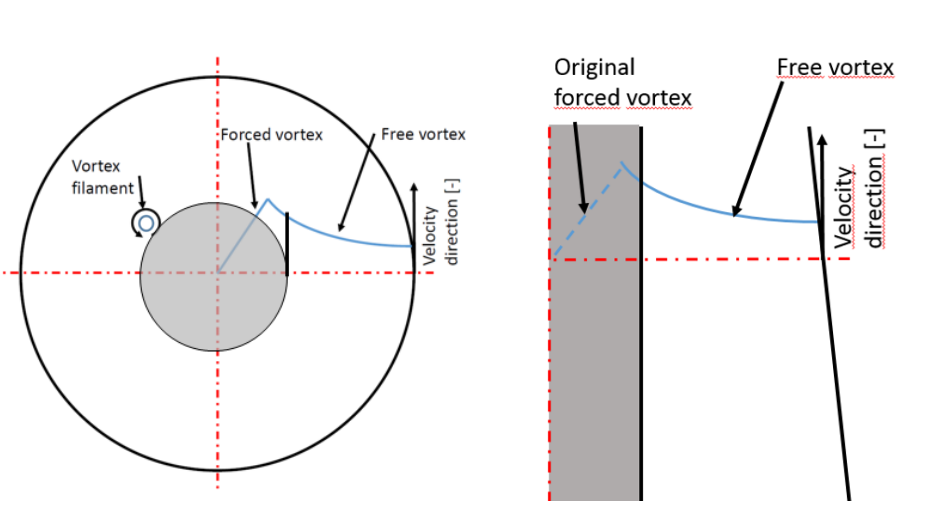

(a) Axial view (b) Cross section

Figure 3.1: FRUCE influence on the tangential velocity. The grey area represents the FRUCE. The inner part of the vortex is removed by the FRUCE.

the runner cone. Two sets bearings for axial and radial forces was used to keep the outer part in place. A cylindrical design was chosen because other results with similar shapes where available for comparison.

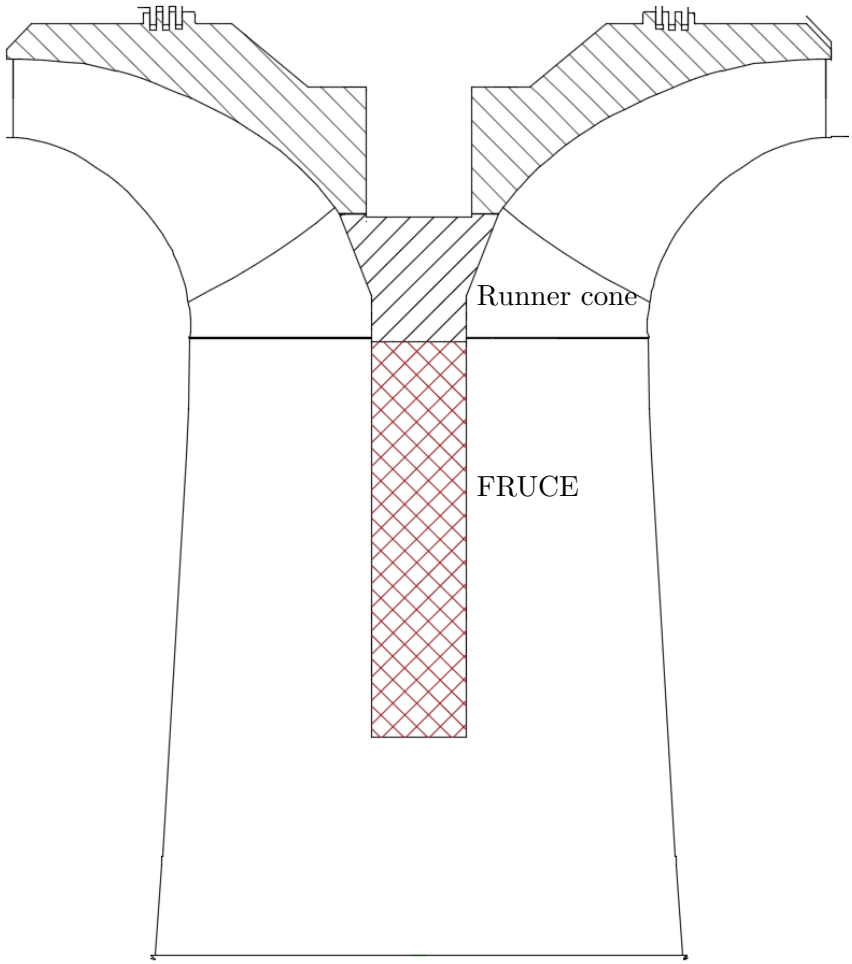

Figure 3.2: Cross section of the FRUCE. The red part is the rotating part of the FRUCE. Inside the outer part are two sets of bearings to keep the outer part in place.

Chapter 4

Experimental setup

This chapter describes the experiments and measurements performed on prototypes and in the laboratory. Prototype measurements were conducted at four different sites. Pressure pulsation measurements were carried out at La Higuera, Leirfossene, Øvre Leirfoss and Nedre Leirfoss. At La Higuera two different air injection methods were investigated along with efficiency measurments. At Øvre Leirfossen and Nedre Leirfossene pressure pulsation measurements were carried out. Leirfossene was the main focus for the FRUCE experiments. Both pressure measurements and efficiency measurements were carried out with and without FRUCE. The FRUCE was first tested in the laboratory before a FRUCE was designed for the prototype in Leirfossene.

4.1 Efficiency measurements

Efficiency measurements were carried out in parallel with the pressure measurements at Øvre Leirfoss and Nedre Leirfoss, but these measurements are not considered part of this thesis. However, the efficiency measurements are used to accurately establish the operating conditions for the pressure measurements. For both La Higuera and Leirfossene the thermodynamic efficiency method was used to measure the efficiency.

The thermodynamic measurement method utilizes the first law of thermodynamics, the principle of conservation of energy, for the energy transfer between the water and the turbine. The specific mechanical energy at the runner is determined by measuring the performance variables; pressure,

temperature, velocity and water levels. In addition the thermodynamic properties of water must be included.

The discharge is challenging to measure in prototype. This is omitted by using the specific mechanical energy together with the specific hydraulic energy. The specific hydraulic energy of the turbine is the difference between the specific energy of water before and after the turbine also known as the known as specific energy head [34].

The efficiency is calculated as the ratio between specific mechanical energy and hydraulic energy. The equations to determine efficiency and uncertainty can be found in the IEC 60041 standard for field acceptance tests [64]

4.2 Prototype measurements

4.2.1 La Higuera HPP

La Higuera HPP is a hydro power plant located in the Andes, south of Chiles capital Santiago. It consist of two units of 77 MW, both equipped with a vertical axis Francis turbine. Power plant data is given in table 4.1.

Table 4.1: Data per unit at La Higuera HPP

La Higuera Hydropower plant	
Number of turbines	2
Nominal net head	375 m
Rated generator output	77 MW
Nominal volume flow	22.7 m/s^3
Nominal speed	600 rpm
Outlet diameter	1.57 m

The power station has suffered from strong vibrations since the start up in 2010. The strong vibrations was one of the causes of the shut down in 2011. The power plant was refurbished and an air injection system was installed. During the recommissioning in 2013 two different methods of air injection, as shown in Figure 4.1, was tested to help reduce the vibrations.

Option A: Air injection through upper cover. This option was installed by the turbine manufacturer. It allows air to pass through the upper cover and enter into the draft tube from the runner cone as shown in Figure 4.1a.

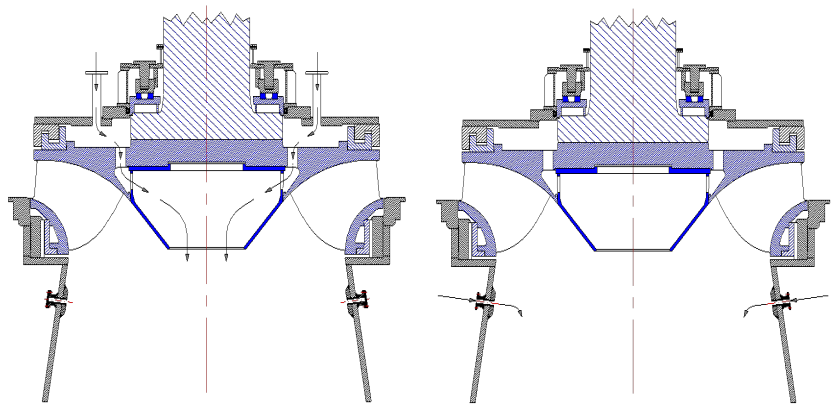

(a) Option A (b) Option B

Figure 4.1: Air injection methods for La Higuera

Option B: Air injection through the draft tube wall which was installed at a later stage. With option B air is injected through four nozzles fitted approximately 250 mm downstream the runner outlet as shown in Figure 4.1b.

Pressure measurements

The pressure measurements were carried out in two set. The first set tested two different setups of air injection (Option A and B) with different amount of air injected at unit 1. The second set was carried out together with efficiency measurements at both units. For the second set of measurements air injection through the draft tube wall (Option B) was used.

Pressure pulsation measurements were performed at La Higuera Power Plant. Two pressure sensor were mounted at the draft tube wall approximately $0.19D_2$ (300 mm) downstream the runner and one pressure sensor was mounted upstream the runner (as shown in figure 4.2). The pressure sensor upstream the runner was mounted upstream the guide vanes, but downstream the main inlet valve. Both pressure sensors in the draft tube were mounted in the same plane with 90° between each other as shown in Figure 4.4. A logging frequency of 2500 Hz and a logging time of 200 s was used. Further pressure sensor data is found in table 4.3. The pressure pulsations were measured in normal operation without air injection, with air injection through

the upper cover (Option A) and air injection through the draft tube wall (Option B).

Table 4.2 shows the measured points and the maximum airflow achieved with the different options. As the best results were found with the highest airflows, the smaller airflows are not included or further discussed.

Table 4.2: Operational points included

Option A			**Option B**		
Load [%]	Air injected [l/s]	% of water flow rate	Load [%]	Air injected [l/s]	% of water flow rate
28.1	138	1.48	29.2	202	2.17
39.3	264	2.27	41.0	214	1.84
49.7	254	1.78	49.7	243	1.70
59.0	198	1.25	59.2	239	1.51
70.8	211	1.23	68.4	248	1.45
77.9	253	1.27	79.6	218	1.09
106.6	0.0	0.00			

For the second set of measurements carried out at unit 2, the pressure sensors were mounted approximately 2 m downstream the runner as seen in Figure 4.3b, due to unfavourable conditions which caused cavitation on the sensor in the original position. These air injection measurements where therefore carried out later alongside the efficiency measurements described in the next section.

Table 4.3: Data per unit at La Higuera HPP

Pressure sensor	Location	Range	Logging frequency
PTX1400	Inlet	0-100 bar a	2500 Hz
PTX1400	Sensor 1	0-10 bar g	2500 Hz
PTX610	Sensor 2	0-10 bar a	2500 Hz

Efficiency measurements La Higuera

The thermodynamic efficiency measurements were carried out at both turbines with and without air injection. The measurements were carried out in accordance with the IEC 60041 [64]. The location of temperature and pressure sensors are shown in Figure 4.5.

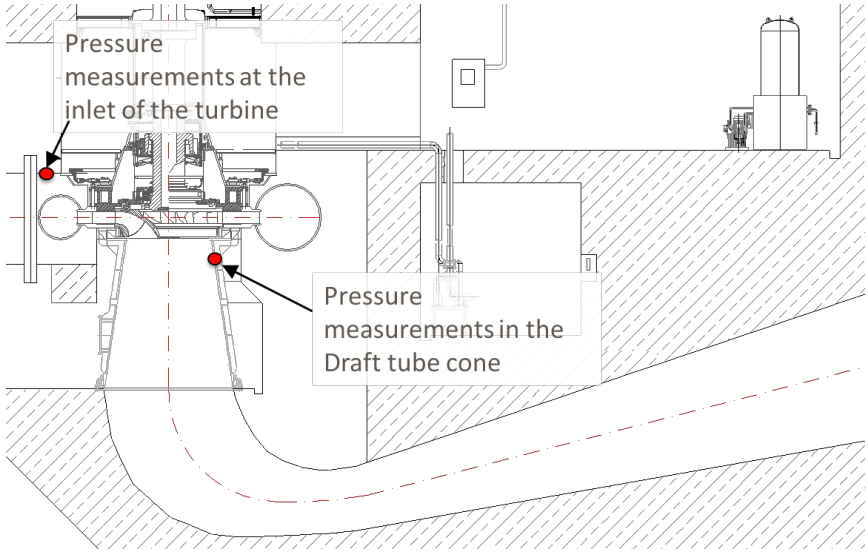

Figure 4.2: Pressure sensor locations at La Higuera HPP

The inlet temperature measurement was done with a probe, as shown in Figure 4.6, inserted in to the main flow upstream the spiral casing. A Seabird SB38 temperature sensor was used to measure the temperature at the inlet with an accuracy of $\pm 0.001°C$. The temperature sensor was thoroughly insulated to eliminate external influence.

The temperature measurements at the outlet were carried out by using a frame and one temperature sensor. The frame, as shown in Figure 4.7, guided water from 31 different locations to the temperature probe. The temperature sensor was the same type, Seabird SB38, as for the inlet.

The pressure measurements were carried out with Digiquarts 9000 series pressure sensors. This was used to measure the inlet pressure, outlet pressure and the atmospheric pressure inside the power plant.

The leakage water was lead into the draft tube. Therefore no measurement of leakage water was carried out.

In total nine measurement points were carried out for unit 1. At unit 2, 17 measurement points was carried out whereof seven were with air injection. An overview can be found in Table 4.4. The operational points measured with air injection along the efficiency measurements are found in Table 4.5.

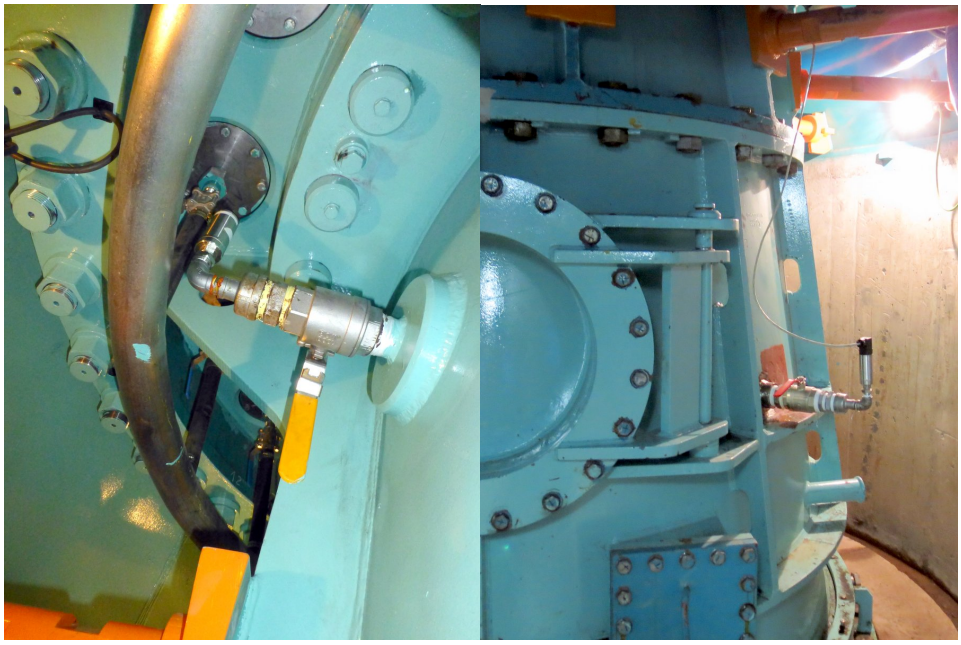

(a) Pressure sensor at unit 1 (b) Pressure sensor at unit 2

Figure 4.3: Pressure sensor mounted at La Higuera HPP. The pressure sensor at unit 1 was mounted $0.19D_2$ downstream the runner outlet, while an unfavourable location at unit 2 lead to remounting $1.3D_2$ downstream the runner outlet

Table 4.4: Operational points included without air injection

Unit 1		**Unit 2**	
Load [%]	MW	Load [%]	MW
40.3	31.0	48.8	37.6
49.4	38.0	59.7	46.0
58.4	45.0	42.5	32.7
58.6	45.1	69.7	53.7
68.4	52.7	81.8	63.0
80.5	62.0	90.6	69.8
91.8	70.7	99.1	76.3
100.1	77.1	99.7	76.8
101.7	78.3		

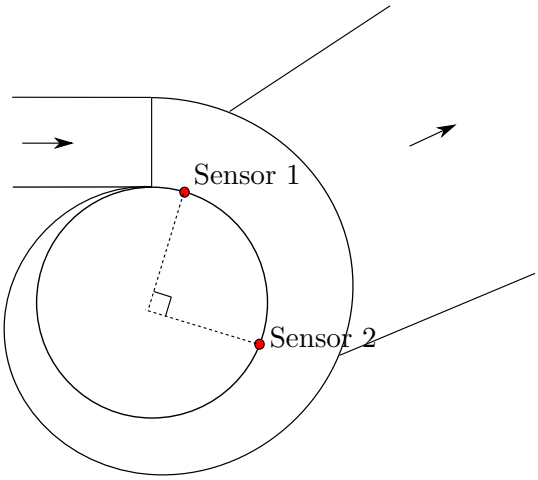

Figure 4.4: Pressure sensor location in the draft tube of La Higuera seen from above

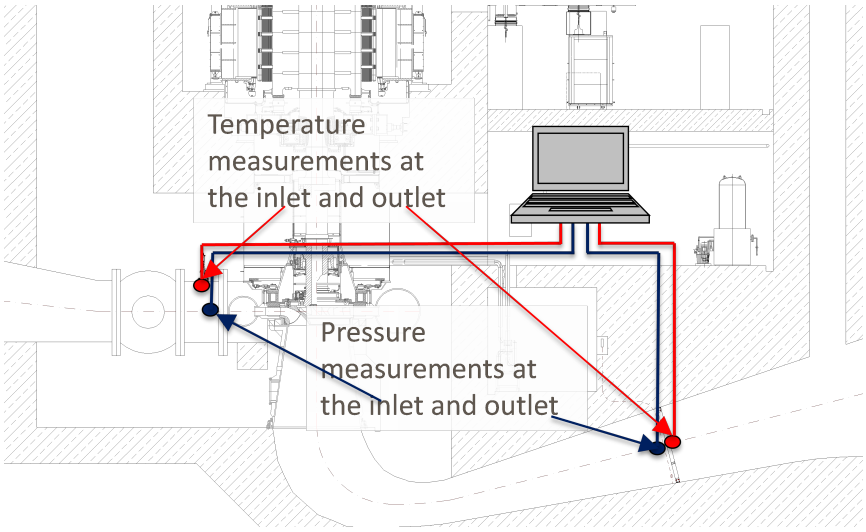

Figure 4.5: Measurement setup at La Higuera

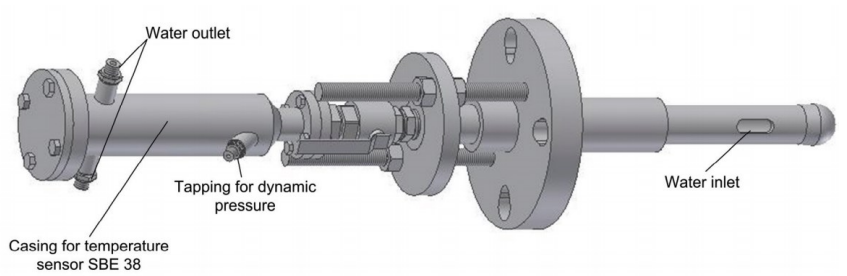

Figure 4.6: Pressure sensor locations

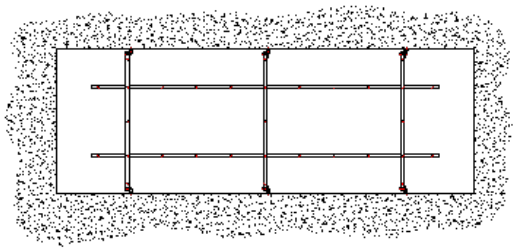

Figure 4.7: Draft tube frame from La Higuera

Table 4.5: Operational points with air injection for Unit 2 at La Higuera HPP

Unit 2			
Load [%]	MW	Air injected [l/s]	% of water flow
42.5	32.7	225	1.87
49.0	37.7	222	1.68
59.7	46.0	212	1.37
69.9	53.8	208	1.18
81.0	62.4	209	1.08
91.2	70.2	212	0.98
98.7	76.0	309	1.32

4.2.2 Øvre Leirfoss and Nedre Leirfoss

Pressure measurements were conducted on the two low head Francis turbines located at Øvre and Nedre Leirfoss Hydro Power Plant. Both hydro power plants are located in Nidelva in Trondheim, Norway. Nedre Leirfoss HPP contains a vertical axis type Francis turbine with a nominal output of 2.5 MW. Øvre Leirfoss HPP is located 2 km further upstream and contains horizontal axis Francis turbine with 3.5 MW nominal output. Further data about the power plants is given in Table 4.6.

Table 4.6: Data per unit at Øvre Leirfoss and Nedre Leirfoss HPP

	Øvre Leirfossen	**Nedre Leirfossen**
Number of turbines	1	1
Nominal net head	32.6 m	25.7 m
Rated generator output	3.5 MW	2.5 MW
Nominal volume flow	10.5 m/s^3	10 m/s^3
Nominal speed	375 rpm	333 rpm
Outlet diameter	1.33 m	1.39 m

The pressure measurements were carried out alongside efficiency measurements of the turbines. For both turbines, five operating points were investigated; 50%, 70%, 90%, 100% (BEP) and 110% load. The pressure sensors were mounted evenly spaced in one plane located $0.27D_2$ downstream the the runner outlet as shown in Figure 4.8. The data were sampled at five different sampling rates of 100 Hz, 500 Hz, 1kHz, 1.5 kHz and 2.5 kHz to investigate the sampling rate influence on the sampled signal. Each measurement series were 500 seconds. Pressure sensor data can be found in Table 4.7.

Table 4.7: Pressure sensors at Øvre and Nedre Leirfoss HPP

Pressure sensor	Location	Range
PTX610	Sensor 1	0-2.5 bar a
PTX610	Sensor 2	0-2.5 bar a
PTX610	Sensor 3	0-2.5 bar a
PTX610	Sensor 4	0-2.5 bar a

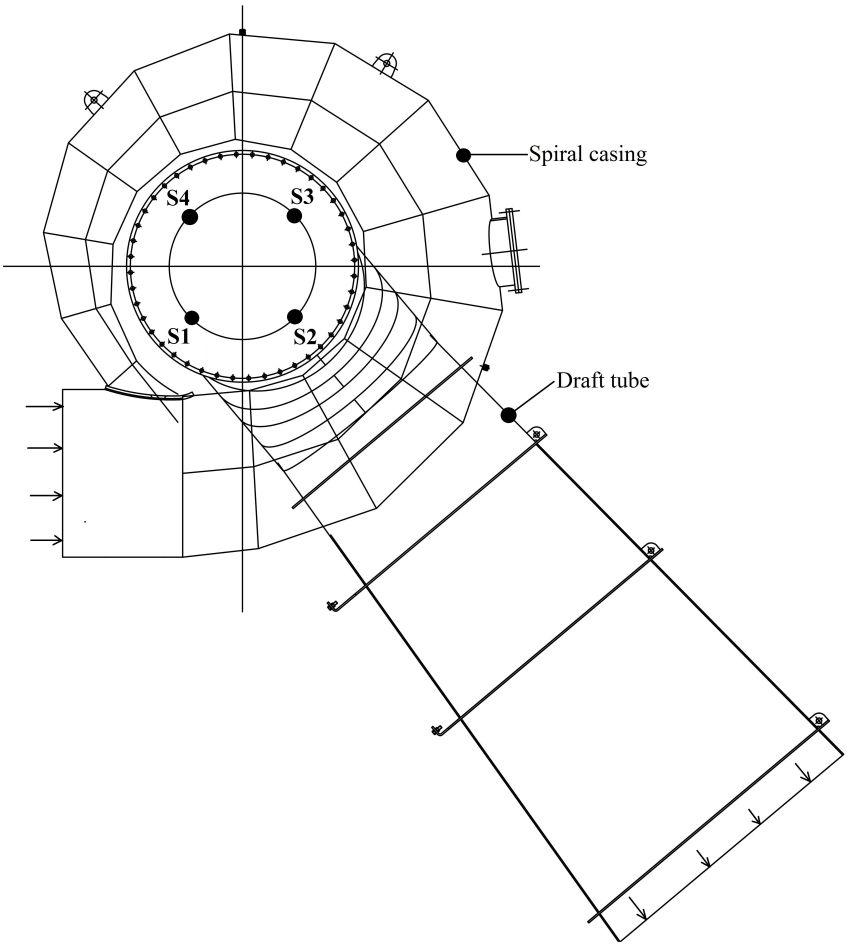

Figure 4.8: Pressure sensor locations at Øvre Leirfoss HPP

4.2.3 Leirfossene hydropower plant

Leirfossene HPP is located by Nidelva in Trondheim. It contains two vertical axis Francis units, both with air injection. The air injection system was installed to reduce the pressure pulsations. The system has been optimized for part load and is controlled by the guide vane opening. The smallest unit, turbine 2, was used for measurements in this thesis. The first measurement series without FRUCE was carried out in May 2016, while the three last series with FRUCE were carried out in the beginning of September 2016. Data for Unit 2 is given in Table 4.8.

Table 4.8: Data for Unit 2 at Leirfossene HPP

Leirfossene HPP	
Nominal net head	58 m
Rated generator output	16 MW
Nominal volume flow	30 m/s^3
Nominal speed	333 rpm
Outlet diameter	1.88 m
Runner blades Unit 2	11
Guide vanes Unit 2	24

Pressure measurements

The pressure measurements were performed with eight pressure sensors mounted at the draft tube . The sensors were mounted in pairs 180° apart in four planes as shown in Figure 4.9 and 4.10. DT 1 was mounted in the inner section of the bend as shown in Figure 4.9. DT 3, DT 5 and DT 7 was mounted directly below DT 1 as shown in Figure 4.10. DT 1, DT 3, DT 5 and DT 7 is referred to as the odd side off the draft tube. While the other side containing DT 2, DT 4, DT 6 and DT 8 is referred to as the even side as shown in Figure 4.10. The even numbered sensors were mounted closer to the outer section of the bend as shown in Figure 4.9. Pressure sensor data can be found in Table 4.9.

The pressure signals were obtained with a logging card which included a antialiasing filter which gave an alias free bandwidth up to $0.453 f_s$, where f_s is the sampling rate.

The pressure sensors were connected to a separate logging system from the efficiency measurements. Two separate logging series of 300 seconds each

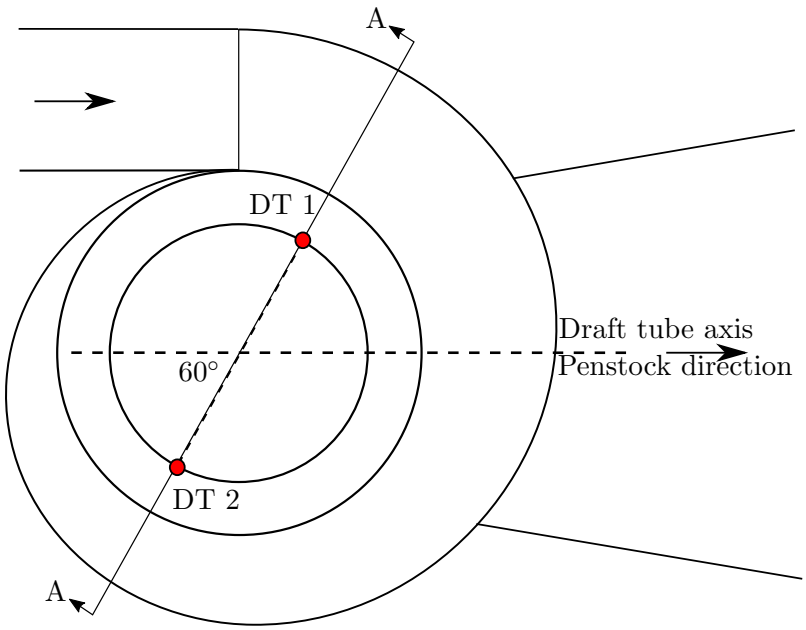

Figure 4.9: Cross section of the draft tube from Leirfossene seen from above.

were obtained for each operational point with a logging frequency of 2 kHz.

Efficiency measurements

Leirfossene has a head of only 58 m, as mentioned in Table 4.8. This is less than 100 m head which IEC 60041 recommend as a lower limit for use of the thermodynamic measuring method. However, under highly favourable conditions, the range can be extended to cover lower heads.

The inlet temperature measurement was done with a probe inserted in to the main flow upstream the spiral casing. A Seabird SB38 temperature sensor was used to measure the temperature at the inlet with an accuracy of $\pm 0.001°C$. The temperature sensor was thoroughly insulated to eliminate external influence. It was only possibly to insert the probe approximately 230 mm into the main flow due to the position of the butterfly valve upstream.

The temperature measurement at the outlet was carried out with a frame and three temperature sensors located as shown in Figure 4.11. Each level of the frame guided water from 10 different positions in the horizontal plane

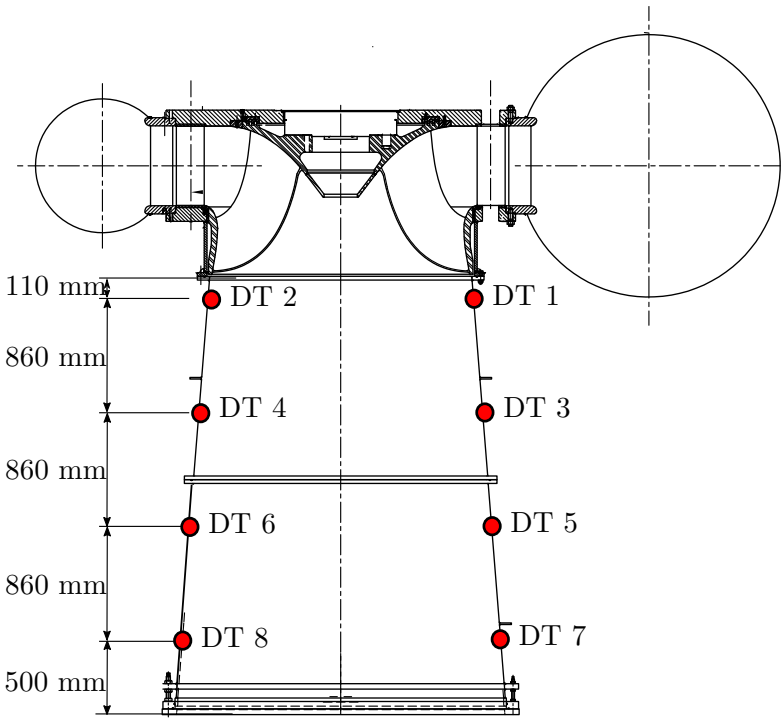

Figure 4.10: Vertical cross section of the draft tube in Leirfossene HPP. The cross section is marked as A-A in Figrue 4.9. DT 1-8 marks the eight pressure sensors located in the draft tube.

Table 4.9: Pressure sensors at Leirfossene HPP

Pressure sensor	Location	Range	Logging frequency
PTX1830	DT1	0-5 bar a	2000 Hz
PTX1830	DT2	0-5 bar a	2000 Hz
PTX1830	DT3	0-5 bar a	2000 Hz
PTX1830	DT4	0-5 bar a	2000 Hz
PTX1830	DT5	0-5 bar a	2000 Hz
PTX1830	DT6	0-5 bar a	2000 Hz
PTX1830	DT7	0-5 bar a	2000 Hz
PTX1830	DT8	0-5 bar a	2000 Hz

to the temperature sensors. The temperature sensors were all Seabird SB38.

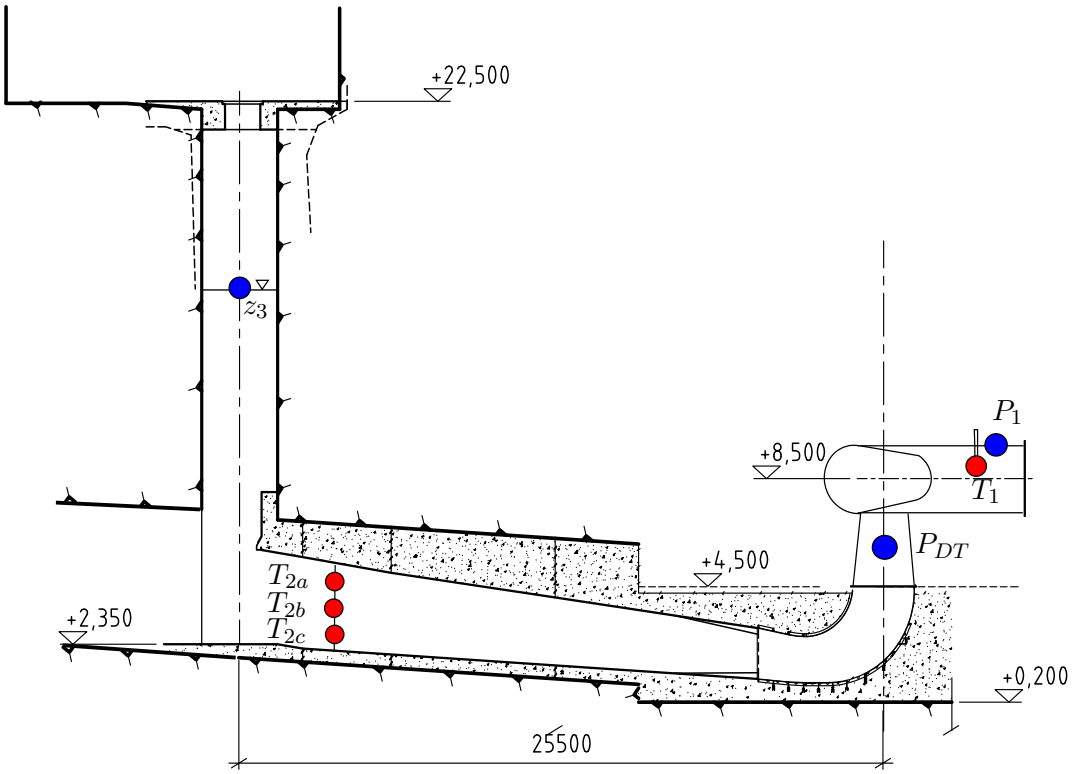

Figure 4.11: Location of temperature sensors at Leirfossene HPP

The inlet pressure were measured with a PTX610 0-10 bar absolute sensor

located in the same cross section as the temperature sensor. The atmospheric pressure was measured with a PTX610 0-2.5 bar absolute sensor. Sensor data can be found in Table 4.10.

The leakage water was lead into the draft tube, so no measurement of leakage water was carried out.

Table 4.10: Sensors at Leirfossene HPP

Sensor	Location	Range	Logging frequency
Seabird SB38	Inlet	-5 - +35 °C	0.3 Hz
Seabird SB38	Outlet 1	-5 - +35 °C	0.3 Hz
Seabird SB38	Outlet 2	-5 - +35 °C	0.3 Hz
Seabird SB38	Outlet 3	-5 - +35 °C	0.3 Hz
PTX610	Inlet	0 - 10 bar a	2000 Hz
PTX610	Temp. probe	0 - 10 bar a	2000 Hz
PTX610	Atm	0 - 2.5 bar a	2000 Hz

In total nine operational points was investigated, where 13 MW (81% of nominal load) was a repetition point. An overview of the operational points is given in 4.11. Measurements with air injection was also carried out for the two lowest loads. Pressure and temperature was logged for 15 minutes minimum for the efficiency measurements.

Table 4.11: Operational points for Leirfossene HPP

Nominal load [%]	Load [MW]	Air injection
47	7.5	on
56	9.0	on
66	10.5	off
75	12.0	off
81	13.0	off
91	14.5	off
100	16.0	off
106	17.0	off

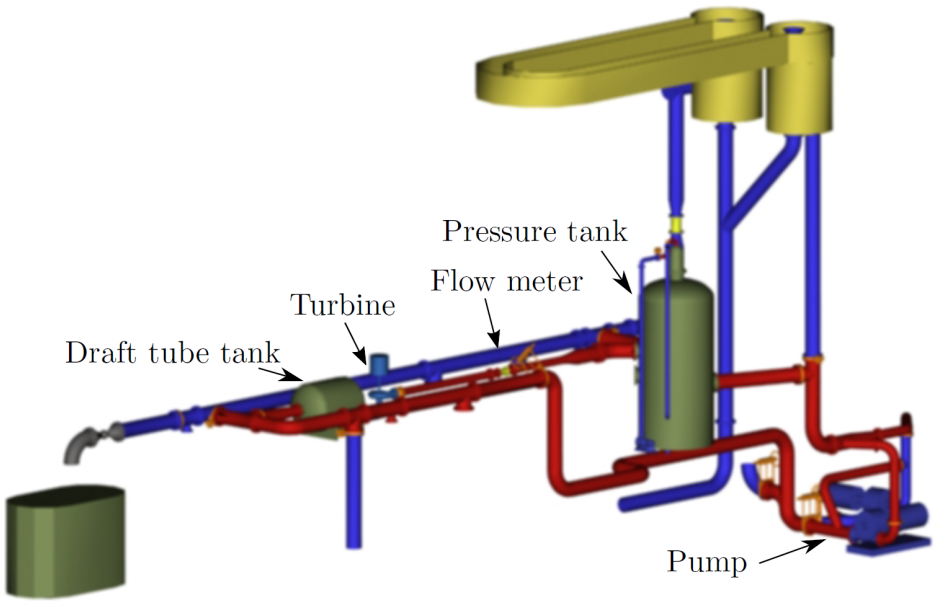

Figure 4.12: Overview of the Waterpower Laboratory. The closed loop used for the measurements is marked in red.

4.3 Laboratory measurements

The Waterpower Laboratory is located in Trondheim at the Norwegian University of Science and Technology (NTNU). It has been a research facility for hydraulic machinery since it was built in 1917. The laboratory was refurbished in 2001 to further meet the increasing demand in turbine performance improvement research. The Francis test rig certified to IEC 60193 *Hydraulic turbines, storage pumps and pump-turbines - Model acceptance testes* [65], enabling performance guarantee tests of Francis and pump turbines.

The measurements at the Waterpower Laboratory were carried out in a closed loop configuration as shown in red in Figure 4.12. The water is supplied by one of the two 287 kW variable speed pumps located in the basement. The water flows through the pressure tank and the flow meter before entering the turbine. Downstream the draft tube, the draft tube tank is used to regulate the submergence of the runner. From there the water is returned to the pumps.

The runner cone extension was designed for the Francis model runner at the Waterpower Laboratory. Pressure measurements were performed with and

without runner cone extension to investigate the impact on the flow. The Francis-99 model runner, which is a high head Francis runner, was used for the experiments. This turbine is also the model runner used as a reference in Francis-99 workshops [19]. Turbine data can be found in Table 4.12. The test was carried out with constant head of 12 m and constant rotational speed of 333 rpm.

Table 4.12: Turbine data for Francis model runner

Francis model runner	
Operating Head	12 m
Runner blades	15 + 15 (splitter blades)
Guide vanes	28
Speed number	0.27 [-]
Inlet diameter	0.63 m
Outlet diameter	0.349 m
Runner inlet height	0.06 m

In total five different test series were carried out including the original design, three FRUCEs and a locked runner cone extension. The FRUCEs are hereafter referred to as mFRUCE. The different FRUCEs are shown in Figure 4.13, where the free rotating part is shown in red. The lengths of FRUCEs were; mFRUCE S = $0.62D_2$, mFRUCE M = $0.86D_2$ and mFRUCE L = $1.20D_2$, where D_2 is the outlet diameter. The locked runner cone extension had the same length as mFRUCE L; $1.20D_2$. NI Labview was used to acquire the data. The different operating points are shown in Table 4.13.

Pressure measurements were carried out with four Kistler 701A dynamic pressure sensors, flush mounted as shown in Figure 4.15. Two sensors were mounted in each plane, directly opposite to each other. Additional pressure sensors were mounted at inlet and downstream the runner cone. The pressure data was amplified and acquired with a logging frequency of 2777.8 Hz with NI 9239 logging card. The logging card provide an alias free bandwidth up to $0.453f_s$.

The efficiency was calculated from the measured pressure, torque, rotational speed and volume flow. Temperature of the water was also measured to calculate the correct density of water.

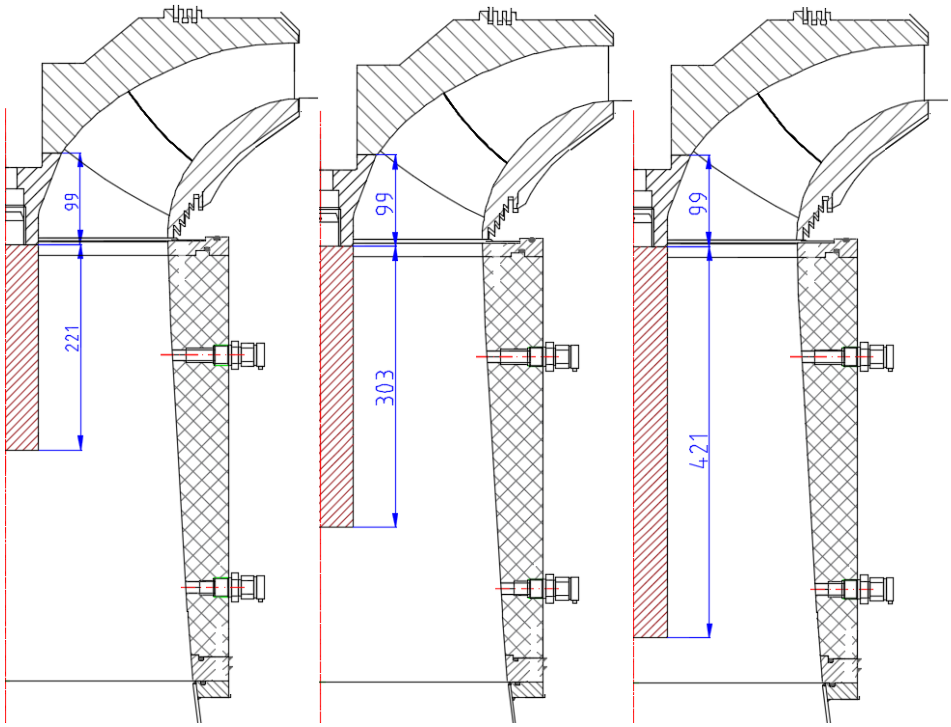

(a) FRUCE 1 (b) FRUCE 2 (c) FRUCE 3

Figure 4.13: Free rotating runner cone extension tested at the Waterpower Laboratory. The length of the FRUCEs are; mFRUCE S = $0.62D_2$, mFRUCE M = $0.86D_2$ and mFRUCE L = $1.20D_2$. The FRUCE diameter is $0.21D_2$. The rotating part is shown in red. The measurements in the drawings are given in millimetres.

Table 4.13: Operational points for laboratory measurements

Operational points	Guide vane opening [degrees]	Volume flow $[m^3/s]$	Relative Volume flow Q/Q_{BEP} [-]
1	4.00	0.086	0.43
2	5.01	0.106	0.53
3	6.02	0.127	0.63
4	7.03	0.147	0.73
5	8.13	0.169	0.84
6 (BEP)	9.89	0.202	1.00
7	11.03	0.223	1.11
8	12.00	0.241	1.20
9	13.05	0.256	1.29

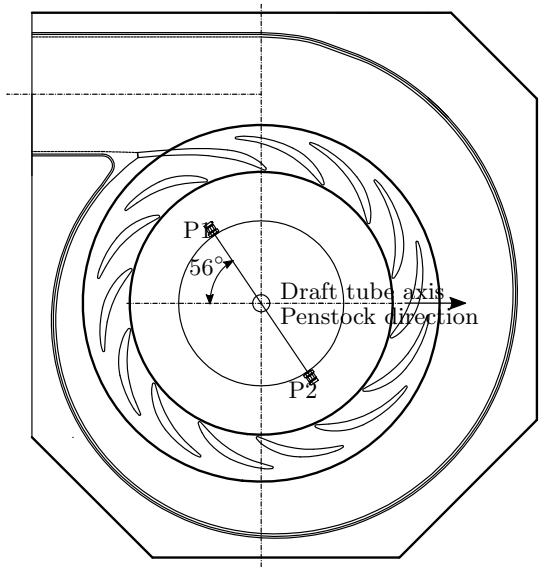

Figure 4.14: Axial position of pressure sensors in the draft tube in the Waterpower Laboratory. Sensor P1 and P3 was located closest to the inlet, while P2 and P4 are located on the opposite side of the draft tube.

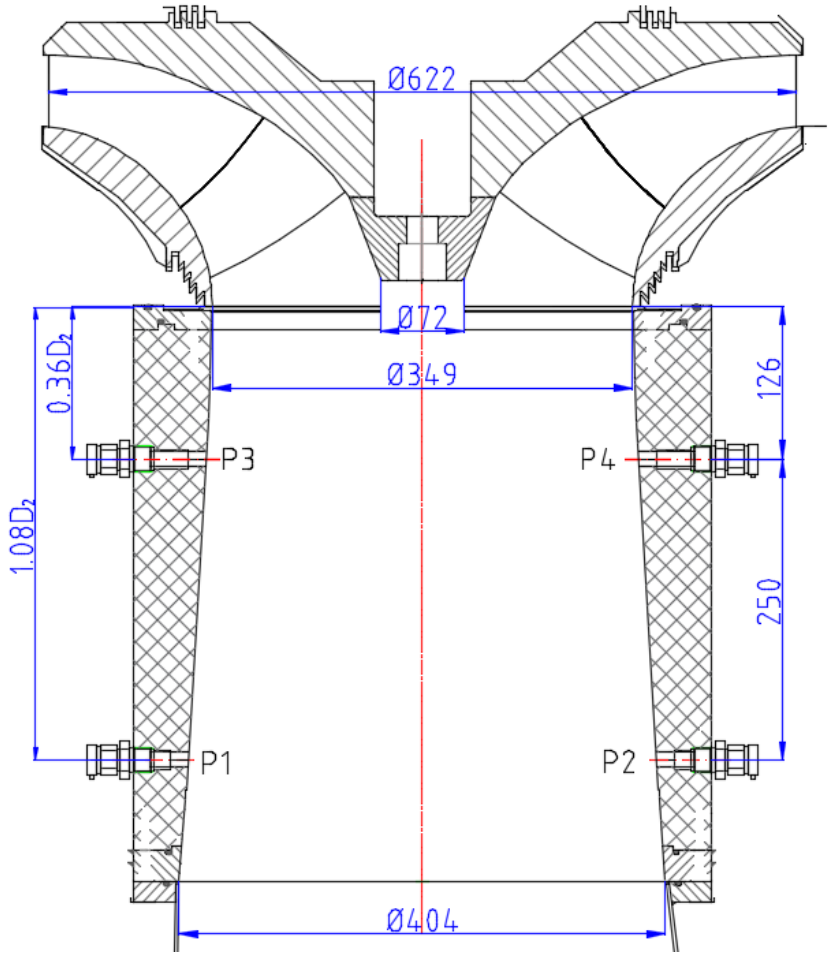

Figure 4.15: Pressure sensor locations at the Waterpower Laboratory. The dimension in the drawing is given in millimeters

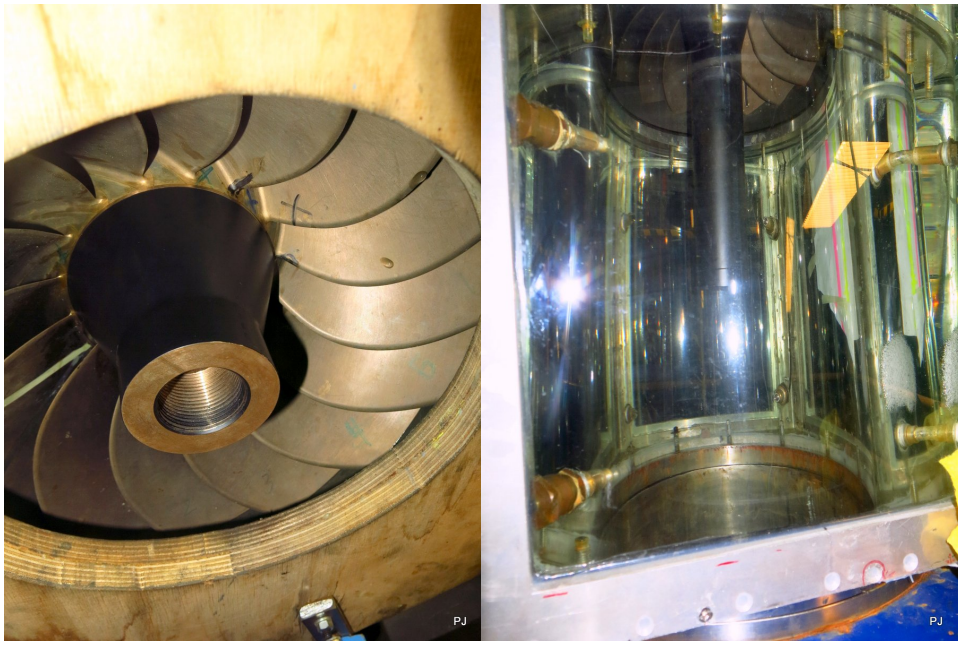

(a) Modified runner cone for FRUCE (b) FRUCE

Figure 4.16: Pictures from the model test at the Waterpower Laboratory. The modified runner cone can be seen to the left, while mFRUCE S mounted to the runner cone can be seen to the right

Chapter 5

Analysis methods

5.1 Pressure measurement analysis

To analyse the pressure fluctuations in the draft tube, several methods have been applied. First an investigation of the average pressure in the different sections of the draft tube has been evaluated. The peak-to-peak values have been obtained using a 99% confidence interval to investigate the magnitude of the pressure fluctuations in the draft tube. Further, the pressure signals have been decomposed to analyse the different frequency components. This was done by obtaining frequency spectra with the Welch method [27, 25, 53].

The pressure fluctuation caused by the rotating vortex rope can again be decomposed into a rotating and a plunging component also known as an asynchronous and synchronous component.

5.2 Amplitude analysis

When investigating the amplitude of a random signal a statistical method is needed to obtain unambiguous results. In general, two methods are used; rms or peak-to-peak values. In this thesis the a peak-to-peak method is chosen to evaluate the amplitudes of the signals. The peak-to-peak values give an impression of the pressure pulsation amplitudes independent of the frequencies occurring in the system.

The IEC 60193 [65] suggests to define the amplitude as the variation which contains a certain percentage of the sample. A Probability Density Function

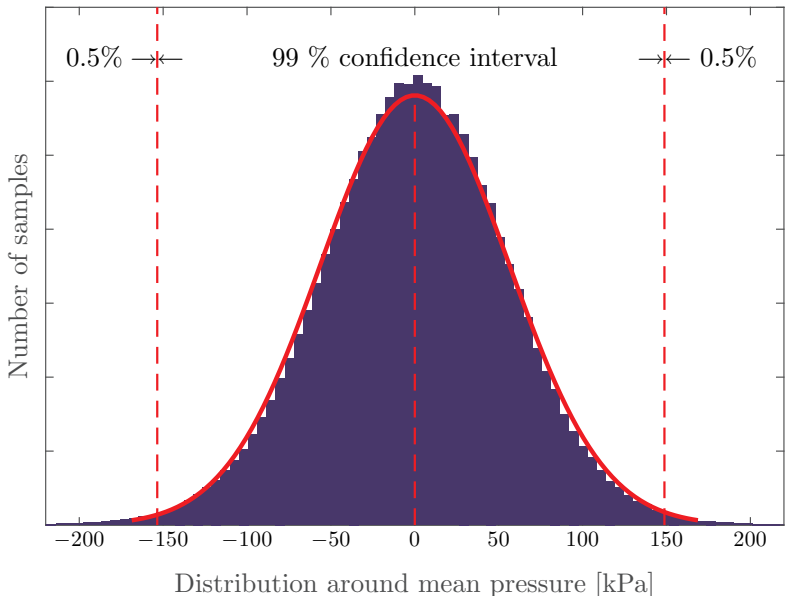

Figure 5.1: Probability density function curve for a time series is shown in red and actual values from the time series is seen in purple. 99% confidence interval is shown between the dashed lines.

(PDF) was therefore applied to find the peak-to-peak values of the pressure signal [14]. The peak-to-peak values will depend on the percentage level chosen. Figure 5.1 show the PDF with a 99% confidence interval which was chosen [14]. The IEC 60193 suggests 97% in a footnote, but is rather non-committal. A comparison of different percentage level is shown by Dörfler et al. [13]. As for the laboratory results, the signal was filtered and the effective confidence interval will therefore be less than 99%.

5.3 The Welch Method

The Welch method was chosen because it is known to give a good approximation of the frequency amplitudes [25]. The method is well described in Heinzel et al. [27], Harris [25] and Proakis and Manolakis [53]. The Welch method returns the periodogram spectrum density (PSD) which is a statistical estimate of the power in different frequencies of a signal. The method divides the sampled data into overlapping sections. A process called win-

dowing is then applied to the sections before computing their Fast Fourier Transform. Windowing reduces spectral leakage in the transformation. The result is averaged over the sections and returned as PSD.

5.4 Discrete Fourier Transform

The fast Fourier transform is an algorithm which computes the discrete Fourier transform (DFT) of a sequence or its inverse. The method is named after M. Fourier and his work on heat propagation [20]. Applying the FFT to a time domain signal, $f(t)$, the signal is converted into the frequency domain $F(\omega)$. The method allows to identify the different frequency components of a time signal, which otherwise would be impossible to distinguish. The Fourier transform is defined in equation 5.1 [27, 25] .

$$F(\omega) = \int_{-\infty}^{+\infty} f(t)e^{-j\omega t}dt \tag{5.1}$$

When applied the signal is discrete with a sampling frequency of $1/T$. A finite approximation must therefore be used as shown in equation 5.2, where nT is the sample time and N is even [25].

$$F(\omega) = \sum_{-N/2}^{+N/2} f(nT)e^{-j\omega nT} \tag{5.2}$$

5.4.1 Windowing

The FFT implicitly assumes that the signal is periodical with a whole oscillation period or multiples of it coinciding with the measurement period [27]. This assumption is rarely true and the data needs to be preconditioned. This is done by a window function which is multiplied with the signal. The window function starts near zero and rises to maximum at the the center of the time series before it decreases towards zero again. Overlapping the windows would seem to be using the same data twice, but the spectral leakage is reduced significantly when windowing is applied. The technique is well described by several authors [27, 25, 28].

Different windows can be applied depending on the nature of the dataset. The Hann window is a well suited for handling trigonometric functions. It weighs the centre values of the sinusoidal rather than the extremities [29]. The extremities creates non continuity when periodic extension of the sequence are made. Reducing the non continuity will reduce the spectral leakage, and in turn the loss in amplitude. The disadvantage is the slightly reduced frequency resolution [27, 28] .

5.4.2 Sampling rate, Nyquist frequency and aliasing

The sampling rate defines how many samples per second which are acquired. This implies that any digital sampling will be discontinuous. The resolution is highly dependent on sampling rate. The Nyquist sampling theorem explains relationship between the minimum sample rate and the frequency of the measured signal as shown in equation 5.3. The sample rate must be twice the highest frequency of interest [27]. This frequency is often referred to as the Nyquist frequency, f_N

$$f_s > 2 \cdot f_N \tag{5.3}$$

Aliasing occurs if the analog signal is sampled with a too low sampling rate relative to the highest frequency in the system. A digital signal will not have an upper frequency component, which means that the aliasing effect will always be present [30]. Oversampling and filtering can be used to reduce the effect of aliasing. Oversampling means sampling with a frequency multiple times the Nyquist frequency. Oversampling is often done to increase the frequency resolution, reduce the effect of aliasing, phase distortion and noise in the measurements. It also reduces the need for filtering.

5.5 Missing data problem

The FFT requires uniform sampling, i.e. constant Δt, to correctly transform the data. In the La Higuera measurement, a logging error occurred. The logging program wrote a file once a second, which led to a small time gaps between each measuring block. Due to the pauses in the logging program, a missing data point problem occurred in the spectral analysis. The constant time step requirement of the FFT was not longer fulfilled.

The increased Δt which occurred every second can be considered as loss of data points. The loss of data points is a loss of information of the physical process. A truncation of the time series before applying the FFT algorithm would cause non-physical and spurious distortion which is seen in the low frequency band. If not all frequencies are known, the spurious errors can not be identified.

A FFT of each measuring block with constant time step could be an option to study higher frequencies. Due to the short length of each block, this will give a far from satisfactory frequency resolution. The relative uncertainty caused by white noise would also increase by this method.

The missing data point problem is well known within geophysics from satellite transmissions. The received satellite signal transmitted is often disrupted by the satellite passing through a transmission shadow. To compensate for the lost data, the least-square spectral analysis was developed [42], commonly known as Lomb normalized periodogram. Instead of weighting data 'per time interval' basis as in FFT, the method weights data on 'per point' basis. This allows for a non-uniform time steps in the time series and avoiding truncation, zero insertion and extrapolation [73]. The drawback of the method is that the computational costs are significantly increased, from less than a second to more than an hour. Another aspect to be aware of is that the Nyquist frequency is not respected by the Lomb normalized periodogram [42, 73]. Hence, frequencies higher than the Nyquist frequency appearing in are disregarded.

Chapter 6

Results and discussion

6.1 La Higuera

Measurements from La Higuera showed a dampening in pressure fluctuations when air was injected. However, the pressure pulsation amplitudes related to rotating vortex rope was not dampened. A small increase in amplitude could be found when air was injected independent of air injection method.

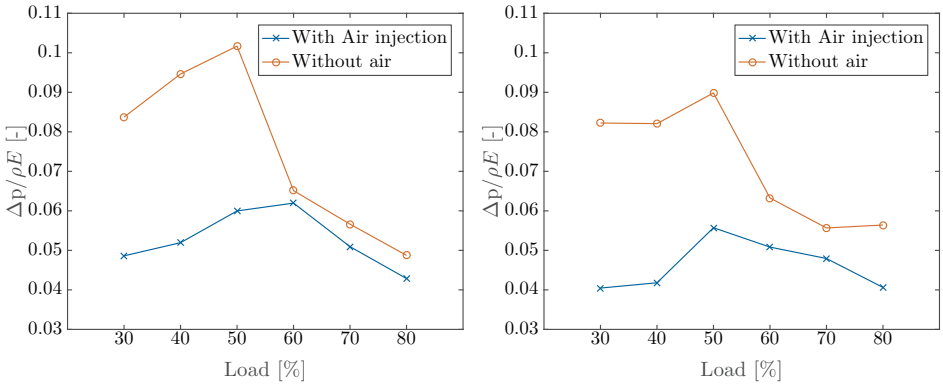

(a) Option A

(b) Option B

Figure 6.1: Peak-to-peak values at La Higuera. The peak-to-peak values are given in % of ρE where $\rho E = 3\ 677$ kPa.

The peak-to-peak values with 99% confidence interval for the two different

air injection options are shown in Figure 6.1. The peak-to-peak values are significantly reduced in both cases. The variation in peak-to-peak amplitudes without air injection is most likely related to difference in operational points and water condition as the measurements were done at separate days.

The highest amplitudes were found at deep part load and this also were the reduction in peak-to-peak values is largest. The maximum amplitudes can be seen for the 50% load for the both with and without air injection. There is a significant change in peak-to-peak amplitudes from 50% to 60% load and the dampening effect of air injection is relatively small. This is normally an operational range where the rotating vortex rope is present.

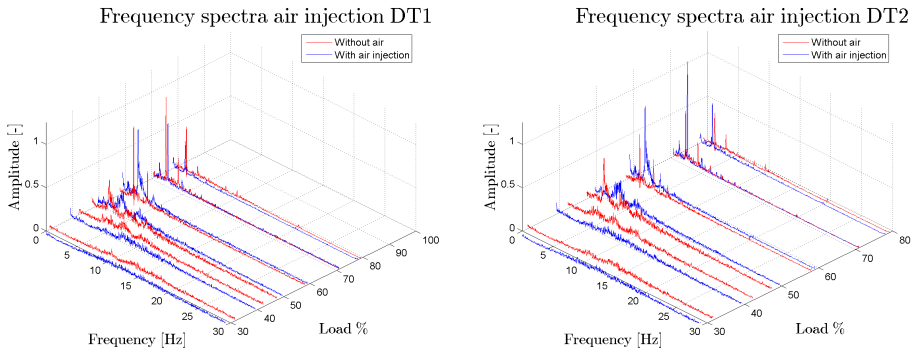

(a) Sensor 1 (b) Sensor 2

Figure 6.2: Frequency spectrum for Option A

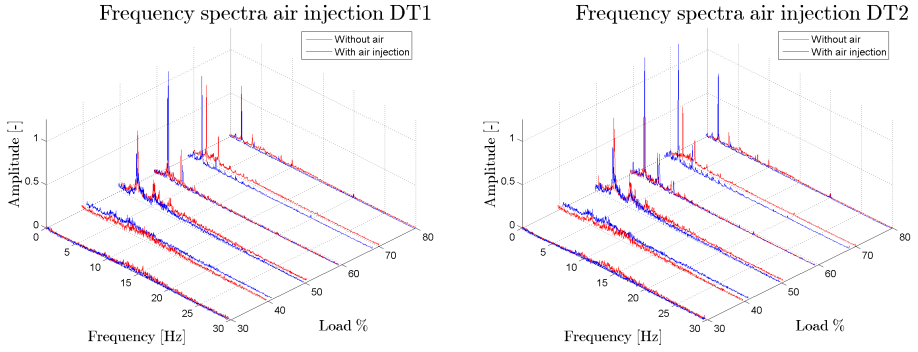

(a) Sensor 1 (b) Sensor 2

Figure 6.3: Frequency spectrum for Option B

As seen in Figure 6.2 and 6.3 the dominant frequency at part load (60-80% P/P_n) was found at 1.2-1.4 Hz, confirming the presence of a vortex rope. These amplitudes of the vortex rope frequency are significantly increased at Sensor 2 when air is injected, while at Sensor 1, minor changes can be observed. The vortex rope frequency is also slightly shifted towards a higher frequency when air is injected.

The frequency spectra clearly show the presence of a vortex rope at high part load (60-80% P/P_n). The air injection is increasing the amplitude of the vortex rope significantly at sensor 2. However, for the same operating range, the peak-to-peak values are reduced with air injection. The air injection does not have a dampening effect on the vortex rope frequency in this case.

For the deep part load range (30-40% P/P_n) the vortex rope frequency is not present, but a significant peak-to-peak value reduction is found. This again can be related to dampening of the high frequency range of noise. The vortex rope frequency can be found at 50% P/P_n which can be seen in the test of option B. At this operational point, the amplitude of the vortex rope frequency is reduced by approximately 25% for Option B and not found with air injection for Option A. At 50% P/P_n the air injection seem to have dampening effect also on the vortex rope frequency.

There may be two reasons for not achieving a dampening of amplitudes at the rotating vortex rope (RVR) frequency. The first reason can be that the amount of air injected was to small to dampen the RVR frequency. Previous investigations of air injection shows that the air flow should be about 1.5-2.5% of the turbine discharge [47]. The maximum airflow reached was 2.27% of the water flow rate, but in most cases it was less than 1.8% of the flow rate. Second, the air injection may not work on dampening large slow pulsations as the RVR frequency. The results showed a dampening of the frequencies of higher amplitude, reduced noise, and reduced peak-to-peak values. Different means might be needed to reduce the RVR amplitudes.

6.1.1 Efficiency measurements

The efficiency measurements were carried out at later stage than the pressure pulsation measurements. The pressure measurements were carried out at Unit 1 in the first measurement series and therefore only two measurement points with air injection at Unit 1 were carried out as seen in Figure 6.4.

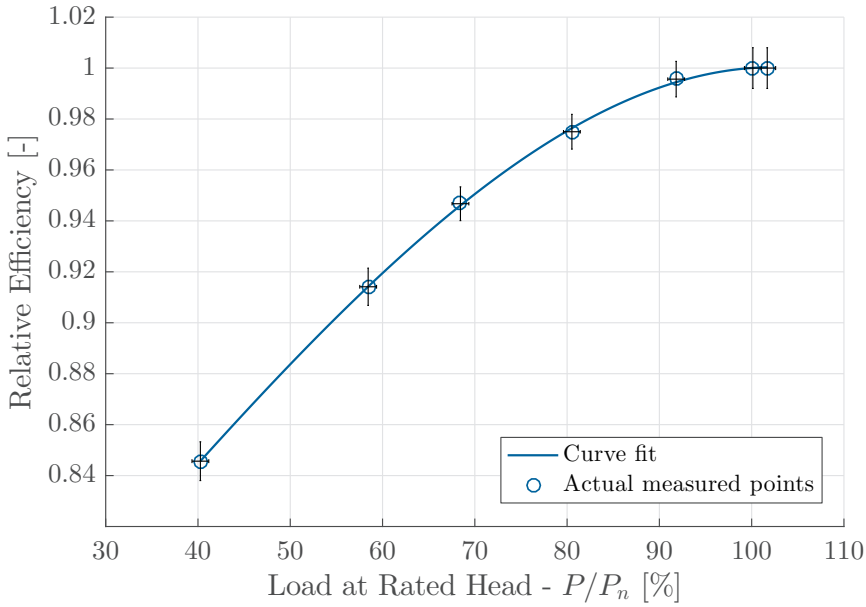

Figure 6.4: Efficiency of Unit 1 La Higuera HPP. The two points in red are with air injection.

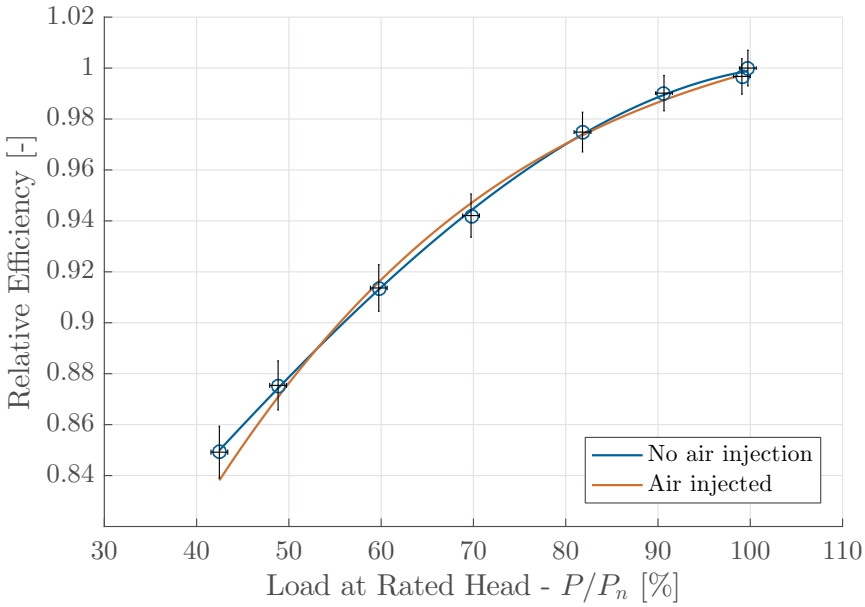

Figure 6.5: Efficiency of Unit 2 La Higuera HPP. The measured operating points without air injection are shown in black with uncertainty

The efficiency measurement at Unit 2 were carried out with and without air injection as shown in Figure 6.5. The efficiency with air injection is well within the uncertainty of the measurements done without air injection except for the lowest measured load. No significant reduction in efficiency was found when air was injected. As the amount of air injected is very small in comparison to the turbine discharge, the energy used to compress the air is also small. This energy would be considered as a loss in efficiency.

6.2 Nedre Leirfoss and Øvre Leirfoss

Draft tube pressure pulsation measurements was carried out for both Øvre and Nedre Leirfoss. A summary of the results are presented here, while the details can be found he attached papers in chapter II.

6.2.1 Nedre Leirfossen

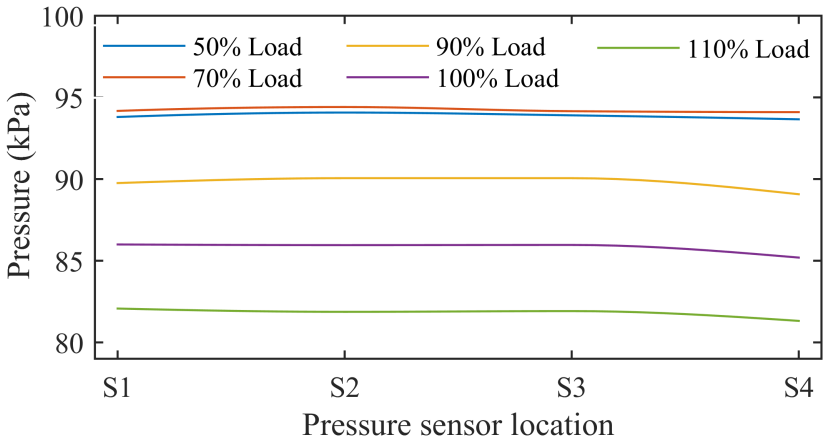

Figure 6.6: Average draft tube pressure at Nedre Leirfoss

The pressure measurements were carried out at 50%, 70%, 90%, 100% and 110% load at steady state conditions. The average pressure was highest at 50% and 70% load as seen in Figure 6.6, while it decreased with increasing load for the other operational points. The fluctuations in pressure was largest at 50% and 70% load where the standard deviation was 4.2 kPa and 5.4 kPa respectively. Further investigation showed that the full scale pressure pulsations were around 5.5% of ρE at 50% and 70% load, where

ρE = 247.27 kPa. For 100% and 110% load, the pressure pulsations was around 1% of ρE.

A signal-to-noise-ratio (SNR) was performed to distinguish pressure pulsations related to flow phenomena from random noise. The estimated SNR for 70% load was found positive, indicating the vortex rope frequency amplitude was greater than the noise, i.e. significant vortex rope effects.

The frequency spectra in Figure 6.7 show a significant amplitude for the vortex rope frequency at 70% load. The normalized frequency was found to be 0.24 (f=1.35 Hz) with magnitude approximately 2% of ρE. At 50% load the vortex rope frequency is also dominant, but the magnitude is less than 0.3% of ρE. The dominant frequency at other loads was the runner frequency with amplitude less than 0.006% of ρE.

The synchronous and asynchronous component at 70% load was further investigated by using S1 and S3, which are sensors mounted on opposite sides of the draft tube. The spectral analysis of the sensors are shown in Figure 6.8. The asynchronous component was found dominating for the frequency at 0.24 of the runner frequency, while the harmonic at 0.48 of the runner frequency was dominated by the synchronous component.

6.2.2 Øvre Leirfoss

The pressure measurements were carried out at 50%, 70%, 90%, 100% and 110% load at steady state conditions. The highest average pressure was found at 70% load as shown in Figure 6.9. The pressure difference between the different loads are in order of 1-2 kPa, except for the average pressure 110% load which is 6 kPa lower than 100%. The average pressure also significantly lower at S3 and S4. This is because the turbine is a horizontal axis turbine and these sensors are mounted above the horizontal plane passing through the turbine as shown in Figure 4.8.

The maximum standard deviation was in this case found at 50% load (6.7 kPa), followed by 70% load (5.1 kPa). The standard deviation was found to be higher at S1 and S2, indicating higher pressure pulsations at these locations. The spectral analysis is shown in Figure 6.10 for the different loads. The frequencies are normalized by the runner speed (6.25 Hz) and amplitudes are normalized by reference pressure at BEP, ρE = 319.9 kPa. At 50% load the dominating frequency is 0.16 with an amplitude of 0.1 of ρE. This may be related to the vortex rope frequency, but it has lower frequency

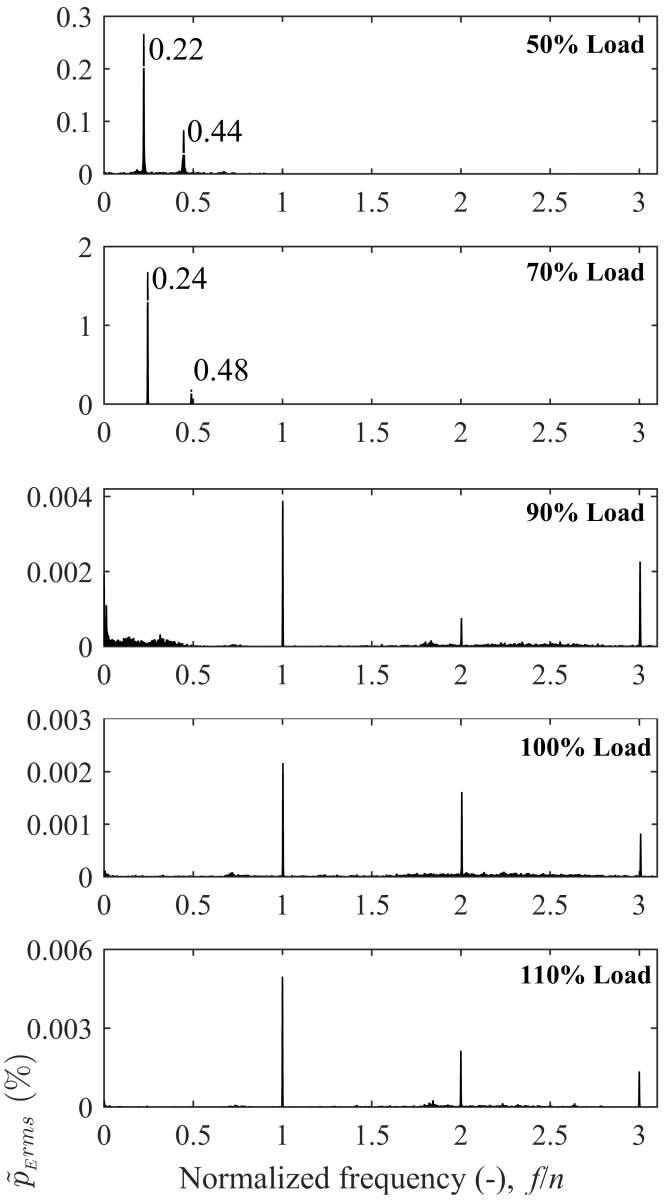

Figure 6.7: Spectral analysis of the time-series at the location S1 for the measured loads. The runner frequency, n, is 5.55 Hz. Note the different scale on the y-axis.

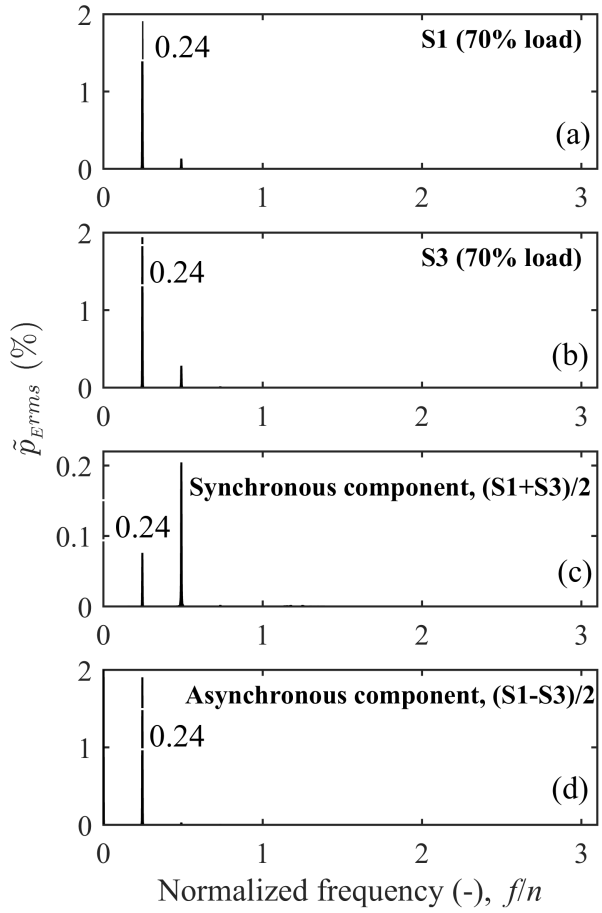

Figure 6.8: Synchronous and asynchronous component at 70% load

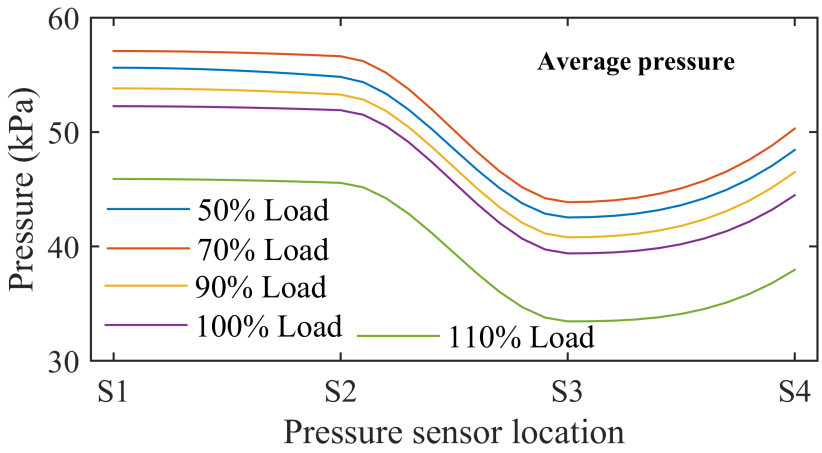

Figure 6.9: Average draft tube pressure at Øvre Leirfoss where S1, S2, S3 and S4 are the different pressure sensors. S3 and S4 are mounted above the horizontal plane as seen in Figure 4.8

than usually seen for the vortex rope. At 70% load the dominant frequency was found at 0.27, which corresponds to the vortex rope frequency. The amplitude is observed to be 0.3% of ρE, which was the highest amplitude found at Øvre Leirfossen. Prominent frequencies at 0.25 and 0.28 was also observed at 90% and 110% respectively, but both loads has an amplitude less than 0.04% of ρE.

The asynchronous and synchronous component were further investigated at 70% load as shown in Figure 6.11. The frequency at 0.27 corresponds to the vortex rope frequency at 1.68 Hz. In this case the synchronous component was found as the dominating with amplitude at 0.3 of ρE. The asynchronous component was only 0.15 of ρE.

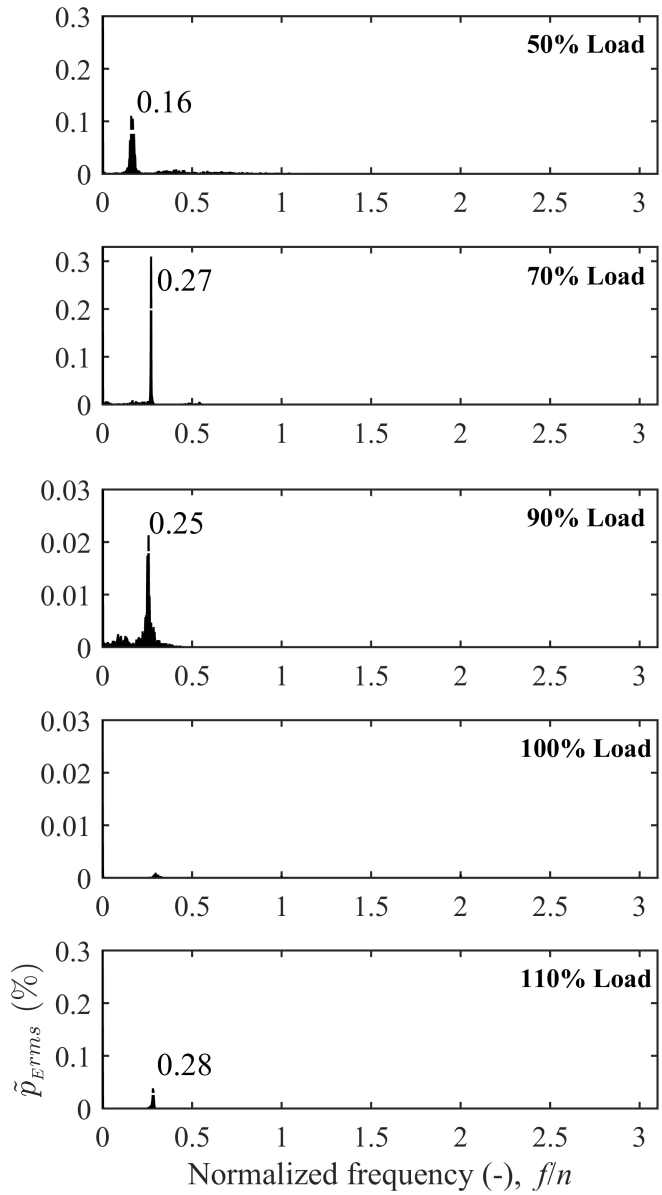

Figure 6.10: Spectral analysis of the time-series at the location S1 for the measured loads. The runner frequency, n, is 6.25 Hz. Note the different scale on the y-axis.

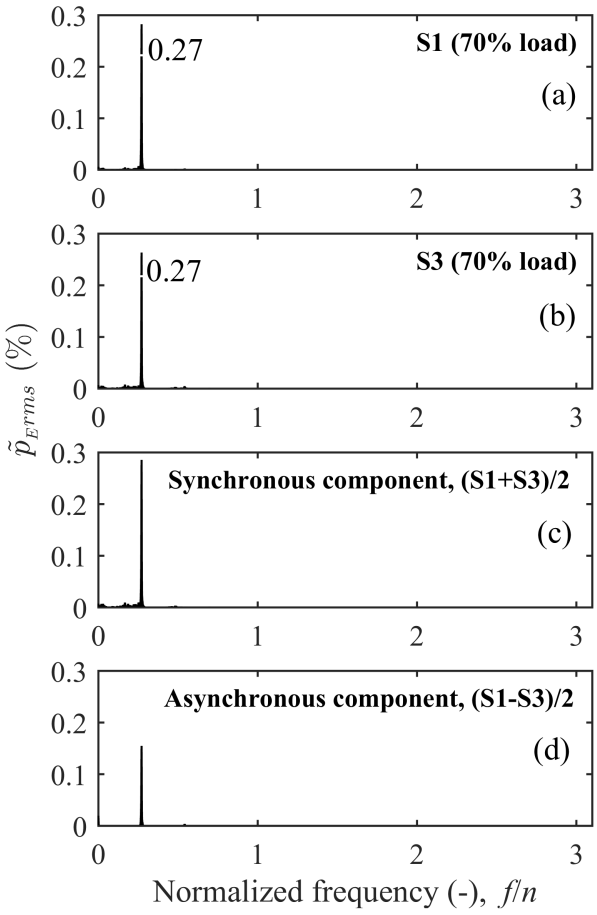

Figure 6.11: Synchronous and asynchronous component at 70% load at Øvre Leirfoss

Both Øvre Leirfoss and Nedre Leirfoss have a low head Francis turbine, but pressure pulsation amplitudes are significantly higher in Nedre Leirfoss compared to Øvre Leirfoss. Both turbines has the same manufacturer, but still they perform differently. The results show the synchronous component is stronger in the horizontal axis turbine, indicating this component has a larger influence on the horizontal axis turbine than the vertical axis turbine. The small asynchronous component is indicating the vortex rope is closer to the draft tube centre. There is also a pressure difference from the upper to the lower side of the draft tube due to the fact that the draft tube starts out in a horizontal direction. This may also be influencing the pressure pulsations together with gravity. As for Nedre Leirfoss which has a vertical axis, the peak-to-peak values reaches over 5% of ρE

6.3 Laboratory results

6.3.1 Efficiency

The calculated relative efficiency for the different tests performed in the Waterpower is shown in Figure 6.12. The uncertainty of the efficiency measurements are in the area of $\pm$ 0.2-0.3%, so the deviation in efficiency are not very large, but some trends can still be found. The original design has the best efficiency at full load, while the FRUCE L increases the efficiency at part load. mFRUCE S and M have lower efficiency than the original design in most cases, but the difference is insignificant at part load. It seems that the FRUCE length is important for the efficiency as the FRUCE has the highest efficiency at part load. Overall, the longer the FRUCE, the better the efficiency. Another interesting observation is that mFRUCE L and the locked extension has the same efficiency at BEP and full load.

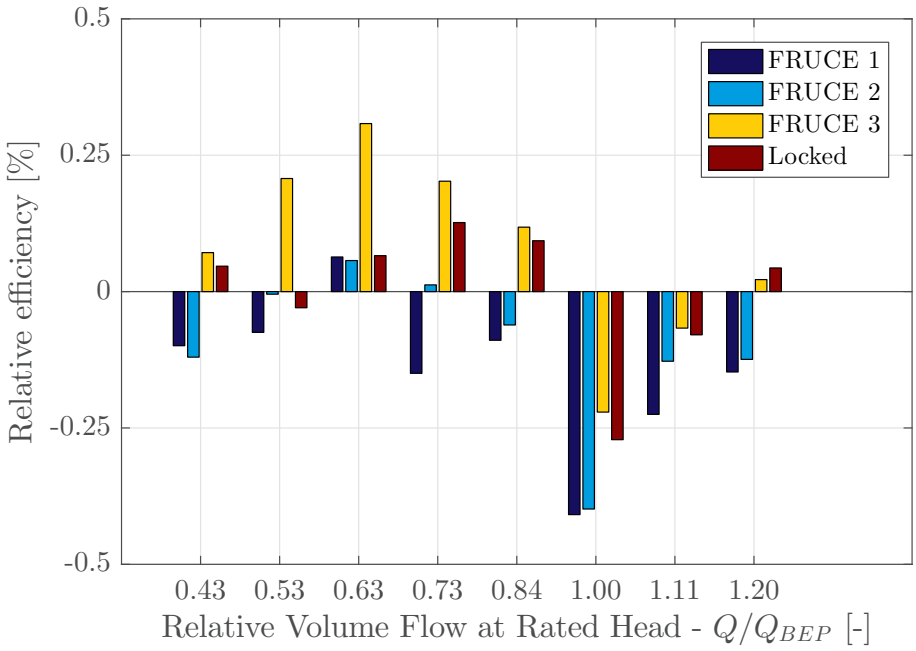

Figure 6.12: Relative efficiency for the different test cases carried out at the Waterpower Laboratory. The efficiency for the original design is 0, so a positive bar indicates increased efficiency and a negative bar indicates reduced efficiency.

The differences in efficiencies are not large, but on the border of the uncertainty within the measurements. The results indicates that the efficiency at high load may be reduced as a consequence of the FRUCE, while at part load it may increase. The increased friction due to the FRUCE can explain the reduced efficiency calculated at high load. The mFRUCE L should than have the lowest efficiency, but the shorter FRUCEs was found to decrease the efficiency more. However, Vekve [74] also found efficiency increases with a locked runner cone extension and longest extension had the highest increase. The increased efficiencies a part load may be a consequence of reduction of reverse flow in the draft tube center and suppression of the RVR.

6.3.2 Velocity measurements

The rotational speed of the FRUCE was measured optically as shown in Figure 6.13. The rotational speed of the FRUCE is given by n_c, while n_t is the rotational speed of the turbine. The rotational speed is in the negative direction for flows higher than Q_{BEP}, meaning the FRUCE is rotating in the opposite direction of the runner. The velocity of the FRUCEs seem to follow a linear relationship between 0.84-1.29Q/Q_{BEP}. The highest negative velocity, at -1.08 (360 rpm), is found at the largest volume flow. The longest FRUCEs reaches a higher negative velocity than the shortest FRUCE. This indicates that full load swirl has a higher rotational speed further downstream in the draft tube. The FRUCE velocity at BEP is approximately 0, indicating there is almost no swirl in the discharge from the runner. At 0.76Q/Q_{BEP} all the mFRUCEs rotates with the same velocity as the runner. When moving towards part load, the volume flow is reduced, and so is the rotational velocity of the FRUCEs. The velocity of mFRUCE S is 9% lower than the runner at lowest load, while mFRUCE L is rotating with 50% lower velocity than the runner. The reduced velocity of the longer FRUCEs indicates that the tangential velocity is reduced further downstream in the draft tube, thereby reducing the velocity of the FRUCEs.

6.3.3 Pressure pulsations

The pressure-time signal was filtered with a zero phase distortion bandpass filter from 0.09-2.16f_n. This was done to remove some rig specific reflection frequencies around 2.5f_n.

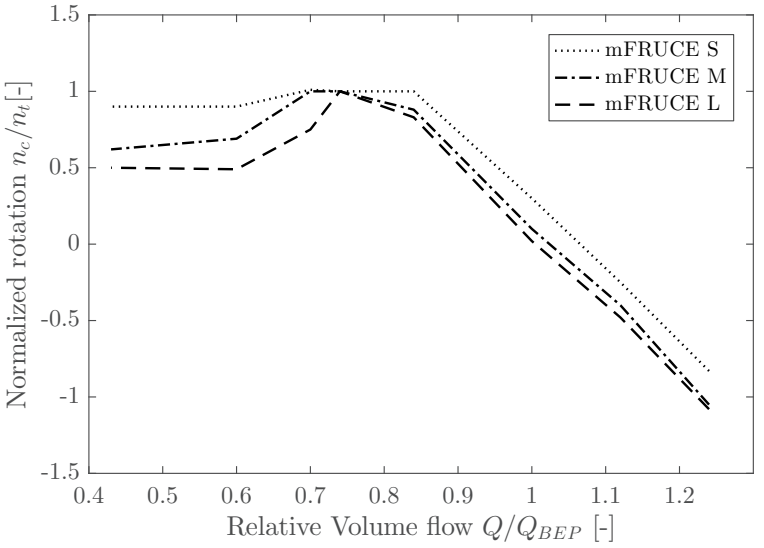

Figure 6.13: Normalized rotational speed for the different FRUCEs. Positive rotation is in the same direction as the runner. The runner speed was 333 rpm.

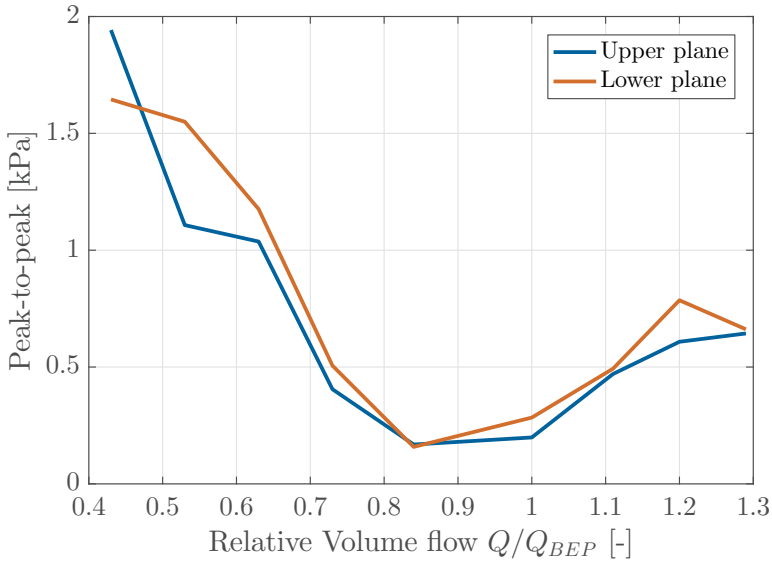

Figure 6.14: Peak-to-peak values for the Francis model runner without FRUCE. A 99% confidence interval has been applied to find the peak-to-peak values for the upper and lower plane.

As seen from 6.14 the highest peak-to-peak values are found at deep part load for the original design. The lowest peak-to-peak values are as expected around BEP, while they increases towards high load. The peak-to-peak values are somewhat higher in the in the lower plane than in the upper plane.

At $0.43Q/Q_{BEP}$ the peak-to-peak values are increasing with length in both plane for the FRUCEs. In the upper plane the peak-to-peak values are reduced 3-10% compared to the original. In the lower plane the differences are smaller. At $0.53Q/Q_{BEP}$ the peak-to-peak values are decreasing with the length of the FRUCE. Though the peak-to-peak values are all higher in the upper plane compared to the original, there is significant reduction in the lower plane for mFRUCE M and L.

At loads above BEP, mFRUCE M is in general the best with significantly lower peak-to-peak values than the original. The locked extension has similar peak-to-peak values at high load.

The FRUCEs only reduce the peak-to-peak values at some operational points. They seem to have minor or negative effect on the peak-to-peak values at the lowest load. This may be because of the swirl number is too high or the FRUCE diameter is too small. At high load, the peak-to-peak values seem to be very sensitive to the FRUCE length.

Based on the peak-to-peak values, mFRUCE L gives the most promising results at part load for volume flows of $0.73Q/Q_{BEP}$ or less. For high load, mFRUCE M has the lowest peak-to-peak values. The FRUCE length seem to be of high importance at high load operation. To reduce the peak-to-peak values, the FRUCE length should be reduced at high load. However, the locked extension has approximately the same peak-to-peak values as mFRUCE M. So an alternative is to lock the FRUCE for higher loads than BEP. However, at high loads the efficiency is reduced with FRUCE. If hydraulic efficiency is a priority, the FRUCE should be removed at high load.

Figure 6.16, 6.17 and 6.18 show the spectral analysis from the three lowest loads investigated. The dominant frequency of FRUCEs, 031-0.42f_n, is most likely related to vortex rope. The original design also has a prominent frequency in the same frequency range. For the locked extension at $0.43Q/Q_{BEP}$ and $0.53Q/Q_{BEP}$, the dominant frequency is very close to the runner frequency. While at $0.63Q/Q_{BEP}$ the dominant frequency for the locked extension is just slightly higher than for the FRUCEs.

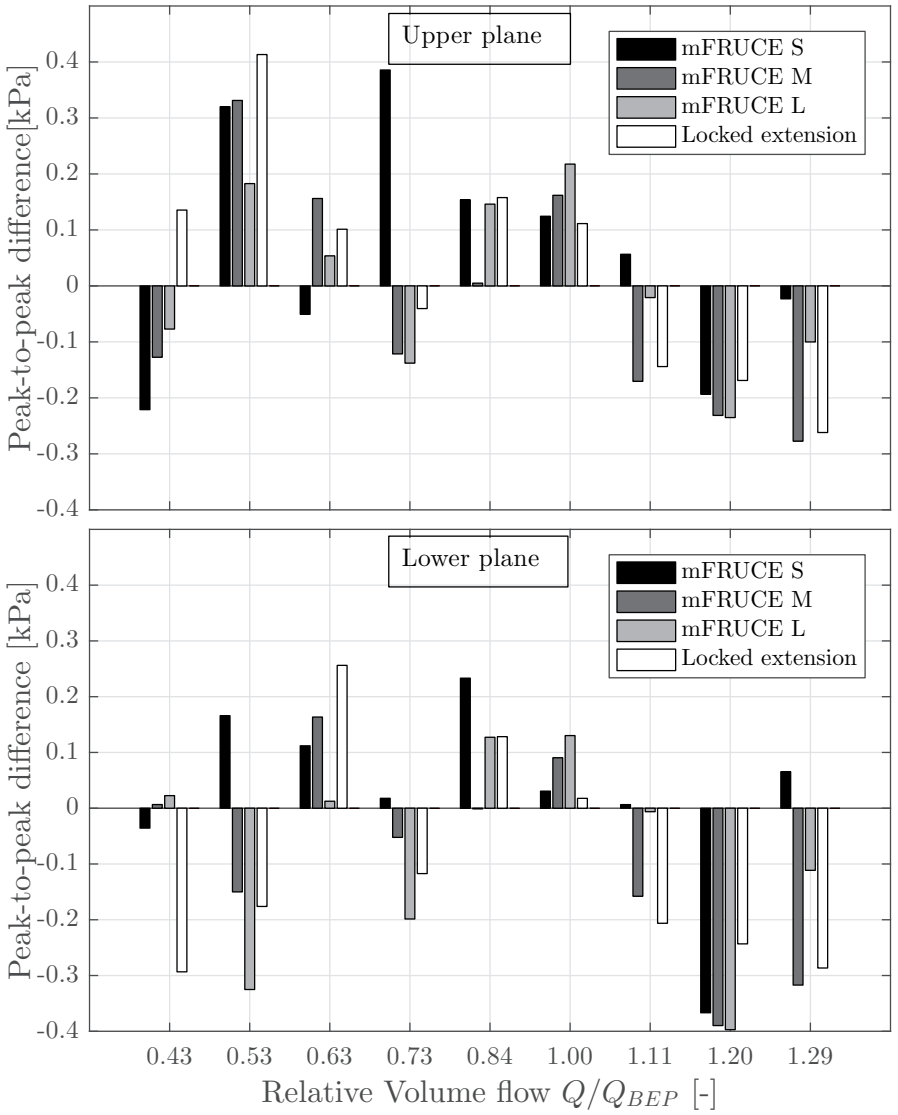

Figure 6.15: Peak-to-peak value differences for the Francis model runner. The peak-to-peak value differences are shown in kPa for the upper (top) and lower (bottom) measuring plane. A 99% confidence interval has been applied to find the peak-to-peak values.

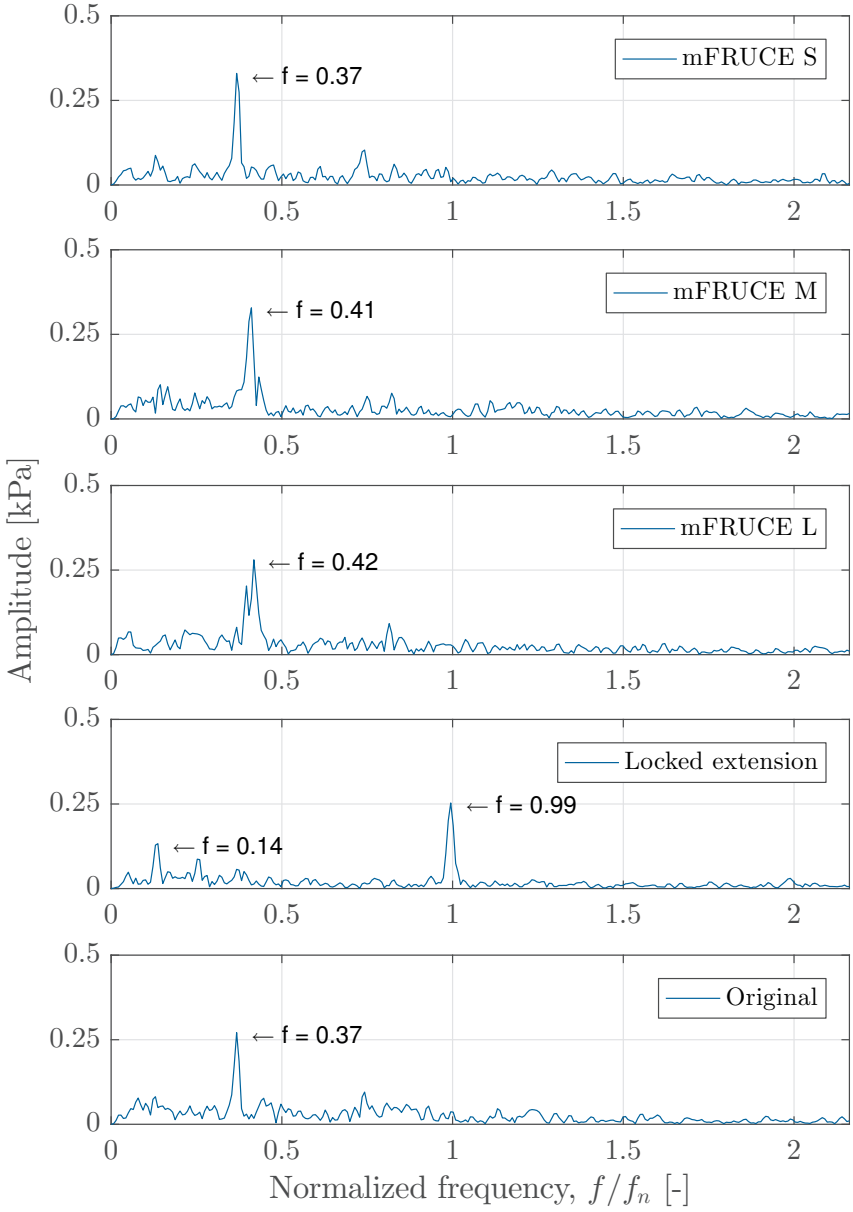

Figure 6.16: Spectral analysis of the time series at sensor P1 at $0.43Q/Q_{BEP}$.

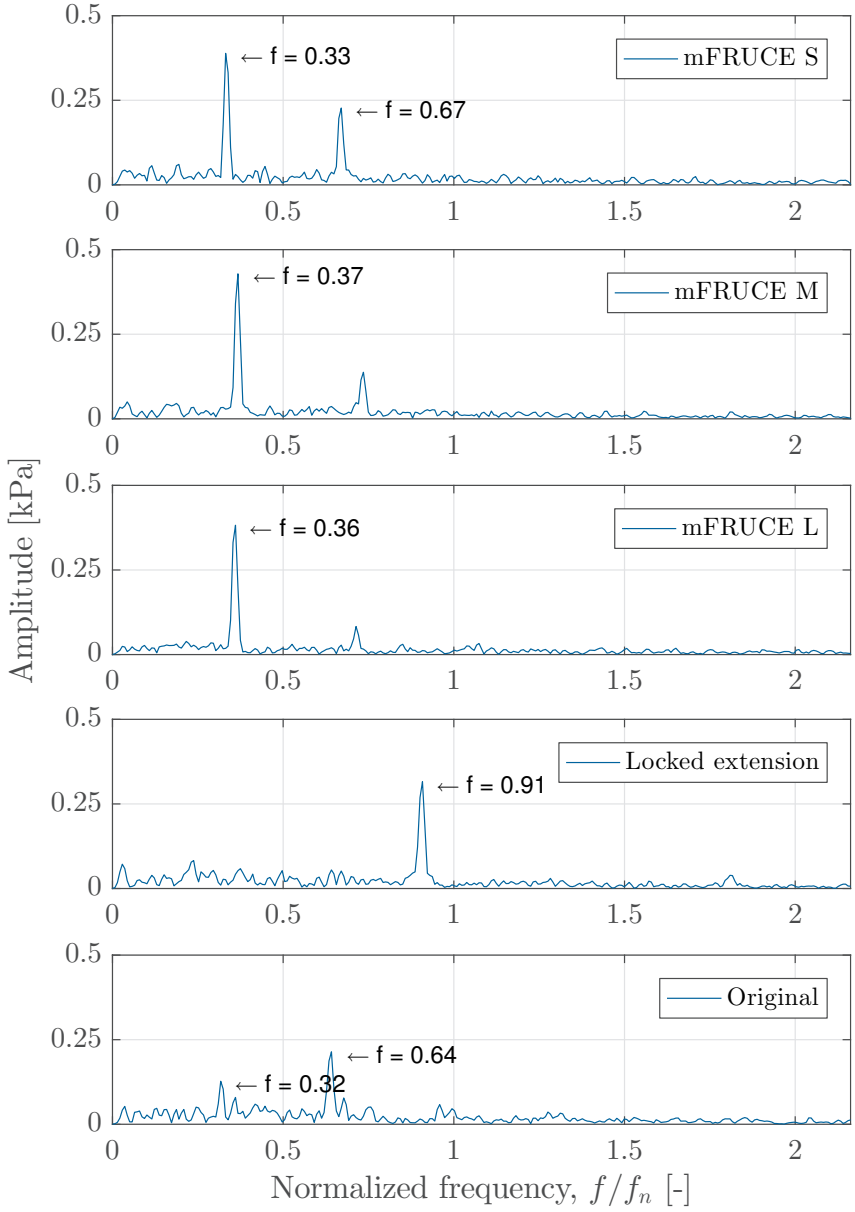

Figure 6.17: Spectral analysis of the time series at sensor P1 at $0.53Q/Q_{BEP}$.

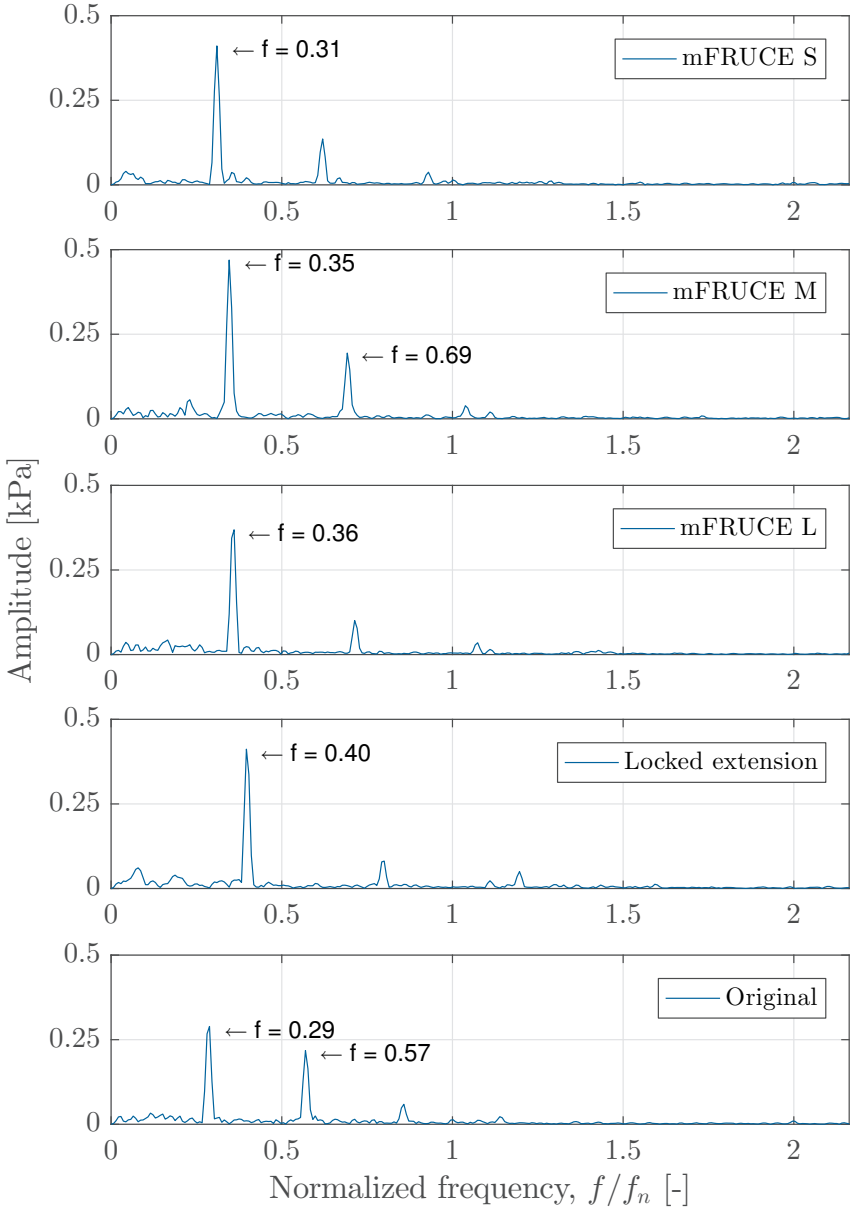

Figure 6.18: Spectral analysis of the time series at sensor P1 at $0.63Q/Q_{BEP}$.

The dominant frequency for the FRUCEs move towards a higher frequency when the FRUCE length increases. The measurements of the rotational speed of the FRUCEs show that the longer FRUCEs rotate slower at part load. A slower rotation of the FRUCEs should indicate a shift towards a lower vortex frequency rather than a shift towards a higher frequency. However, this may be related to energy transfer through the FRUCE from the upper section of the draft tube to the lower section. For turbine discharge of $0.73Q/Q_{BEP}$ and higher, the vortex rope related frequency does not shift.
For the locked runner cone extension, the dominant frequency is shifted almost to the runner frequency. This is most likely because the locked extension increases the swirl in the draft tube as it rotates with the same speed as the runner. However, at $0.63Q/Q_{BEP}$ the dominant frequency shifts back to the same frequency range as the FRUCEs. At this point, the discharge may have increased so the axial velocity of the flow is dominant the tangential flow, so the influence of the rotational speed of the locked extension is reduced compared to lower loads.

6.3.4 Synchronous and asynchronous component

The asynchronous component is as expected the dominant component at part load for the FRUCEs, as displayed for $0.43Q/Q_{BEP}$ in Figure 6.19. The magnitude in the upper plane is larger for the asynchronous component, while the synchronous component remains almost constant. The synchronous component is clearly dominant for the locked extension.

At $0.53Q/Q_{BEP}$ the asynchronous component is increased in amplitude compared to $0.43Q/Q_{BEP}$. The FRUCEs has a significantly asynchronous component than without FRUCE in both planes as can be seen in Figure 6.20. The synchronous component are all in the same order of magnitude for the original design and the FRUCEs, while the locked extension has a significantly higher synchronous component. The synchronous component is still dominant for the locked extension. The asynchronous component is reduced from the upper to the lower plane and for the original design it is reduced to the point that the synchronous component becomes dominant. The synchronous components are more or less in the same order of magnitude for both planes for both the original design and the mFRUCEs.

At $0.63Q/Q_{BEP}$, the asynchronous component has become even more domi-

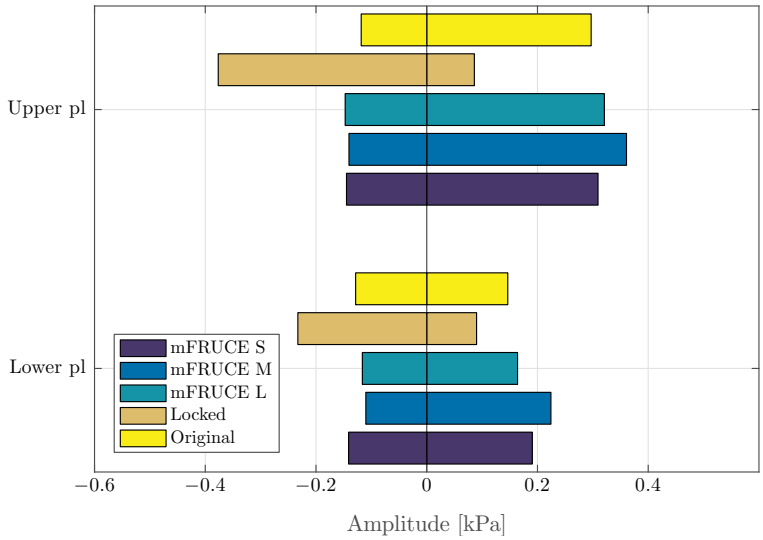

Figure 6.19: Synchronous and asynchronous component at $0.43Q/Q_{BEP}$. The synchronous component is shown in the negative direction and the asynchronous component is shown in the positive direction

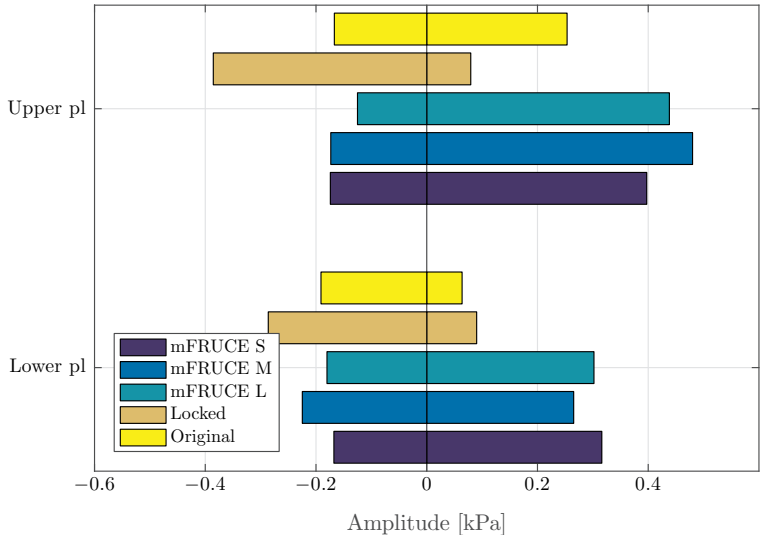

Figure 6.20: Synchronous and asynchronous component at $0.53Q/Q_{BEP}$. The synchronous component is shown in the negative direction and the asynchronous component is shown in the positive direction

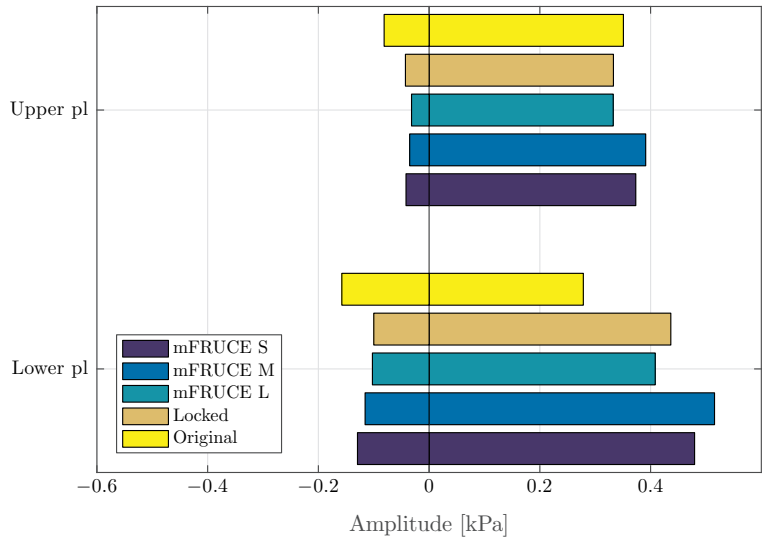

Figure 6.21: Synchronous and asynchronous component at $0.63Q/Q_{BEP}$. The synchronous component is shown in the negative direction and the asynchronous component is shown in the positive direction

nant, also for the locked extension. The dominant frequency for the locked extension has now shifted from close to the runner frequency to the RVR frequency as seen in the previous section. In the upper plane mFRUCE L and the locked extension have the smallest asynchronous component. The shorter mFRUCEs have a larger asynchronous component, while the original design has the largest synchronous component.

In the lower plane, the original design has the largest synchronous component, but the asynchronous component has decreased and is know significantly smaller than all the mFRUCEs. The locked extension and mFRUCE L still have the a smaller synchronous component than the other mFRUCEs. It is also worth noting that the asynchronous components at this load is increasing from the upper to the lower plane compared to the two lower loads.

At the loads presented in this section, the original design has a smaller asynchronous component than the mFRUCEs. This indicates that the FRUCEs do not reduce the tangential velocity in the draft tube or thereby not the frequency amplitude of the vortex rope as seen in the previous section.
The locked extension has a large synchronous component at $0.43Q/Q_{BEP}$ and $0.53Q/Q_{BEP}$ which indicates that the extension is increasing the tangential velocity of the draft tube flow. When the flow is increased to $0.63Q/Q_{BEP}$, this phenomena is suppressed. At $0.63Q/Q_{BEP}$, the RVR seem develop more in the flow direction and the asynchronous components are increasing in the lower plane. However, the asynchronous component of the original design does not increase in the lower plane. It is therefore likely that the mFRUCEs change the behaviour of the RVR and increases its amplitude.

6.4 Leirfossene

6.4.1 Efficiency

The efficiency measured with the thermodynamic method is well within the uncertainty band of the efficiency measured with pressure-time method by a consultant company in 2009, shortly after commissioning. At part load the curve fit has a higher efficiency for the thermodynamic measurement and the difference between measured points increases. The efficiency curve fit in this section is done with a third order equation.

The uncertainty in the thermodynamic measurements are also smaller than for the pressure-time method. The thermodynamic methods uncertainty decreases with decreasing flow as the temperature difference increases. The pressure-time method increases in uncertainty as the flow is reduced due to a decrease in pressure difference.

A comparison of the efficiencies with and without FRUCE is shown in Figure 6.23. For all the FRUCEs, a drop in efficiency at full load can be observed. As seen in Figure 6.24 the actual measured points at the two highest loads are outside the uncertainty band of the original design. This is a significant drop of up to 2.5% in the worst case for FRUCE 3. The maximum efficiency is somewhat lower for FRUCE 1 and 3. The measured points for the original design and FRUCE 2 are approximately 0.5% higher. There are minor

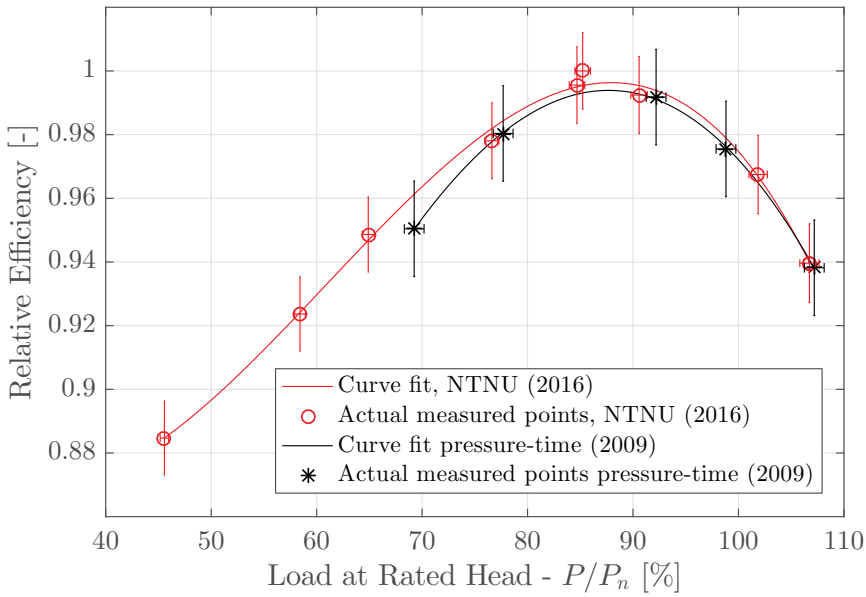

Figure 6.22: Efficiency for Unit 2 at Leirfossene HPP. The efficiency measurements carried out with the thermodynamic measurements by NTNU (2016) compared to previous measurements carried out with the pressure-time method in 2009.

differences in efficiency at part load. However, the efficiency of FRUCE 2 decreases more towards the lowest load and is almost outside the uncertainty band of the original design.

6.4.2 Pressure pulsations

There are eight pressure sensors in the draft tube, which are placed in pairs in four horizontal planes. These planes are referred to as Plane 1 to 4, where Plane 1 is the upper plane with sensors DT1 and DT2. DT 3,5 and 7 are located directly downstream DT 1 and is referred to as the odd side. On the opposite side, DT 4, 6 and 8 are located directly downstream DT 2 and is referred to as the even side. The nominal load referred to is the load given by the turbine manufacturer. This is however not the best efficiency point.

The highest average pressure is observed to be 182 kPa at the lowest load, 47%. The highest pressure is found at DT8, i.e. furthest downstream. In

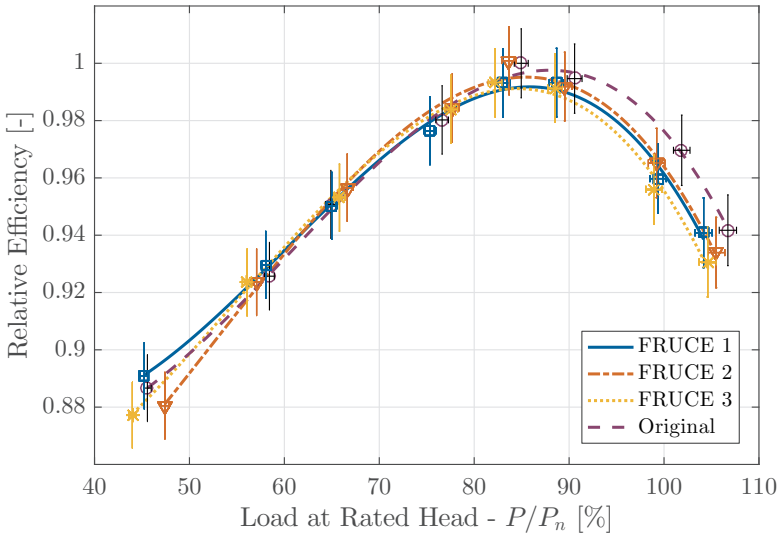

Figure 6.23: Efficiency comparison for the different FRUCEs. The dashed line and errorbars represent the original design without FRUCE

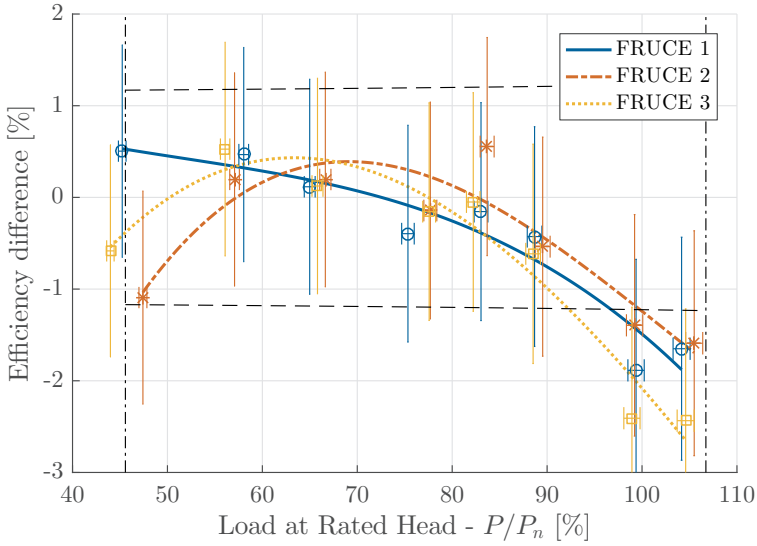

Figure 6.24: Efficiency difference for the different FRUCEs. The uncertainty band for the original design is given with dashed horizontal lines. The vertical dashed lines indicates the lowest and highest load measured with the original design.

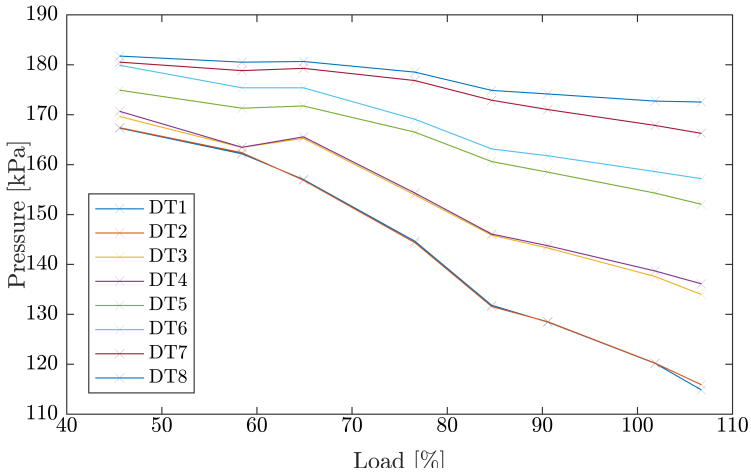

Figure 6.25: Average pressure in the draft tube at different loads without FRUCE

the two top planes, the average pressure values are close to constant for the whole load area. The standard deviation for 47% load is in the order of 11 kPa (2% of the head). In the two lower planes, the average pressure is higher in the outer section of the draft tube than towards the inner side of the draft tube. The pressure difference is 1-6 kPa for Plane 4 and 3-5 kPa for Plane 3. A pressure difference is visible in the lowest plane in the draft tube, it may be a consequence of an asymmetric flow pattern. A higher velocity in the outer section of the draft tube due to the bend may be the cause. Also, the standard deviation is significantly greater than the measured pressure difference between the two side of the draft tube. The pressure difference between the different sides of the draft tube may not be significant. The same pressure difference can be seen also with the FRUCEs.

The static pressure difference between each plane is increasing with the flow, except between 56% and 66% load. The pressure jump between 56% and 66% load is obvious in the second plane from the top (DT3 and DT4), but can also be seen in the planes below. The pressure jump cannot be seen with FRUCE, which makes it likely to be flow related. It also dampens out in the lower part of the draft tube, which may relate it to the swirl.

Figure 6.26 to 6.31 displays the peak-to-peak amplitudes of the pressure signal, ΔP_{pp}, at different levels of the draft tube for different loads. DT 7 and 8 are the furthest downstream the draft tube. The peak-to-peak values

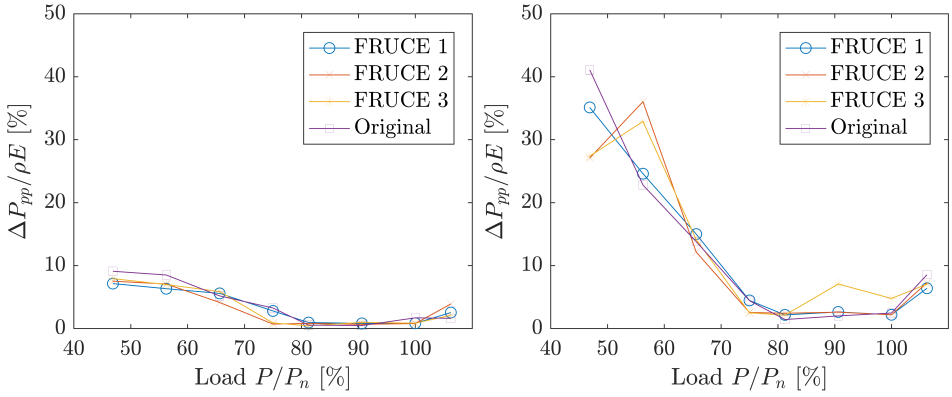

(a) DT 7 (b) DT 8

Figure 6.26: Peak-to-peak values for Plane 4 with different FRUCEs

on each side of the draft tube differs significantly in size. Peak-to-peak values at DT 8 are between 30-40% of ρE, which is suspiciously high. A frequency analysis of each pressure signal showed that a wide band of frequencies from 600-800 Hz was present at DT 8 at 47% load. This band of frequencies had typically no dominant peak. The range shifted with operational point from 150-250 Hz and up to 800-950 Hz. It was also only found at part load from 47%-66% load. Typical frequencies which occur in the range of 150-950 Hz are blade passage and harmonics, von Kármán vortex street, flow turbulence and cavitation noise [13]. The band of frequencies only occurred at some of the sensors, DT 1, DT 2, DT 4, DT 5 and DT 8, and it was not necessarily in the same frequency range occurring at alThis indicates that the FRUCEs do not reduce the tangential velocity in the draft tube or thereby not the frequency amplitude of the vortex rope as seen in the previous section." This indicates that the FRUCEs do not reduce the tangential velocity in the draft tube and therefore not the frequency amplitude of the vortex rope as seen in the previous section l the sensors at the same operating point. The occurrence of the high frequency band shifts from operational point and differs from each sensor, it is therefore most likely a local phenomenon related to sensor position.

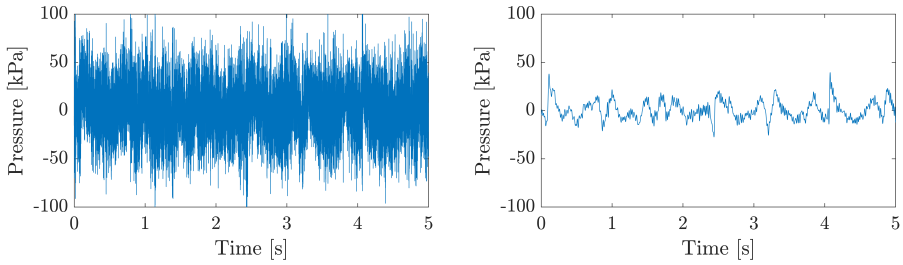

(a) raw signal (b) Filtered signal

Figure 6.27: Acquired and filtered pressure data for DT 8 at 47% load

The blade passage frequency is typically one peak, which in this case was 61.5 Hz, and its harmonics will be multiple this frequency. The blade passing frequency not therefore likely to be the cause this frequency band. As the frequency band only occur at part load it is likely it is related to flow turbulence and cavitation. The location of the pressure sensors may also cause local cavitation at the sensor, inducing increased amplitudes in a wide frequency range.

Local cavitation is the most likely explanation as this also was seen at La Higuera. In La Higuera two sensor was damaged due to cavitation on pressure sensor membrane.

The signal was therefore filtered with a low pass filter with zero phase distortion with cut-off frequency at $9f_n$ (50 Hz). The unfiltered and filtered signal is shown in Figure 6.27.

As seen in Figure 6.28 the maximum peak-to-peak values are 10-11% of ρE at 47% load. For 47% and 56% load one or more of the FRUCEs reduces the peak-to-peak values. At 66% load, the original design has the lowest peak-to-peak values at DT 1. At full load, all the FRUCEs increase the peak-to-peak values. In Plane 2, all the FRUCE peak-to-peak values are significantly lower than the original design. The FRUCE peak-to-peak values are also lower than in Plane 1. The same trend as in Plane 1 can be seen. Peak-to-peak values for the FRUCEs are lower at 47% and 56% and the peak-to-peak value of the original design drops significantly at 76% load.

As seen in Figure 6.30 and 6.31 for every operational point at part load, one of the FRUCEs reduce the peak-to-peak value compared to the original.

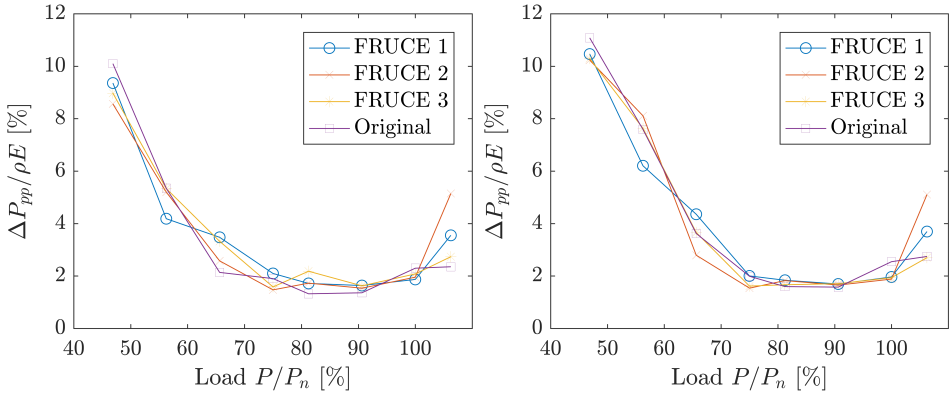

(a) DT 1 - odd side (b) DT 2 - even side

Figure 6.28: Peak-to-peak values for Plane 1 with different FRUCEs

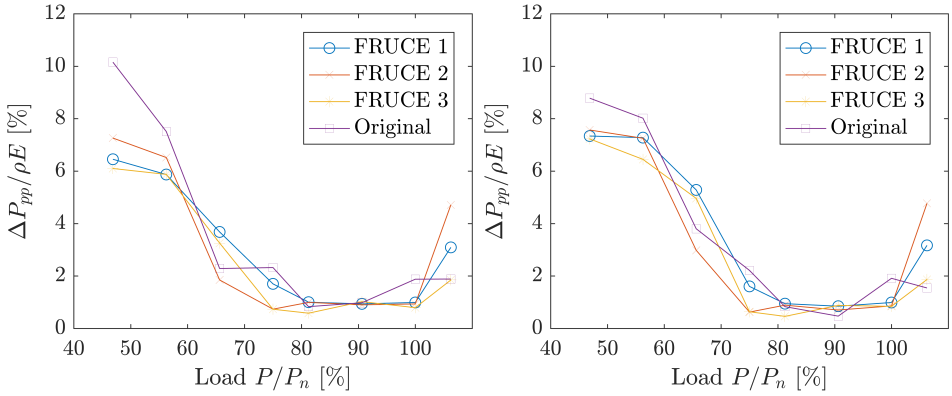

(a) DT 3 (b) DT 4

Figure 6.29: Peak-to-peak values for Plane 2 with different FRUCEs

The original has consequently the lowest peak-to-peak value at full load. The FRUCEs has dampening effect on the peak-to-peak values in the lower frequency range at part load. From 80-92% load the peak-to-peak values are the smallest and the difference between FRUCE and the original design is minor. At 100% load the peak-to-peak value of the original design increase before it drops when full load is reached. The peak-to-peak values of the FRUCEs does not increase before full and have about 50% lower peak-to-peak values than the original design at 100% load.

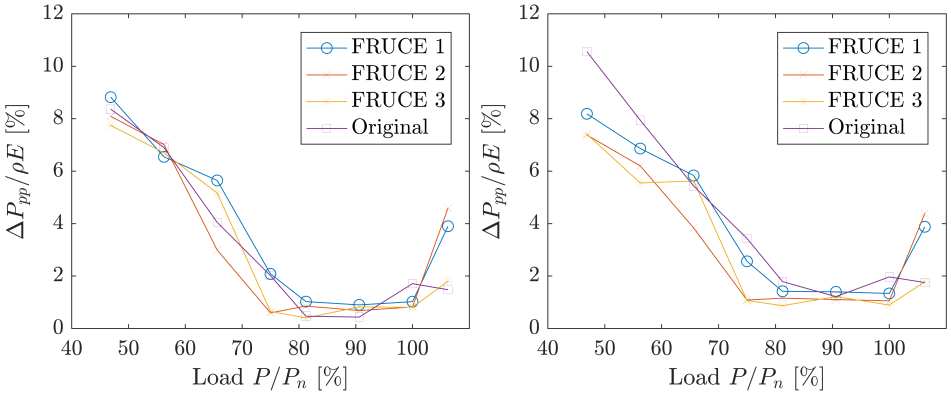

(a) DT 5 (b) DT 6

Figure 6.30: Peak-to-peak values for Plane 3 with different FRUCEs

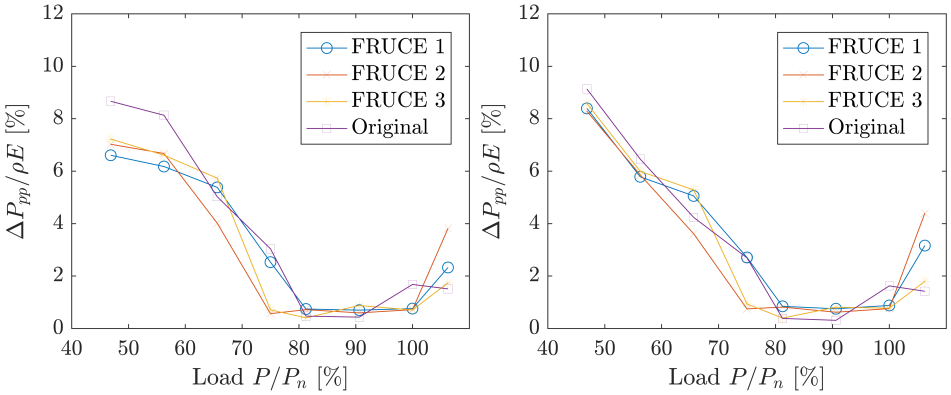

(a) DT 7 (b) DT 8

Figure 6.31: Peak-to-peak values for Plane 4 with different FRUCEs

6.4.3 Frequency analysis

The part load investigation includes four operational points at 47%, 56%, 66% and 75% load. The results for the low frequency range from 1-15 Hz is presented. As expected, the dominant frequency in this range is the RVR frequency. The dashed lines seen in the following figures at $f/f_n = 1$ and $f/f_n = 2$ are the marking the position of the runner frequency and the harmonic. The figures are also normalized with regards to the maximum

amplitude with the original design at the given load.

47% load

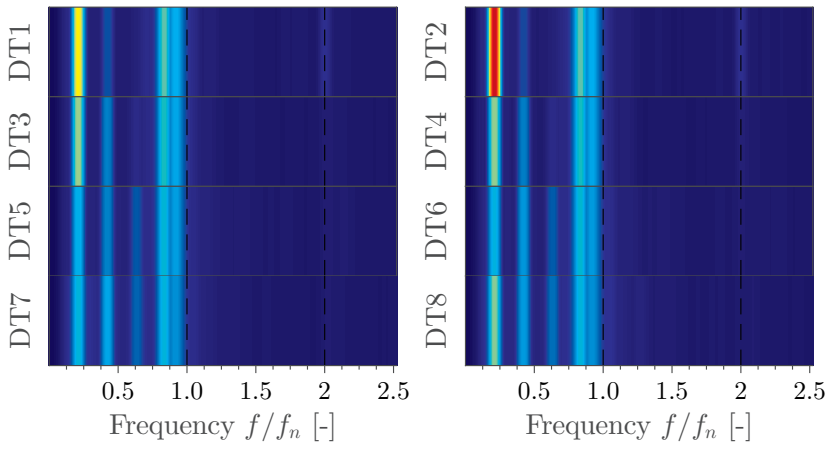

Figure 6.32: Frequency spectrum for original design at 47%. The maximum amplitude is 2.25% ρE found at DT 2.

The highest peak-to-peak values were found at 47% load, and this is also where the RVR frequency reached the highest amplitude. The highest amplitude can be found at DT2 for all cases and the second highest peak is found at DT1. These are the two sensors closest to the runner, so this is not unexpected. From DT2 and downstream at the even side of the draft tube, the RVR frequency becomes weaker. At the opposite side, there is also an amplitude reduction downstream, but a small increase can be noticed from DT6 to DT7. Due to the difference in RVR frequency amplitude, the vortex rope is not axissymetric. The RVR frequency amplitude is found to be lowest without FRUCE at 2.25% of ρE. The FRUCEs increases the maximum amplitude with 14-24%, where FRUCE 2 had the smallest increase.

56% load

At 56% load the frequency amplitudes indicates the FRUCEs have a dampening effect with regards to the RVR frequency. The highest amplitude for the original design was found at DT 2, with 2.5% of ρE. This is an increase compared to 47% load. FRUCE 1, shown in Figure 6.35, has a maximum amplitude of 2.09% ρE, which is a 16% reduction. The maximum amplitude has also moved downstream to DT 4. FRUCE 2 and 3 also show a

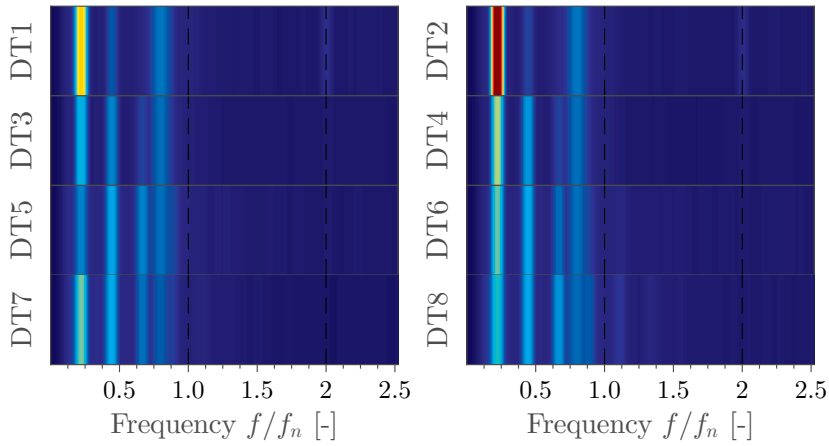

Figure 6.33: Frequency spectrum for FRUCE 3 at 47% load. The maximum amplitude is 2.69% ρE found at DT 2.

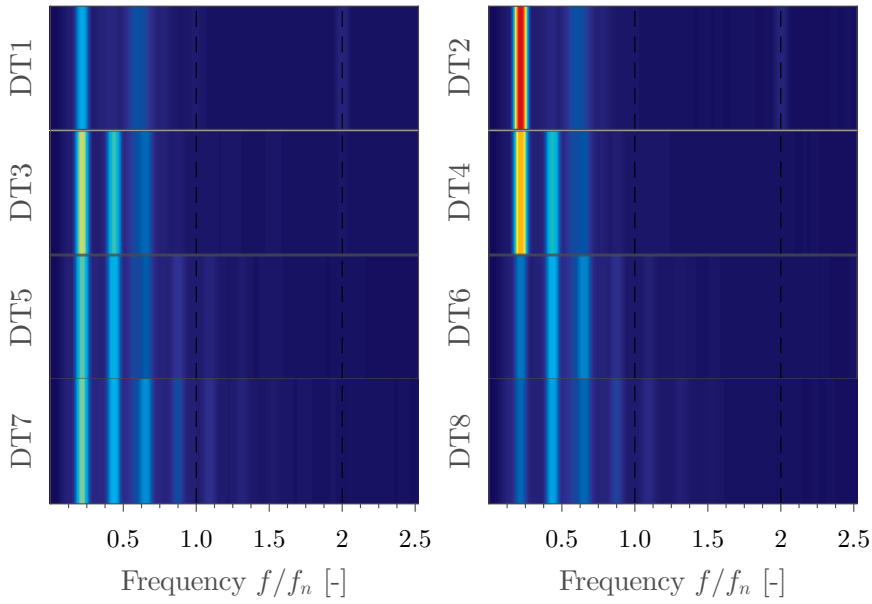

Figure 6.34: Frequency spectrum for the original design at 56% load. The maximum amplitude is 2.50% ρE found at DT 2.

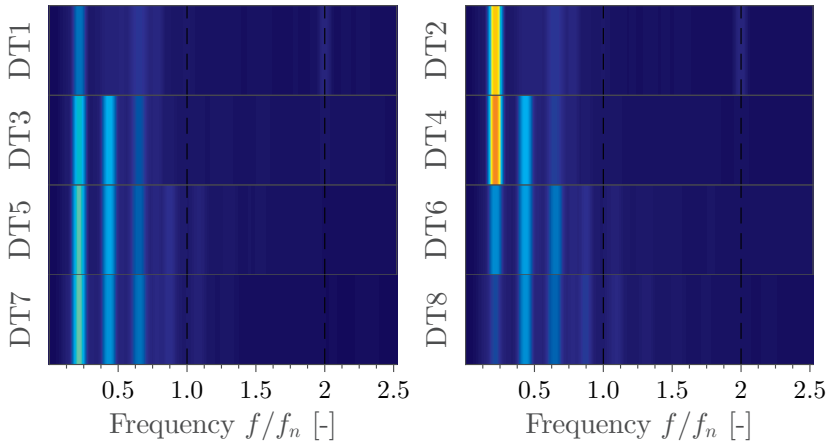

Figure 6.35: Frequency spectrum for FRUCE 1 at 56% load. The maximum amplitude is 2.09% ρE found at DT 4.

reduction in RVR frequency with about 10%, but the highest amplitude is found at DT 2.

66% load

The dominant frequency at 66% load is still the RVR frequency. At this point, there are some notable differences. The maximum amplitude is significantly reduced from the lower loads and is know 1.33% of ρE for the original design. The maximum amplitude is also found further downstream at DT 4 for FRUCE 1 and 3, while for FRUCE 2 it is found at DT 7. The maximum amplitudes for the FRUCE 1 and 3 are 15% and 21% higher, respectively, than without FRUCE. Without FRUCE a similar result is found as for FRUCE 1 and 3. However, it is worth noting that the RVR frequency amplitude is significantly higher at DT2 without FRUCE. For FRUCE 2 the highest amplitude are found at DT7, while DT6 shows the second highest. There is a significant reduction in the amplitude at DT2, DT4 and DT5 compared to without FRUCE. The results indicate that the FRUCE is forcing the initiation point of the vortex rope further downstream in the draft tube.

75% load

At 75% load the highest RVR frequency amplitude is found at DT8 for FRUCE 1 and without FRUCE. The two other FRUCEs show a completely different result, where the dominant frequency is 11.1 Hz at DT1 and DT2.

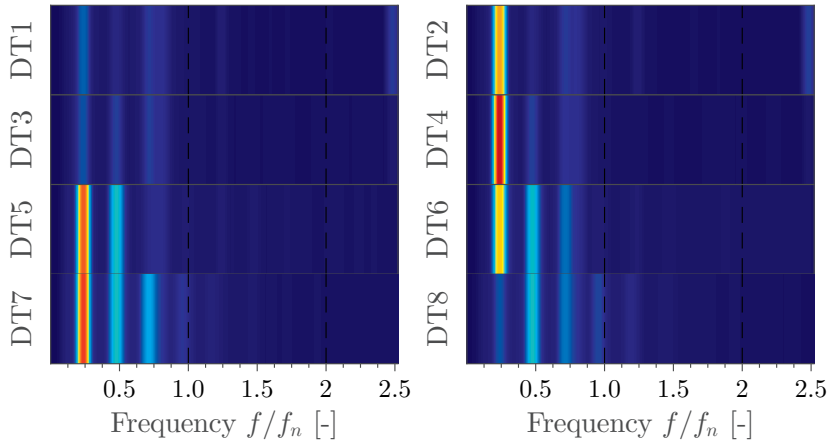

Figure 6.36: Frequency spectrum for the original design at 66% load. The maximum amplitude is 1.33% ρE found at DT 4.

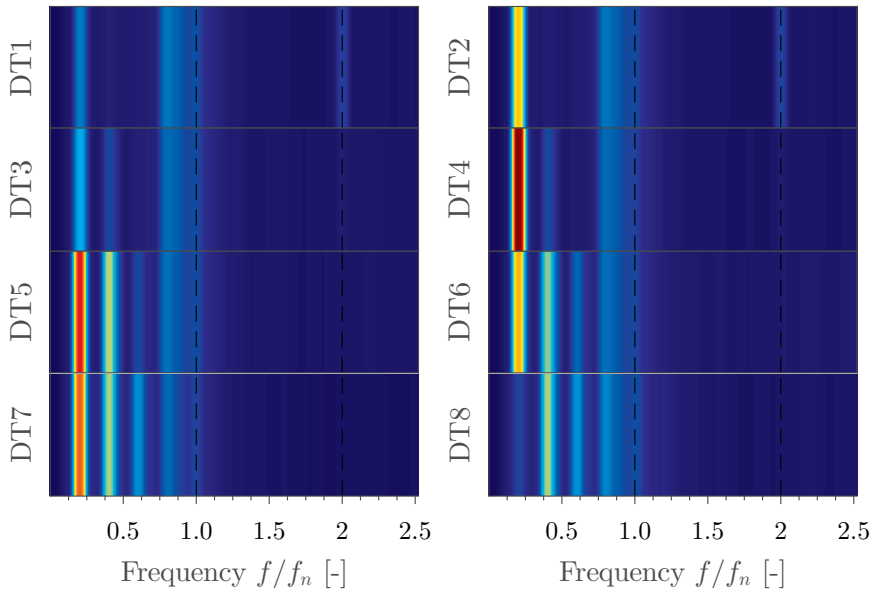

Figure 6.37: Frequency spectrum for FRUCE 1 at 66% load. The maximum amplitude is 1.53% ρE found at DT 4.

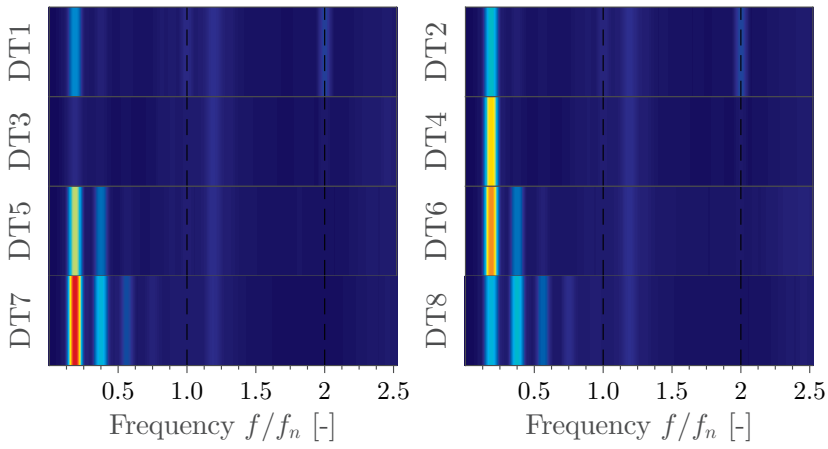

Figure 6.38: Frequency spectrum for FRUCE 2 at 66% load. The maximum amplitude is 1.31% ρE found at DT 7.

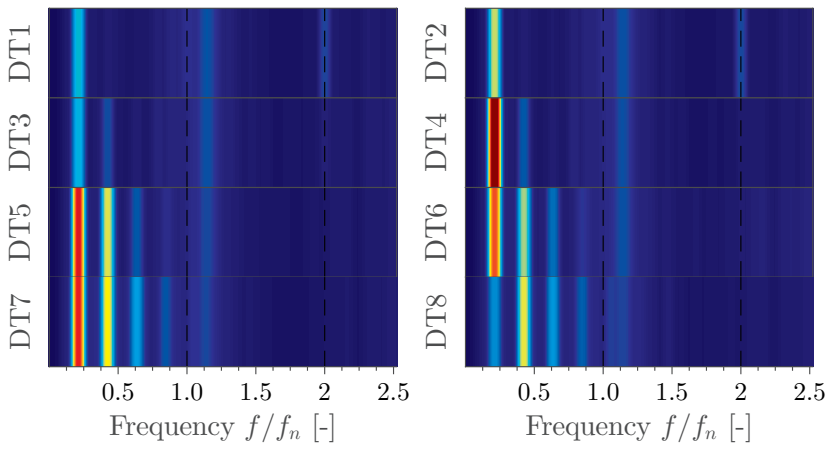

Figure 6.39: Frequency spectrum for FRUCE 3 at 66% load. The maximum amplitude is 1.62% ρE found at DT 4.

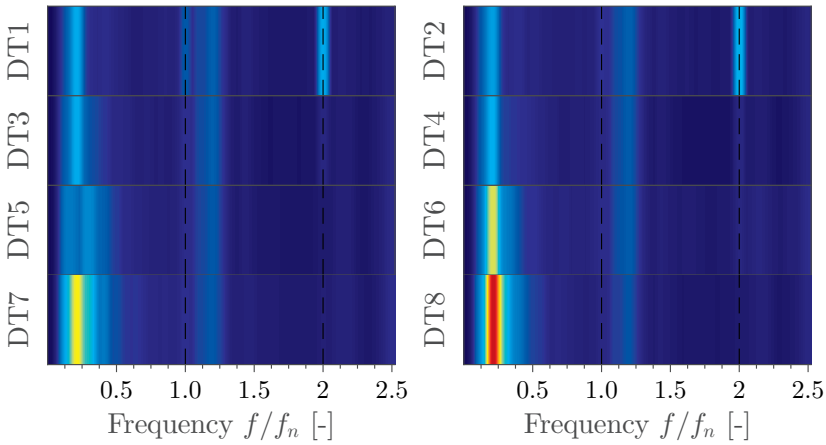

Figure 6.40: Frequency spectrum without FRUCE at 75% load

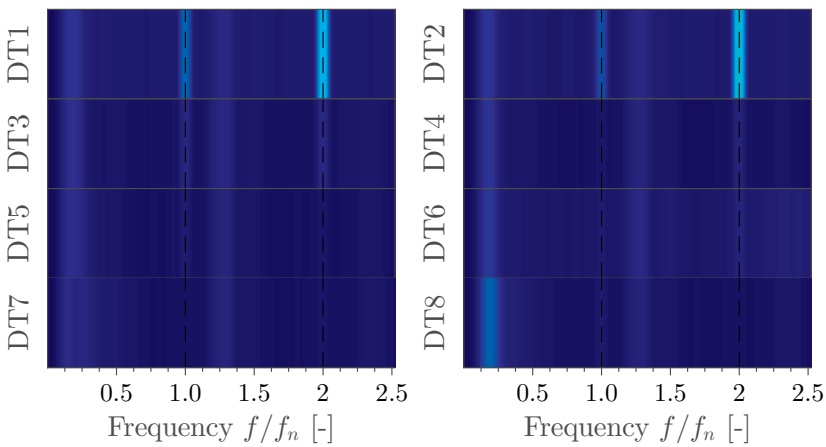

Figure 6.41: Frequency spectrum for FRUCE 2 at 75% load

This matches the second harmonic of the runner frequency. The maximum amplitude is reduced with more than 50%.

81% load BEP

At best efficiency point (BEP) the results for the different options are similar. The runner frequency at 5.55 Hz and its harmonic at 11.1 Hz is clearly visible in the top measurement plane. The second harmonic of the runner frequency is the dominant frequency. The maximum amplitude difference is less than 2% between the different options. For the FRUCEs, two frequencies are visible for all the sensors at around $0.9f_n$ and 1.2 f_n. This are suggested to be reflection frequencies from the free surface at the outlet and the split in outlet channel.

91% load

The results from 0.91% load are not significantly different from BEP. The same frequencies are found and the maximum amplitude is increased by 10%.

100% load

The dominant frequency at 100% load is still the second harmonic of the runner frequency and its amplitude is increased with 35%. The increase in maximum amplitude is probably the cause for the reflection frequencies discussed for BEP to be less prominent. However, a prominent frequency at 4.3 Hz and at 5 Hz are found at operation without FRUCE. The 5 Hz frequency is likely to be the reflection frequency from the free surface at the outlet. The 4.3 Hz frequency may be the beginning of the full load vortex rope.

106% load

The full load vortex rope is now present at operation without FRUCE with a frequency of $0.49f_n$. The second harmony of the runner frequency is still present and the dominant frequency for FRUCE 1 and 3, as well as without FRUCE. Especially FRUCE 1 and 2 has a wide band of prominent frequencies around $0.9f_n$. This is similar to what was observed without FRUCE at 100% load. As the FRUCE now is rotating in the opposite direction of the runner, these may be related to full load vortex rope. FRUCE 3 has clearly smaller amplitudes related to the $0.9f_n$ area than the FRUCEs with smaller diameter. This suggests that the increased diameter helps to reduce the full load vortex rope.

6.4.4 Synchronous vs asynchronous

The synchronous and asynchronous components of the dominant frequency for part load is presented in this section. The dominant frequency at part load is the vortex rope frequency around $0.22 f_n$.

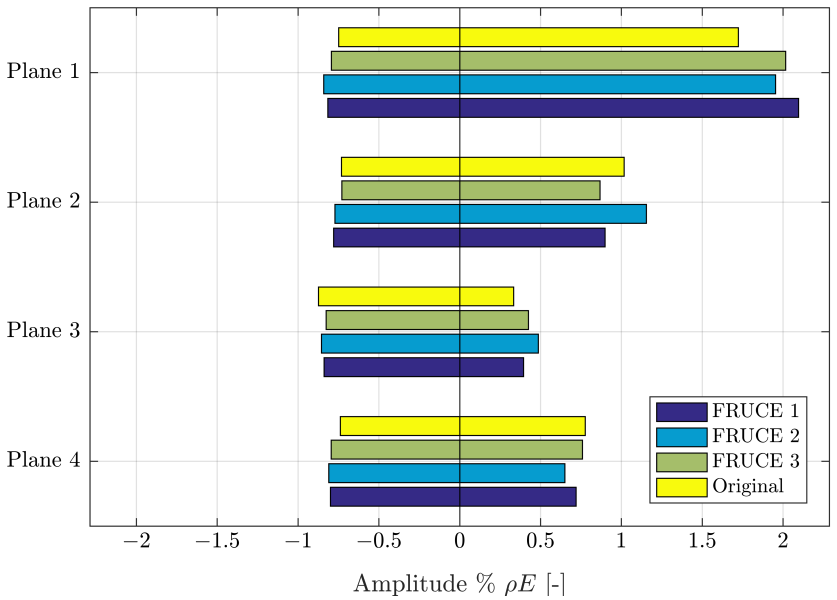

Figure 6.42: Synchronous and asynchronous component at 47% load. The synchronous component shown to the left is almost constant in all the four measuring planes.

Figure 6.42 shows that the synchronous component is almost constant in amplitude in the whole draft tube at 47% load. The asynchronous component is dominant in the upper part of the draft tube and decreases in amplitude when moving downstream.

This indicates that the vortex rope rotational radius gets smaller. The small increase from Plane 3 to Plane 4 may be a consequence of the bend in the draft tube.

The amplitudes of the asynchronous component vary somewhat for the different options, but there is no clear tendency. However, it is clear that the asynchronous component amplitude is higher with FRUCE in Plane 1.

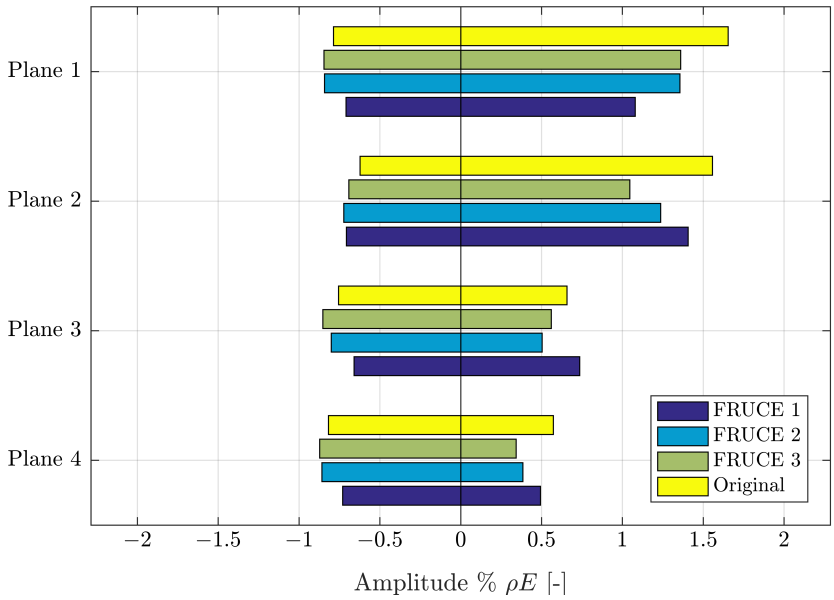

Figure 6.43: Synchronous and asynchronous component at 56% load

Investigating the dominant frequency for the different options, some differences can be found with a FRUCE mounted. The dominant frequency is $0.21f_n$ without FRUCE, and $0.22f_n$ for all the FRUCEs. This indicates that a FRUCE may increase the tangential velocity and shift the dominant frequency. The asynchronous component is also increased in Plane 1 corresponding with the shift in frequency.

At 56% load the asynchronous component is dominant further downstream in the draft tube. The asynchronous amplitude for the original is greatest in the two top planes where the asynchronous component is dominant. The FRUCEs clearly reduce the asynchronous amplitude to some extent. The synchronous has some small changes in amplitude, but no significant trends.

At this load, the vortex rope frequency is different for every option. The dominant frequency for the original $0.23f_n$, while for the FRUCE 1, 2 and 3 they are $0.22f_n$, $0.21f_n$ and $0.20f_n$ respectively. Combining the frequencies and the asynchronous component, there seem to be a relationship between the frequency and the amplitude. However, there FRUCE 1 has the lowest amplitude in Plane 1 and deviates from the possible relationship seen in Plane 2. This might be a consequence of the flow not being axisymmetric.

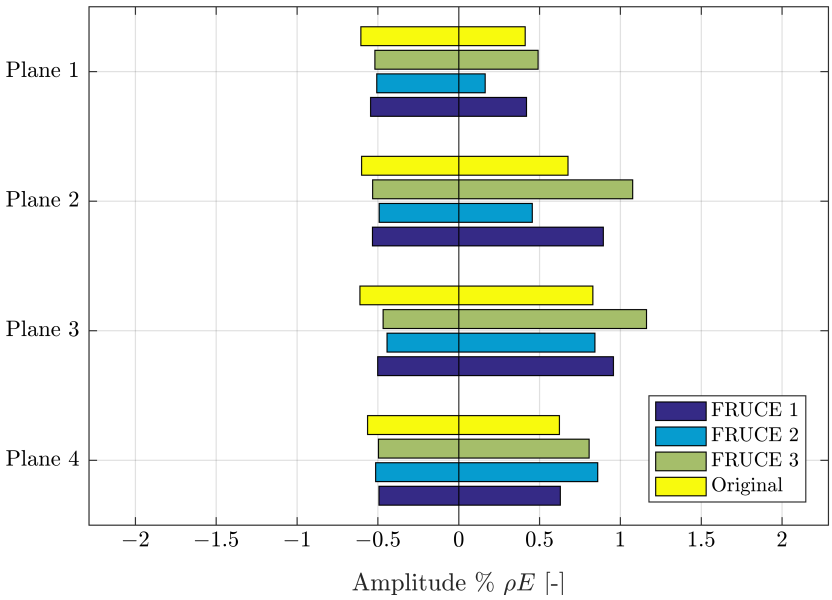

Figure 6.44: Synchronous and asynchronous component at 66% load

Increasing the load to 66% load, the behaviour changes drastic, as seen in Figure 6.44. The asynchronous component is more prominent further downstream and the synchronous component is dominant in Plane 1. At this particular load the FRUCE length, seem to be of influence. Plane 3 and 4 looks to be too far downstream the FRUCE for it to have significant influence. In the two upper planes, FRUCE 2 has significantly reduced asynchronous amplitudes compared to the other options. It is assumed this is because the FRUCE forces the initiation point of the vortex rope further downstream.

At this operating point, the asynchronous component is not dominant in Plane 1, but becomes more dominant in Plane 2 and 3. It is also worth noting that the asynchronous component is significantly lower for FRUCE 2 in the two upper planes. This indicates that the vortex rope's initiation point is moved downstream with FRUCE 2.

Investigating the frequencies, FRUCE 2 has the lowest frequency with $0.19f_n$, while FRUCE 1 and 3 have $0.20f_n$ and $0.21f_n$, respectively. Interestingly, the frequency without FRUCE increases to $0.24f_n$ and is now significantly higher than with FRUCE. At 56% and 66% load the vortex rope frequencies show an opposite trend compared to the laboratory measurements. The longest FRUCE has a higher frequency than the shortest FRUCE and the original design in the laboratory. The prototype measurements show the lowest frequency for the longest FRUCE and the highest frequency without FRUCE. The differences in vortex rope frequency is possibly due to the different turbines. The relative FRUCE length at Leirfossene is also shorter than for the laboratory measurements.

6.4.5 Air injection

At Leirfossene HPP, air injection was installed to dampen the pressure pulsations in the turbine. The peak-to-peak measurements with and without air injection are compared in the following section.

It was noted earlier that the high frequency range contributed significantly to the peak-to-peak values, the signals were therefore filtered with a low pass filter with cut-off frequency at $9f_n$.

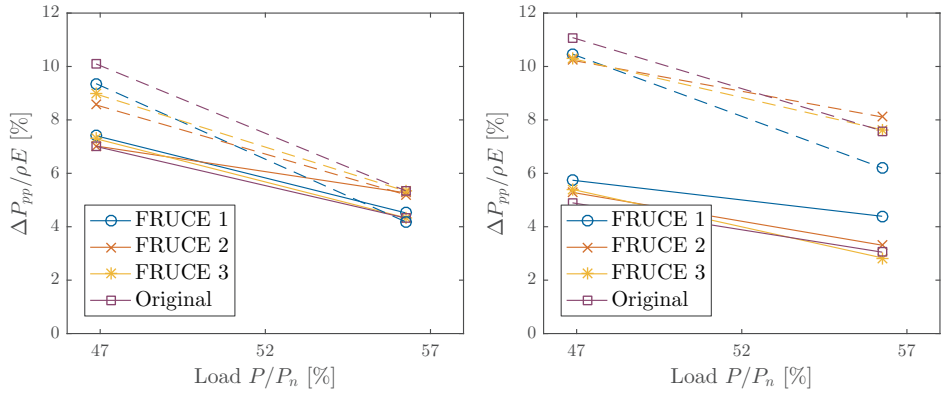

(a) DT 1 (b) DT 2

Figure 6.45: Peak-to-peak values for filtered signals with cut-off frequency at $9f_n$ at Plane 1 with different FRUCEs. The dashed lines are without air injection and the full lines are with air injection.

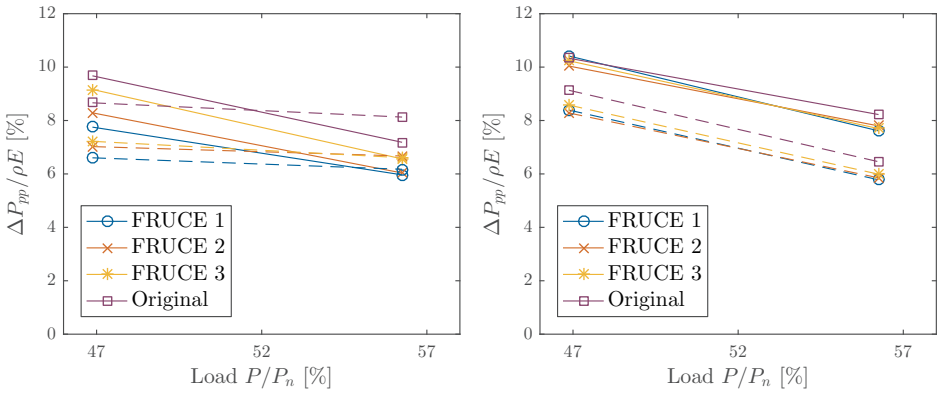

(a) DT 7 (b) DT 8

Figure 6.46: Peak-to-peak values for filtered signals with cut-off frequency at $9f_n$ at Plane 4 with different FRUCEs. The dashed lines are without air injection and the full lines are with air injection.

The filtered signals show there is a reduction in peak-to-peak values in the top plane. The original design has the greatest reduction in peak-to-peak values. This is most likely due to the air injected closer to the turbine. When the FRUCE is mounted, the air enters the draft tube downstream the FRUCE instead of just downstream the runner cone.

In the lower plane, the largest peak-to-peak values can be found with air injection. The air injection does not seem to have the dampen effect in the lower part of the draft tube as in the upper part.

Chapter 7

Conclusion

The main focus of this work has been to investigate methods to reduced pressure pulsations in Francis turbines. Pressure pulsations in four Francis prototypes and one Francis model have been studied. Experimental work on a high head Francis model has been carried out in the Waterpower Laboratory at NTNU in Trondheim, Norway. The prototype measurements have been carried out on three low head Francis turbines and one high head Francis turbine.

The investigation of a high head Francis turbine with air injection was carried out in Chile. Pressure pulsations were investigated at six part load operating points with supplementary efficiency measurements. The pressure measurements carried out revealed that air injection has a positive dampening effect on the peak-to-peak values, but may increase the low frequency amplitudes at part load. Further, the air injection did not affect the efficiency of the turbine.

A free rotating runner cone extension (FRUCE) was developed and tested at the Waterpower Laboratory. The laboratory measurement showed that the peak-to-peak values were reduced in some of the test cases at part load operation, but also increased at other operating points. The amplitude at the rotating vortex rope (RVR) frequency also increased with FRUCE at part load. It was concluded that the diameter of the FRUCE was too small to have a dampening effect on the peak-to-peak values and the RVR frequency amplitude.

Three FRUCE designs with different lengths and diameter were made for testing at Leirfossene Hydro Power Plant (HPP). The prototype measure-

ments from Leirfossene HPP showed that a reduction in pressure pulsations was achieved. At 47% load the peak-to-peak values were reduced with up to 40%. Overall a dampening of the peak-to-peak values was found for part load operation. The longest FRUCE also showed that the initiation point of the RVR was moved downstream in the draft tube at part load. The FRUCE was designed to reduce pressure pulsations at part load, but also reduces the peak-to-peak values at higher loads. A drawback with the current design is reduced efficiency at high load.

A runner cone extension can be used to manipulate the draft tube pressure pulsations. The results from Leirfossene HPP show reduced peak-to-peak values at part load. The results depends on the length and diameter of the FRUCE. A too small diameter of the FRUCE will have minor or negative effect on the pressure pulsations. Active control of the rotational speed, diameter and length is required to efficiently control the draft tube pressure pulsations.

The FRUCE changes to some degree the vortex rope frequency. In the model test it was found to shift the RVR frequency towards a higher frequency, while in the prototype it was shifted towards a lower frequency. A change of the RVR frequency could be an advantage in case of resonance problems.

All in all air injection and FRUCE have their advantages and disadvantages. As the measurements has shown they can both be used to reduce pressure pulsation amplitudes, but they do not eliminate the problem. The FRUCE technology has development potential, but it will require simulations and prototype testing.

Chapter 8

Further Work

A research work is a long process to find answers to a problem. However, during the experimental part of this work some new subjects came to mind.

An interesting aspect would be to first test different diameters of the freely runner cone extension in model turbine. Further, controlling the runner cone extension with some sort of brake would give a possibility to see how different speeds would influence the draft tube flow and pressure pulsations. A step further would be to make the runner cone extension and active form of flow control by allowing it to vary length depending on operating condition. Varying diameter or shape might also be possible. A different approach could be to fit the runner cone extension with fins to use them as flow straighteners.

As the flow and swirl distribution can be challenging to control in a model runner, experiments could be carried out in a simplified draft tube with a swirl generator. This would allow easier control of the swirl parameter. A simplified model could also be easier to perform PIV and Laser Doppler Velocimetry (LDV) measurements.

Another challenge experienced with regards to the field measurements was finding suitable bearings. Bearings made for operation in water are not made for the rotational speeds found in a typical turbine.

Further investigation of the FRUCE with larger diameters should be conducted. Potentially also different shapes. controlling the rotation speed of the FRUCE could prove to be useful. There are man things that could be interesting to measure as well. Using PIV to map the tangential velocities

at different levels in the draft tube could help understanding the flow in the draft tube when a FRUCE is installed.

Bibliography

[1] Alekseenko S, Kuibin P. Stationary vortex structures in intensively swirling flows. Numerical methods in laminar and turbulent flow 1995;9:382–393.

[2] Avellan F. Flow investigation in a Francis draft tube: the FLINDT project. In: Proceedings of the 20th IAHR Symposium, Charlotte, North Carolina, USA No. LMH-CONF-2000-003; 2000. .

[3] Baya A, Muntean S, Câmpian VC, Cuzmoş A, Diaconescu M, Bălan G. Experimental investigations of the unsteady flow in a Francis turbine draft tube cone. IOP Conference Series: Earth and Environmental Science 2010 Aug;12(1):012007.

[4] Benjamin TB. Theory of the vortex breakdown phenomenon. Journal of Fluid Mechanics 1962 Dec;14(04):593–629.

[5] Biela V, Beltran H. Draft tube fins. In: Proc. 19th IAHR Symp. on Hydraulic Machinery and Cavitation, Singapore; 1998. p. 454–461.

[6] Bosioc AI, Tanasa C, Muntean S, Susan-Resiga RF. Unsteady pressure measurements and numerical investigation of the jet control method in a conical diffuser with swirling flow. IOP Conference Series: Earth and Environmental Science 2010 Aug;12(1):012017.

[7] Bosioc AI, Susan-Resiga R, Muntean S, Tanasa C. Unsteady Pressure Analysis of a Swirling Flow With Vortex Rope and Axial Water Injection in a Discharge Cone. Journal of Fluids Engineering 2012;134(8):081104.

[8] Casanova García F, Mantilla Viveros CA. Experimental analysis of the vibration on the draft tube of a Francis hydraulic turbine during operation at different power levels. Revista Facultad de Ingeniería Universidad de Antioquia 2010;55:90–98.

[9] Cassidy JJ, Falvey HT. Observations of unsteady flow arising after vortex breakdown. Journal of Fluid Mechanics 1970 May;41(04):727–736.

[10] Ciocan GD, Iliescu MS. Vortex rope investigation by 3D-PIV method. In: Proceedings of the 2nd IAHR International Meeting of the Workgroup on Cavitation and Dynamic Problems in Hydraulic Machinery and Systems, Timisoara, Romania; 2007. p. 159–172.

[11] Dahlhaug OG. A study of swirl flow in draft tubes. dissertation, NTNU; 1997.

[12] Dörfler PK, Ruchonnet N. A statistical method for draft tube pressure pulsation analysis. IOP Conference Series: Earth and Environmental Science 2012 Nov;15(6):062002.

[13] Dörfler PK, Sick M, Coutu A. Flow-Induced Pulsation and Vibration in Hydroelectric Machinery: Engineer's Guidebook for Planning, Design and Troubleshooting. Springer Science & Business Media; 2012.

[14] Eaton J, Eaton L. Labtutor: a friendly guide to computer interfacing and LabVIEW programming. Oxford University Press; 1995.

[15] Escudier MP, Bornstein J, Zehnder N. Observations and LDA measurements of confined turbulent vortex flow. Journal of Fluid Mechanics 1980;98(01):49–63.

[16] Faler JH, Leibovich S. Disrupted states of vortex flow and vortex breakdown. Physics of Fluids 1977;20(9):1385.

[17] Faler JH, Leibovich S. An experimental map of the internal structure of a vortex breakdown. Journal of Fluid Mechanics 1978 May;86(02):313–335.

[18] Fjærvold KT. Sprekker i nye Francisløpehjul sett i lys av spenninger og trykkpulsasjonsmålinger. Gardermoen, Norway; 2012. .

[19] Fossen C, Francis-99. NVKS; 2016. `http://www.ntnu.edu/nvks/francis-99`.

[20] Fourier J. The analytical theory of heat. The University Press; 1878.

[21] Foust J, Etter J, Fisher R. Predicting Dissolved Oxygen and Nitrogen Uptake During Turbine Aeration. Proceedings of HydroVision 2008 2008;.

[22] Francke HH. Increasing hydro turbine operation range and efficiencies using water injection in draft tubes. dissertation, NTNU; 2010.

[23] Grein H. Vibration phenomena in Francis turbines: Their causes and prevention. ESCHER WYSS NEWS 1982;55(1):37–42.

[24] Hardin JC. The velocity field induced by a helical vortex filament. Physics of Fluids 1982;25(11):1949.

[25] Harris, F J . On the use of windows for harmonic analysis with the discrete Fourier transform. Proceedings of the IEEE 1976;66(1):51–83.

[26] Harvey JK. Some observations of the vortex breakdown phenomenon. Journal of Fluid Mechanics 1962;14(04):585–592.

[27] Heinzel G, Rüdiger A, Schilling R. Spectrum and spectral density estimation by the Discrete Fourier transform (DFT), including a comprehensive list of window functions and some new at-top windows. Max-Planck-Institut für Gravitationsphysik (Albert-Einstein-Institut) Teilinstitut Hannover; 2002.

[28] Instruments N, The Fundamentals of FFT-Based Signal Analysis and Measurement in LabVIEW and LabWindows/CVI; 2009. `http://www.ni.com/white-paper/4278/en/`, accessed: 23.11.2016.

[29] Instruments N, Understanding FFTs and Windowing; 2015. `http://www.ni.com/white-paper/4844/en/`, accessed: 23.11.2016.

[30] Instruments N, Acquiring an Analog Signal: Bandwidth, Nyquist Sampling Theorem, and Aliasing; 2016. `http://www.ni.com/white-paper/2709/en/`, accessed: 23.11.2016.

[31] Jonsson PP, Mulu BG, Cervantes MJ. Experimental investigation of a Kaplan draft tube – Part II: Off-design conditions. Applied Energy 2012 Jun;94:71–83.

[32] Keller JJ. On the interpretation of vortex breakdown. Physics of Fluids 1995;7(7):1695.

[33] Kirschner O, Schmidt H, Ruprecht A, Mader R, Meusburger P. Experimental investigation of vortex control with an axial jet in the draft tube of a model pump-turbine. IOP Conference Series: Earth and Environmental Science 2010 Aug;12(1):012092.

[34] Kjølle A. Hydraulisk måleteknikk (Hydraulic measurement techniques). Trondheim: NTNU; 2003.

[35] Kobro E. Measurement of pressure pulsations in Francis turbines. dissertation, NTNU; 2010.

[36] Kurokawa J. J-Groove Technique for Suppressing Various Anomalous Flow Phenomena in Turbomachines. International Journal of Fluid Machinery and Systems 2011;4(1):1–13.

[37] Kurokawa J, Kajigaya A, Matsui J, Imamura H. Suppression of Swirl in a Conical Diffuser by Use of J-Groove. In: Proceeding of the IAHR Symposium on Hydraulic Machinery and systems International Association of Hydraulic Research (IAHR); 2000. .

[38] Kurokawa J, Matsui J, Kitahora T, Saha SL. A New Passive Device to Control Rotating Stall in Vaneless and Vaned Diffusers by Radial Grooves. In: Proceedings of JSME International Conference on Fluid Engineering, vol. 2 Japan Society of Mechanical Engineers; 1997. .

[39] Lambourne N, Bryer D. The bursting of leading-edge vortices: some observations and discussion of the phenomenon. HM Stationery Office; 1962.

[40] Leibovich. Vortex stability and breakdown - Survey and extension. AIAA Journal 1984 Sep;22(9):1192–1206.

[41] Leibovich S. The Structure of Vortex Breakdown. Annual Review of Fluid Mechanics 1978;10(1):221–246.

[42] Lomb NR. Least-squares frequency analysis of unequally spaced data. Astrophysics and space science 1976;39(2):447–462.

[43] Lucca-Negro O, O'Doherty T. Vortex breakdown: a review. Progress in Energy and Combustion Science 2001;27(4):431–481.

[44] March P. Hydraulic and Environmental Performance of Aerating Turbine Technologies. In: EPRI, Palo Alto, California, Proceedings of EPRI/DOE Conference on Environmentally-Enhanced Hydropower Turbines: Technical Papers Report; 2011. .

[45] Muntean S, Susan-Resiga R, Campian VC, Dumbra C, Cuzmos A. In situ unsteady pressure measurements on the draft tube cone of the Francis turbine with air injection over an extended operating range. Proc of the 6th Int Conference on Energy and Environment (CIEM) 2013;.

[46] Muntean S, Susan-Resiga R, Bosioc A, Stuparu A, Baya A, Anton LE. Mitigation of Pressure Fluctuation in a Conical Diffuser with Precessing

Vortex Rope Using Axial Jet Control Method. In: Proceedings of the 24th IAHR Symposium on Hydraulic Machinery and Systems, Foz do Iguassu, Brazil; 2008. .

[47] Nakanishi K, Ueda T. Air Supply into Draft Tube of Francis Turbine. Fuji Electric Review 1964;10(3):81–91.

[48] Nishi M. Surging characteristics of conical and elbow type draft tubes. In: Proc. 12th IAHR Symposium on Hydraulic Machinery and System, Stirling, 1984; 1984. p. 272–283.

[49] Nishi M, Wang X, Yoshida K, Takahashi T, Tsukamoto T. An experimental study on fins, their role in control of the draft tube surging. In: Hydraulic Machinery and Cavitation Springer; 1996.p. 905–914.

[50] Nishi M, Liu S. An Outlook on the Draft-Tube-Surge Study. International Journal of Fluid Machinery and Systems 2013;6(1):33–48.

[51] Nishi M, Yoshida K, Yano M, Okamoto M, Miyagawa K, Liu S. A Preliminary Study on the Swirling Flow in a Conical Diffuser with Jet Issued at the Center of the Inlet. In: Proceedings of the 2nd IAHR International Meeting of the Workgroup on Cavitation and Dynamic Problems in Hydraulic Machinery and Systems, Timisoara, Romania; 2007. .

[52] Papillon B, Sabourin M, Couston M, Deschenes C. Methods for Air Admission in Hydro Turbines. In: 21st IAHR Symposium on Hydraulic Machinery and Systems, Lausanne, Switzerland, September; 2002. p. 9–12.

[53] Proakis J, Manolakis D. Digital Signal Processing: Principles, Algotithms, and Applications. Prentice Hall; 1996.

[54] Qian ZD, Li W, Huai WX, Wu YL. The effect of runner cone design on pressure oscillation characteristics in a Francis hydraulic turbine. Proceedings of the Institution of Mechanical Engineers, Part A: Journal of Power and Energy 2012 Feb;226(1):137–150.

[55] Rheingans WJ. Power Swings in Hydroelectric Power Plants. Transaction of ASME 1940;62:171–184.

[56] Åril B. Sønnå Høy - Løpehjulshavari. Gardermoen, Norway; 2009. .

[57] Rocha G, Sillos A. Power swing produced by hydropower units. In: Proceedings of 11th IAHR Symposium, vol. 2; 1982. p. 44.

[58] Ruprecht A, Grupp J, Al-Salaymeh A, Kirschner O. Experimental and numerical investigation of vortex control in a simplified straight draft tube model. In: In Proc. 24th IAHR Symposium on Hydraulic Machinery and Systems, Foz do Iguassu, Brazil; 2008. .

[59] Sarpkaya T. On stationary and travelling vortex breakdowns. Journal of Fluid Mechanics 1971;45(03):545–559.

[60] Sarpkaya T. Vortex Breakdown in Swirling Conical Flows. AIAA Journal 1971;9(9):1792–1799.

[61] Sarpkaya T. Effect of the Adverse Pressure Gradient on Vortex Breakdown. AIAA Journal 1974 May;12(5):602–607.

[62] Sloan DG, Smith PJ, Smoot LD. Modeling of swirl in turbulent flow systems. Progress in Energy and Combustion Science 1986;12(3):163–250.

[63] Squire H. Analysis of the vortex breakdown phenomenon. Imperial College of Science and Technology, Aeronautics Department; 1960.

[64] Standard I. IEC 60041: Field acceptance tests to determine the hydraulic performance of hydraulic turbines, storage pumps and pump-turbines. International Electrotechnical Commission; 1991.

[65] Standard I, IEC 60193: Hydraulic turbines, storage pumps and pump-turbines - Model acceptance testes. International Electrotechnical Commission; 1999.

[66] Stensby KE. Økt installasjon i eksisterende vannkraftverk. NVE; 2011.

[67] Susan-Resiga R, Muntean S, Bosioc A, Stuparu A, Milos T, Baya A, et al. Swirling flow apparatus and test rig for flow control in hydraulic turbines discharge cone. In: 2nd IAHR International Meeting of the Workgroup on Cavitation and Dynamic Problems in Hydraulic Machinery and Systems, Timisoara, Romania, Scientific Bulletin of the "Politehnica" University of Timisoara, Transactions on Mechanics, vol. 52; 2007. p. 203–217.

[68] Susan-Resiga R, Vu TC, Muntean S, Ciocan GD, Nennemann B. Jet control of the draft tube vortex rope in Francis turbines at partial discharge. In: Proceedings of the 23rd IAHR Symposium on Hydraulic Machinery and Systems; 2006. p. 17–21.

[69] Tanasa C, Susan-Resiga R, Bosioc A, Muntean S. Mitigation of pressure fluctuations in the discharge cone of hydraulic turbines using flow-

feedback. IOP Conference Series: Earth and Environmental Science 2010 Aug;12(1):012067.

[70] Thicke RH. Practical Solutions for Draft Tube Instability. Water Power & Dam Construction 1981;Februray 1981:31–37.

[71] Tănasă C, Bosioc A, Susan-Resiga R, Muntean S. Flow-Feedback for Pressure Fluctuation Mitigation and Pressure Recovery Improvement in a Conical Diffuser with Swirl. International Journal of Fluid Machinery and Systems 2011 Mar;4(1):47–56.

[72] Tănasă C, Susan-Resiga R, Muntean S, Bosioc AI. Flow-Feedback Method for Mitigating the Vortex Rope in Decelerated Swirling Flows. J Fluids Eng 2013 Apr;135(6):061304–061304.

[73] Van Dongen H, Olofsen E, Van Hartevelt J, Kruyt E. A procedure of multiple period searching in unequally spaced time-series with the Lomb–Scargle method. Biological Rhythm Research 1999;30(2):149–177.

[74] Vekve T. An experimental investigation of draft tube flow. dissertation, NTNU; 2004.

Part II

Papers

Paper 1

Evaluation of runner cone extension to dampen pressure pulsations in a Francis model turbine
Peter Joachim Gogstad and Ole Gunnar Dahlhaug
IOP Conference Series: Earth and Environmental Science, vol 1, 082019 2016

IOP Conf. Series: Earth and Environmental Science **49** (2016) 082019 doi:10.1088/1755-1315/49/8/082019

Evaluation of runner cone extension to dampen pressure pulsations in a Francis model turbine

Peter Joachim Gogstad and Ole Gunnar Dahlhaug
Waterpower Laboratory, NTNU, 7491 Trondheim, Norway
E-mail: peter.j.gogstad@ntnu.no

Abstract. Today's energy market has a high demand of flexibility due to introduction of other intermittent renewables as wind and solar. To ensure a steady power supply, hydro turbines are often forced to operate more at part load conditions. Originally, turbines were built for steady operation around the best efficiency point. The demand of flexibility, combined with old designs has showed an increase in turbines having problems with hydrodynamic instabilities such as pressure pulsations. Different methods have been investigated to mitigate pressure pulsations. Air injection shows a significant reduction of pressure pulsation amplitudes. However, installation of air injection requires extra piping and a compressor. Investigation of other methods such as shaft extension shows promising results for some operational points, but may significantly reduce the efficiency of the turbine at other operational points. The installation of an extension of the runner cone has been investigated at NTNU by Vekve in 2004. This has resulted in a cylindrical extension at Litjfossen Power Plant in Norway, where the bolt suffered mechanical failure. This indicates high amplitude pressure pulsations in the draft tube centre. The high pressure pulsation amplitudes are believed to be related to high tangential velocity in the draft tube. The mentioned runner cone extension has further been developed to a freely rotating extension. The objective is to reduce the tangential velocity in the draft tube and thereby the pressure pulsation amplitudes.

1. Introduction

Hydropower is a renewable energy source with high efficiency. Moreover, its storage capacity and flexibility in power generation makes hydropower an excellent form of energy generation to ensure steady power supply. Increased amount of intermittent energy generation introduced the last years has increased the flexibility demand of the energy market. This has led to increased part load operation of hydro turbines. Originally, turbines were built for steady operation around the best efficiency point. The demand for flexibility, combined with old designs has shown an increase in turbines having problems with hydrodynamic instabilities such as pressure pulsations. Direct consequences of pressure pulsations may be cavitation erosion and fatigue damages.

Mitigation of pressure pulsations is considered an important task to reduce fatigue damages in order to increase the turbine lifetime. There is a strong coupling between the axial and tangential velocity profiles in the draft tube at part load operation [1]. The radial pressure gradient and the presence of vortex rope is influenced by the tangential velocity [2]. To reduce the tangential velocity, experiments with a freely rotating runner cone extension (FRUCE) has been carried out. Introducing a runner cone extension in the draft tube has previously shown

Content from this work may be used under the terms of the Creative Commons Attribution 3.0 licence. Any further distribution of this work must maintain attribution to the author(s) and the title of the work, journal citation and DOI.
Published under licence by IOP Publishing Ltd

promising result with regards to reduce pressure pulsation amplitudes. When the runner cone extension is rotating freely it will only be driven by the free vortex in draft tube and thereby reduce the tangential velocity and pressure pulsation amplitudes.

2. Background

Rotating machinery such as turbines tend to create periodic pressure fluctuations known as pressure pulsations. Vortex breakdown occurring in the draft tube is recognized as the primary cause of severe flow instabilities and pressure pulsations [3]. Cassidy and Falvey [4] discovered that a helical vortex could form downstream of the vortex breakdown. This phenomenon is often referred to as the rotating vortex rope (RVR) in the hydropower literature [5]. One of the strongest pressure pulsation amplitudes is often related to the RVR. For fixed blade runners, such as Francis, a vortex rope tends to occur in the draft tube at part load operation.

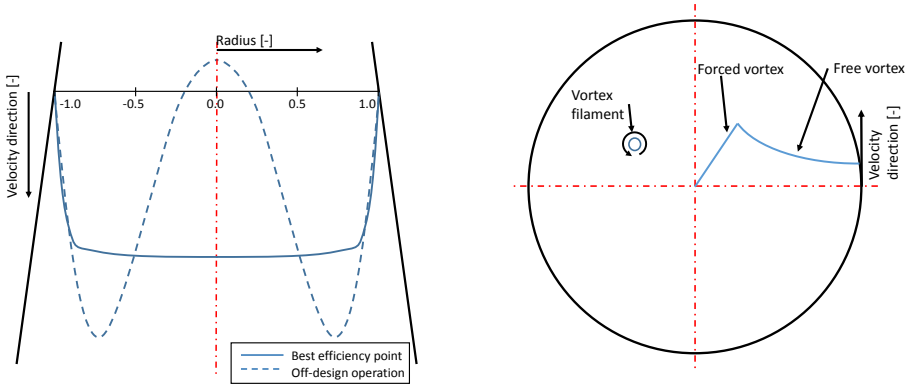

(a) Axial velocity profile

(b) Tangential velociy profile with vortex filament

Figure 1. Theoretical velocity profiles in a turbine draft tube

For Francis runners, performance is influenced by the design of the runner, guide vanes and draft tube. The flow regime in the draft tube is normally described by two velocity components: axial and tangential as illustrated in Figure 1. The tangential velocity is known to be the driving force of the RVR. The tangential velocity profile is generally assumed to be a Rankine vortex, i.e. a combination of a forced and free vortex, as shown in Figure 1b. It illustrates an ideal Rankine vortex which is referred to in the present work. In a typical Francis turbine, the profile of the trailing edge will define the tangential velocity profile at the inlet of the draft tube. The tangential velocity component is also known as the swirl component, as it is the component describing the swirl. The definition of swirl number is as follows;

$$S = \frac{\int_{R_i}^{R_0} v \cdot w \cdot r^2 \cdot dr}{\int_{R_i}^{R_0} v^2 \cdot r \cdot dr} \tag{1}$$

Where w is the tangential velocity component and v is the axial velocity component. For swirl numbers larger than 0.10, a Rankine vortex is present [6][7]. The vortex filament within swirl flow was described analytically by Hardin [8] and Alekseenko and Kuibin [9]. If the swirl is sufficiently strong, the vortex filaments may easily roll up into a single vortex core [10]. This type of filament is also found in draft tubes, where it is observed as a helix or spiral rotating

around the draft tube center [10][11]. In the field of hydropower, the spiral vortex filament is known as a vortex rope. If the pressure is low enough, the vortex rope is visible due to vapor core.

The remaining hydraulic energy in the draft tube is divided between pressure and kinetic energy. The kinetic energy is again divided into three velocity components, where the tangential and axial velocity are dominating. Due to the strong coupling between the axial and tangential velocity components in the draft tube at off design condition [1], the axial velocity profile will change according to Dahlhaug [7] and the static pressure in the radial direction will change. For swirl numbers higher than one, vortex breakdown occurs and the axial flow in the central region of the draft tube will reach zero and reverse flow may occur. The vortex rope is located in the shear layer between the central stalled region and the swirling main-flow with a low pressure zone in the center of the vortex rope [10]. Particle Image Velocimetry (PIV) measurements performed by Ciocan and Iliescu [12] demonstrated the movement of the rotating vortex rope. The movement of the vortex rope was also documented with Laser Doppler Vibrometer (LDV) by Vekve [2]. Reducing the maximum tangential velocity seems to be one of the keys to mitigate pressure pulsations in the draft tube, as this approach reduces the swirl number.

Different methods have been investigated to mitigate pressure pulsations, such as air injection, water injection and other passive installations in the turbine. Different methods of air injection have been investigated by different authors [3][13][14][15][16]. Results are case dependent, meaning a decrease in pressure pulsation amplitudes at one turbine, does not mean the same result in another. Both an increase and a decrease in pressure pulsation amplitudes were observed by Muntean et.al. [16], depending on operational point. Further, March [14] pointed out there may be significant efficiency losses, up to 4% related to air injection. The efficiency loss is dependent on method of air injection and amount of air. Increased air volume flow lead to increased losses as shown by March [14].

Passive installation such as fins and runner cone extension has been tested by different authors [2][17][18][19]. A runner cone extension tested at NTNU by Vekve [2] showed promising results in reduction of pressure pulsation amplitudes. Vekve tested two different lengths with three different diameters of $0.1D_2$, $0.21D_2$ and $0.41D_2$. The longest runner cone extension with largest diameter showed the best dampening of pressure pulsastion amplitudes. This resulted in a full scale test at Litjfossen Hydro Power Plant in Norway. The test showed minor reduction in efficiency ($\tilde{0}.5\%$), but 30-40% reduction in pressure pulsation amplitudes at part load. Vekve concluded that the shaft extension moves the initiation point of the vortex rope further downstream and can reduce the strength of the vortex rope (i.e., the amplitude of the RVR). The further downstream the vortex breakdown occurs, the shorter the distance the RVR has available for longitudinal development. Eventually, the bolt keeping the runner cone extension in place suffered mechanical failure, and the runner cone extension was found further downstream. This indicates high amplitude pressure pulsations in the draft tube centre.

A numerical investigation of a counter rotating cone in a Kaplan elbow was performed by Cervantes [20]. Though he did not extend the runner cone, he found that a slower rotation than the runner increased pressure recovery and reduced the losses. The results also found a stationary runner cone to be beneficial for the draft tube performance. This paper will further investigate a freely rotating runner cone extension at a model turbine. The focus of the paper will be possible improvements with a freely rotating runner cone extension (FRUCE).

3. Experimental setup

The experiment was carried out at the Waterpower Laboratory at NTNU in Trondheim. The Tokke model runner, which is a high head Francis runner, was used for the experiments. This turbine is also the model runner used as a reference in Francis-99 workshops [21]. In order to investigate the pressure fluctuations in the draft tube cone, four Kulite 701A dynamic pressure

Table 1. Operational points

Operational points	Guide vane opening [degrees]	Volume flow $[m^3/s]$	Relative Volume flow Q/Qbep [-]
1	3,999	0,086	0,43
2	5,009	0,106	0,53
3	6,020	0,127	0,63
4	7,031	0,147	0,73
5	8,129	0,169	0,84
6 (BEP)	9,887	0,202	1,00
7	11,030	0,223	1,11
8	11,997	0,241	1,20
9	13,051	0,256	1,29

sensors were flush mounted as shown in Figure 2. Two sensors in the upper cone labeled P1 and P2, and two in the lower cone labeled P3 and P4. Two and two sensors were mounted directly opposite to each other. Additional pressure sensors were mounted at inlet and downstream the runner cone, but the analysis from these will not be included in this paper. The rotation of the runner cone extension was measured optically.

The measurements was carried out with a constant head of 12 m and constant rotational speed at 333 rpm. NI Labview was used to acquired the data. The pressure data was amplified and acquired with a logging frequency of 2777.8 Hz with NI 9239 logging card. The different operating points are shown in Table 1.

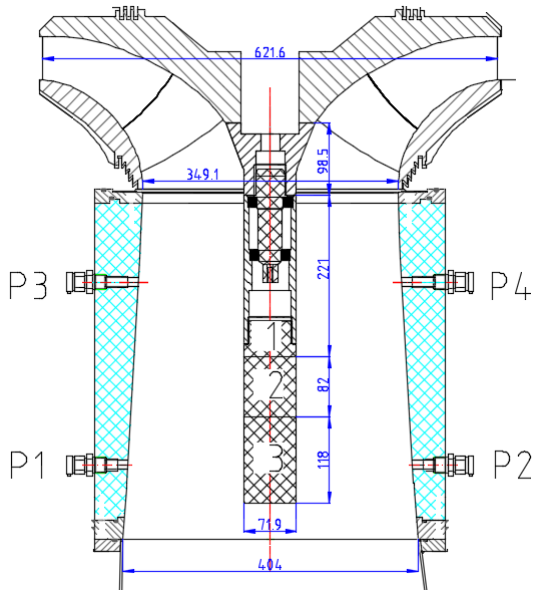

Figure 2. Freely rotating runner cone extension with the different lengths; FRUCE 1 = $0.62D_2$, FRUCE 2 = $0.86D_2$ and FRUCE 3 = $1.20D_2$. The location of pressure sensors can be seen on the draft tube wall. The dimension in the drawing is given in millimeters

4. Freely rotating runner cone extension

The runner cone extension was designed as a cylinder. The runner cone was modified to fit the extension. Figure 2 shows the drawing of the modified runner cone and with the extension. A transition part with bearings was fitted between the runner cone and the extension to allow the extension to rotate freely. The runner cone extension was tested with three different lengths; $0.62D_2$, $0.86D_2$ and $1,20D_2$, where is D_2 the outlet diameter. The diameter of the runner cone extension, D_s, was $0.21D_2$ for all lengths.

5. Data processing

The pressure data was processed to investigate the frequency spectra, peak-to-peak values. For this paper the data was resampled to a frequency of 500 Hz. An antialiasing Finite Impulse Response (FIR) lowpass filter was applied and the time delay introduced by the filter was compensated for. Further, a lowpass Butterworth filter was applied with a cut-off frequency of $2.2f_n$, where f_n is the runner frequency equals to 5.55 Hz. The cut-off frequency was chosen to filter out rig specific frequencies at 15 Hz and 40 Hz. Peak-to-peak values was found by using a 99% confidence interval. The effective confidence interval is lower than 99% since a filter has been applied to the data. Fast Fourier Transform (FFT) was applied to achieved the frequency spectra.

6. Results and discussion

6.1. Measurements of rotation

The rotation of the runner cone extension was measured optically and shown in Fig. 2. The largest rotational speed is reached at full load, where the FRUCE is rotating the opposite direction of the turbine. The rotational speed reached -1.08 relative speed for the longest FRUCE. The velocity of FRUCE seems to have linear relationship from $0.84Q/Q_{BEP}$ to full load at $1.29Q/Q_{BEP}$. At full load there is not much separating the different FRUCEs.

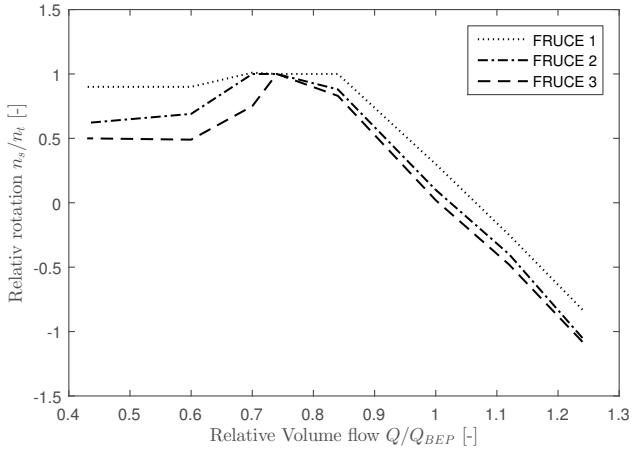

Figure 3. FRUCE rotation as a function of flow rate. The relative speed is given by the FRUCE rotational speed, n_s, and the runner speed, n_t.

Compared to a locked runner cone extension, the velocity of the FRUCE is reduced at low load. The lowest rotational speed is found for the longest FRUCE. This is due to the tangential

velocity in the lower part of the draft tube is reduced. The lower tangential velocity is helping to reduce the speed of the runner cone. This is also the area where the largest amplitudes related to the Rheingans frequency is found.

At part load the length clearly has influence on the rotational speed of the FRUCE. All the three FRUCEs reached runner speed at $0.73Q/Q_{BEP}$, but they never increase above rotational speed of the runner. The longest FRUCE reduces the speed first and reached the lowest speed when moving toward lower flow rate.

6.2. Pressure analysis

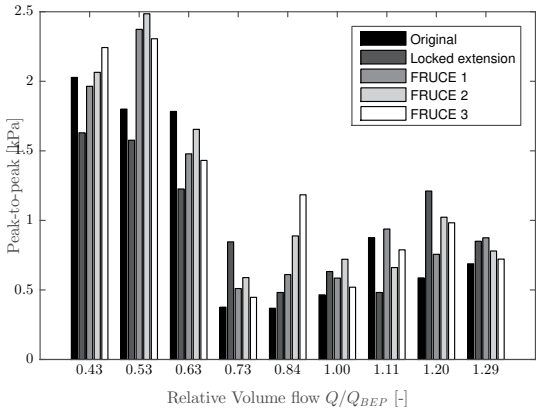

Figure 4. Peak-to-peak values for a 99% confidence interval for the upper measuring plane of the Francis model draft tube

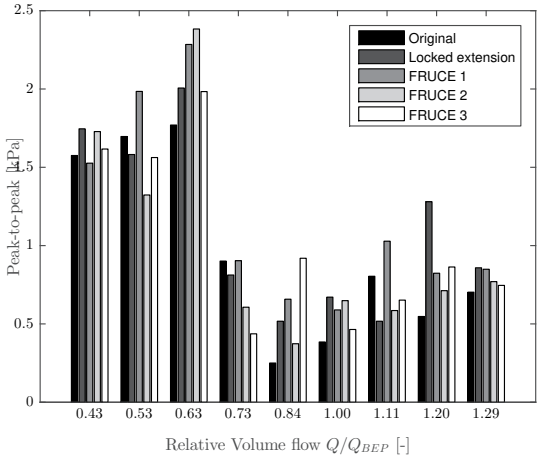

Figure 5. Peak-to-peak values for a 99% confidence interval for the lower measuring plane of the Francis model draft tube

The peak-to-peak values with a 99% confidence interval for the upper plane is shown in Figure 4 and in Figure 5 for the lower plane. The locked runner cone extension clearly has an dampening effect on the amplitudes in the upper plane at part load. However, the difference in the lower plane is minor. In both cases the locked runner cone extension has a negative effect at $1.2Q/Q_{BEP}$. The FRUCEs have increased peak-to-peak values in the upper plane at $0.53Q/Q_{BEP}$, while a small dampening can be seen for the two longest FRUCEs in the lower plane. The opposite effect can be observed when the flow is increased to $0.63Q/Q_{BEP}$. Higher amplitudes for the FRUCEs in the lower plane, but dampened in the upper plane.

The high peak-to-peak values at the upper plane is probably a consequence of the FRUCE diameter. It removes the forced votex in the draft tube center and allow the free vortex to develop towards the FRUCE diameter. The free vortex will therefore reach a higher velocity at the surface of the FRUCE than it would without. The authors assume this is the reason for the increasing pressure amplitude. Considering conservation of angular momentum, the tangential velocity profile will change due to the expansion of the draft tube cone. The tangential velocity profile will therefore reach a lower velocity at the FRUCE as shown with the modified velocity profile in Figure 6. The speed of the FRUCE will be influenced by the sum of the viscous forces working in tangential direction.

At $0.63Q/Q_{BEP}$ the peak-to-peak values are lower in the upper plane, than in the lower. A small dampening can be found in comparison to the original design in the upper plane. The authors have no explanation for this phenomenon. However, the FRUCE velocity is increased at this flow rate compared to lower flow rate where the FRUCE speed is fairly constant. This may cause a transmission of energy to lower measuring plane and therefore an increase in peak-to-peak values.

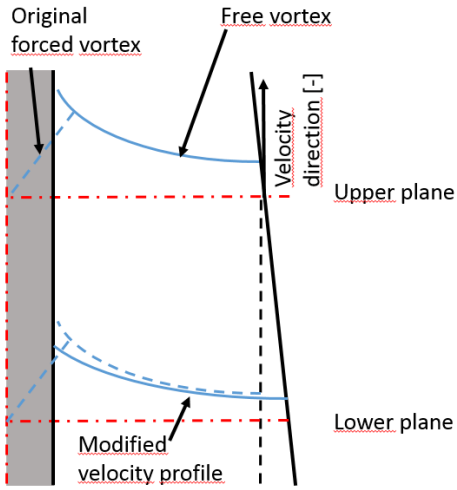

Figure 6. Ideal tangential velocity profiles at upper an lower measuring plane with FRUCE. The ideal velocity profile is shown with a dashed line in the lower plane and the modified velocity profile is shown with a solid line.

At high load the FRUCEs generally performs better than the locked runner cone extension for flows larger than $1.2Q/Q_{BEP}$. The peak-to-peak values are clearly more consistent from upper to lower plane with higher flows than $0.73Q/Q_{BEP}$. From $0.84Q/Q_{BEP}$ and higher, the original design shows the smallest peak-to-peak values except at $1.11Q/Q_{BEP}$.

The frequency spectra presented are focused on the low frequency amplitudes, especially related to the RVR. The runner frequency, f_n, is 5.5 Hz for all operational points as the runner speed was kept constant.

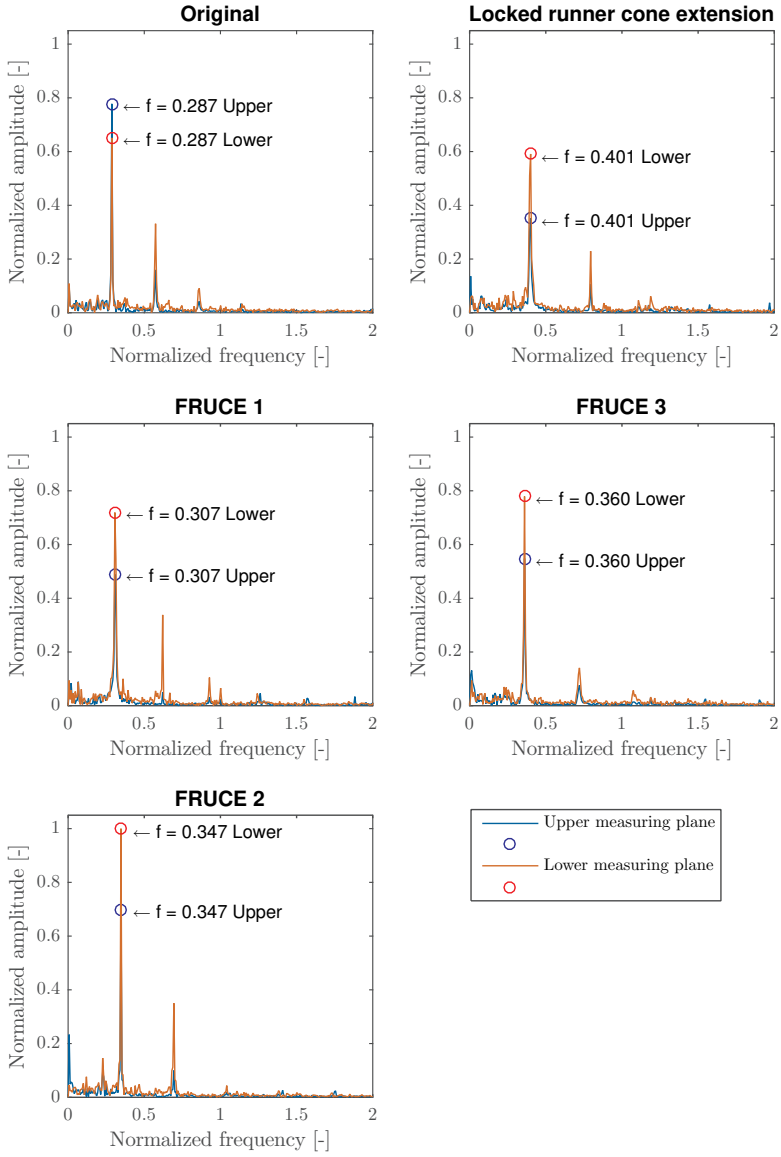

Figure 7. Frequency analysis for $0.63Q/Q_{BEP}$ with upper and lower measuring plane

The frequency spectra from upper and lower measuring plane shown in Figure 7 show two significant peaks at $0.29f_n$ and $0.57f_n$. The dominant frequency at $0.29f_n$ is the vortex rope frequency for the original design. In the lower measuring plane this frequency has an increased amplitude for FRUCEs while a small dampening can be noted for the locked runner cone extension. However, in the upper measuring plane there are a significant dampening for all runner cone extensions. The amplitude for the dominating frequency for FRUCE 3 is decreased by 30%, while for the locked runner cone extension the reduction in amplitude is 55%. The reduction in amplitudes are greater than what can be seen from the peak-to-peak analyses. The vortex rope frequency is also shifted towards a higher frequency with the installation of the FRUCEs. The trend is the longer FRUCE, the higher dominating frequency. However, the locked runner cone extension produces the highest frequency.

7. Conclusion

The results show that the freely rotating runner cone extension has an dampening effect in some cases at part load. However, only the locked runner cone extension shows better dampening effect in most cases. From $0.84Q/Q_{BEP}$ and higher, the original design shows the smallest peak-to-peak values expect at $1.11Q/Q_{BEP}$.

The tangential velocity of the water is highest at $0.73Q/Q_{BEP}$. However, the highest peak-to-peak values are found at lower flow rate than $0.73Q/Q_{BEP}$.

The FRUCE did not achieve the dampening which was hoped for. This is most likely due to a to small diameter of the FRUCE. Previous results from Vekve [2] shows improvement with increased diameter. An increased diameter will also increase the axial velocity more and thereby decrease the swirl number.

References

[1] Lucca-Negro O and O'Doherty T 2001 *Progress in Energy and Combustion Science* **27** 431–481 ISSN 0360-1285
[2] Vekve T 2004 *An experimental investigation of draft tube flow* Ph.D. thesis
[3] Baya A, Muntean S, Câmpian V C, Cuzmoş A, Diaconescu M and Bălan G 2010 *IOP Conference Series: Earth and Environmental Science* **12** 012007 ISSN 1755-1315
[4] Cassidy J J and Falvey H T 1970 *Journal of Fluid Mechanics* **41** 727–736 ISSN 1469-7645
[5] Jonsson P, Mulu B and Cervantes M 2012 *Applied Energy* **94** 71–83 ISSN 03062619
[6] Sloan D G, Smith P J and Smoot L D 1986 *Progress in Energy and Combustion Science* **12** 163–250 ISSN 0360-1285
[7] Dahlhaug O G 1997 *A study of swirl flow in draft tubes* Ph.D. thesis
[8] Hardin J C 1982 *Physics of Fluids* **25** 1949 ISSN 00319171
[9] Alekseenko S and Kuibin P 1995 *Numerical methods in laminar and turbulent flow.* **9** 382–393
[10] Nishi M and Liu S 2013 *International Journal of Fluid Machinery and Systems* **6** 33–48
[11] Dörfler P, Sick M and Coutu A 2012 *Flow-Induced Pulsation and Vibration in Hydroelectric Machinery: Engineers Guidebook for Planning, Design and Troubleshooting* (Springer Science & Business Media)
[12] Ciocan G D and Iliescu M S 2007 Vortex rope investigation by 3D-PIV method *Proceedings of the 2nd IAHR International Meeting of the Workgroup on Cavitation and Dynamic Problems in Hydraulic Machinery and Systems, Timisoara, Romania* pp 159–172
[13] Papillon B, Sabourin M, Couston M and Deschenes C 2002 Methods for Air Admission in Hydro Turbines *21st IAHR Symposium on Hydraulic Machinery and Systems, Lausanne, Switzerland, September* pp 9–12
[14] March P 2011 Hydraulic and Environmental Performance of Aerating Turbine Technologies *EPRI, Palo Alto, California, Proceedings of EPRI/DOE Conference on Environmentally-Enhanced Hydropower Turbines: Technical Papers Report*
[15] Casanova Garcia F and Mantilla Viveros C A 2010 *Revista Facultad de Ingeniera Universidad de Antioquia* 90–98
[16] Muntean S, Susan-Resiga R, Campian V C, Dumbra C and Cuzmos A 2013 *Proc. of the 6th Int. Conference on Energy and Environment (CIEM)*
[17] Qian Z D, Li W, Huai W X and Wu Y L 2012 *Proceedings of the Institution of Mechanical Engineers, Part A: Journal of Power and Energy* **226** 137–150 ISSN 0957-6509, 2041-2967

[18] Thicke R 1981 *Water Power & Dam Construction* **Februray 1981** 31–37
[19] Nishi M, Wang X, Yoshida K, Takahashi T and Tsukamoto T 1996 An experimental study on fins, their role in control of the draft tube surging *Hydraulic Machinery and Cavitation* (Springer) pp 905–914
[20] Cervantes M J 2009 Counter rotating runner cone in a Kaplan elbow draft tube for increased efficiency *3rd IAHR International Meeting of the Worksgroup on Cavitation and Dynamic Problems in Hydraulic Machinery and Systems*
[21] Fossen C Francis-99 URL `http://www.ntnu.edu/nvks/francis-99`

Paper 2

Investigation of the Unsteady Pressure Pulsations in the Francis Turbine Prototypes-Part 1: Steady State Operating Conditions
Chirag Trivedi, Peter Joachim Gogstad and Ole Gunnar Dahlhaug
Submitted to Mechanical Systems and Signal Processing 2016

Is not included due to copyright

Paper 3

Investigation of the Unsteady Pressure Pulsations in the Francis Turbine Prototypes-Part 2: Transient Operating Conditions
Chirag Trivedi, Peter Joachim Gogstad and Ole Gunnar Dahlhaug
Submitted to Mechanical Systems and Signal Processing 2016

Is not included due to copyright

Paper 4

Experimental investigation of air injection in high head Francis turbine

Peter Joachim Gogstad and Ole Gunnar Dahlhaug

Submitted to Hydropower and dams 2017

Experimental investigation of air injection in high head Francis turbine

Peter Joachim Gogstad and Ole Gunnar Dahlhaug
Waterpower Laborotory, NTNU, Trondheim, Norway
E-mail: peter.j.gogstad@ntnu.no

Abstract. Pressure pulsations caused by unsteady flow can lead to instability of operation. Air injection into the turbines draft tube is a well-known method used to mitigate pressure pulsations. Investigation of two different methods of air injection into the high head turbines in La Higuera power plant were carried out for part load operation. The turbines have a nominal power of 77 MW each and 375 m head. Two methods of air injection were investigated; air injection through the upper cover and air injection through the draft tube wall. Pressure pulsations were measured at the inlet and in the draft tube.

1. Introduction

Today's energy market has a high demand of flexibility due to introduction of other renewables as wind and solar. To ensure steady power supply, hydro turbines are forced to operate more at part load. The turbine itself will be exposed to variation in pressure, discharge, rotational speed and torque. These phenomena are strongly linked to the flow structure at the outlet and leads to hydrodynamic instabilities [1]. Hydrodynamic instabilities as pressure pulsations, in combination with natural frequencies that may result in a resonance effect, leading to draft tube surge and grid instabilities [2]. Swirling flows in turbines have for a long time been subject to intensive research. For Francis turbines operating at part load, swirl in the draft tube is present due to the fixed blade of the Francis runner. Rheingans [2] found the swirling flow to have a frequency of 1/3 of the runner frequency. The vortex breakdown occurring in the draft tube is recognized as the main cause of severe flow instabilities and pressure fluctuations [3]. The pressure pulsations are known to generate heavy vibrations and noise [4], which may give high fatigue load and ultimately lead to mechanical failure [3][5]. Consequently, research on design and methods to mitigate pressure pulsations have been intensified.

Different authors have proposed and tested several methods to mitigate pressure pulsations. The most well-known method is perhaps air injection into the draft tube. However, water injection [6, 7] and fins [8] have also been investigated with varying results. Air injection has been done in different ways, air injection over the stay vanes [9, 10] or air admission directly into the draft tube [11]. A case study of Hirakud Power Plant shows a significant reduction of vibrations with air injection below the runner [12]. Garcia [10] reached the conclusion that an air discharge equal to 0.34% of the water discharge was enough to improve the hydraulic stability. However, air injection may also have negative effects. In an extreme case the amplitude was increased by 41.8%. Measurements of Baya et.al. [3] indicates that the highest amplitudes are found closest to the turbine, while Susan-Resiga [13] finds the highest amplitudes to be further

downstream. The design of the turbine and draft tube are therefore an important factor in how the pressure pulsations amplitudes propagates in the draft tube.

2. La Higuera Hydropower Plant Case Study

La Higuera Hydro Power Plant is located in the Andes south of Chiles capital Santiago. It consist of two vertical axis units of 77 MW each. Turbine data is listed in table 1

The power station has suffered from strong vibrations since the start up in 2010. Different circumstances caused it to close down in 2011. During the recommissioning in 2013 different methods of air injection was tested to help reduce the vibrations. The methods are further described in the next section.

Table 1: Data per unit at La Higuera HPP

La Higuera power plant	
Number of turbines	2
Nominal net head	375 m
Rated generator output	77 MW
Nominal volume flow	22.7 m/s^3
Nominal speed	600 rpm
Outlet diameter	1.57 m

3. Experimental Setup

Two different setups of air injection were tested as shown in Figure 1.

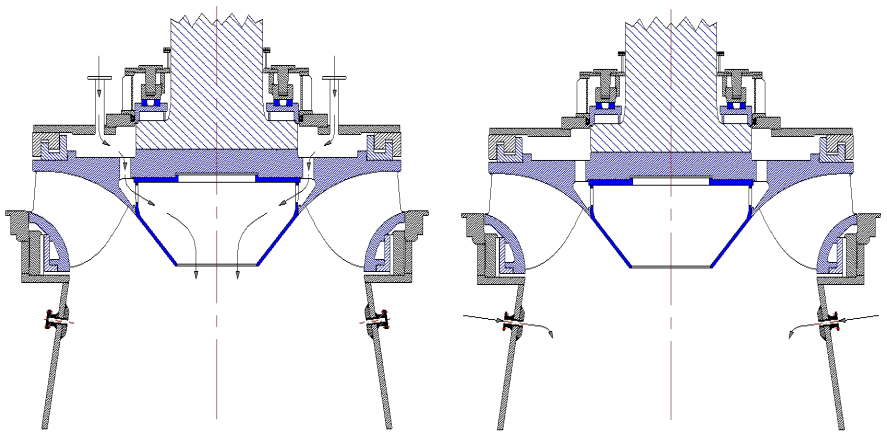

(a) Option A: Air injection through upper cover (b) Option B: Air injection through draft tube wall

Figure 1: Air injection methods for La Higuera

Option A: Air injection through upper cover. The turbine manufacturer installed this option. It allows air to pass through the upper cover and enter in the draft tube from the runner cone as shown in figure 1a.

Option B: Air injection through the draft tube wall. This was installed during the period the power station was unoperational. Air is injected through four nozzles around the draft tube fitted approximately 250 mm downstream the runner outlet as shown in Figure 1b.

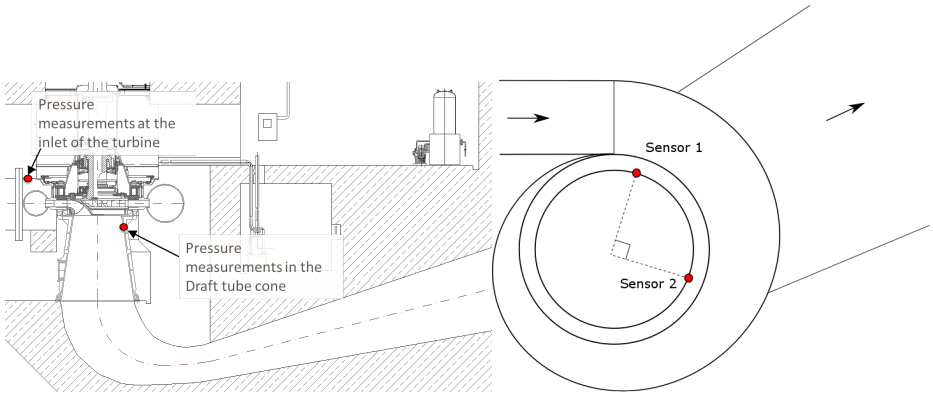

(a) Crossection (b) Pressure sensors at the draft tube

Figure 2: Mounted pressure sensors

The experimental investigation was performed at 13 operating points, where the 13 point was the reference at best efficiency point (BEP) with 6 measuring points for each air injection option. A complete list of the measuring points can be found in Table 2. The load was varried from 28% to 80% of best efficiency point. Operating at loads above 80% was not considered a problem and therefore not further investigated. Table 2 includes the amount of air injected at each measurement point. The amount of air injected was limited due to the capacity of the compressor. This removed the possibility to investigate the dynamic behavior of the draft tube flow with higher air ratios. No optimization of air injection was done due to compressor limitations. Measuring time for each operational point was 200 seconds.

In order to measure the pressure pulsations in the draft tube, two sensors were fitted approximately 0.3 m downstream the runner and one sensor was placed upstream the turbine as shown in Figure 2. The sensors on the draft tube wall were mounted with approximately 90° between each other in a horizontal plane. The atmospheric pressure was measured on the turbine floor.

Pressure measurements were only performed in one plane in the draft tube. It is therefore not possible to conclude if the pressure pulsation amplitudes will increase or decrease downstream the measurement plane.

High-speed pressure sensors were used for the measurement with a logging frequency of 2500 Hz. Upstream the turbine, a PTX1400 (0-100 bar a) sensor was used. Downstream, one PTX610 (0-10 bar a) and one PTX1400 (0-10 bar g) was used to measure pressure pulsations. The sensor signals was logged digitally with LabView.

Table 3 show a list over expected frequencies based on the turbine data. The blade passing frequency and the rotational frequency is independent of operational point. The Rheingans frequency is expected to change somewhat depending on operational point due to the change in the swirl of the flow.

Table 2: Operational points included

Option A			Option B		
Load [%]	Air injected [l/s]	% of water flow	Load [%]	Air injected [l/s]	% of water flow
28.1	138	1.48	29.2	202	2.17
39.3	264	2.27	41.0	214	1.84
49.7	254	1.78	49.7	243	1.70
59.0	198	1.25	59.2	239	1.51
70.8	211	1.23	68.4	248	1.45
77.9	253	1.27	79.6	218	1.09
106,6	0,0	0,00			

Table 3: Expected frequencies

Frequency	Range [Hz]
Blade passing frequency	170
Rotational speed	10
Rheingans frequency	2-4

4. Analysis Method

The peak to peak value was investigated to identify changes in the pressure pulsations. The peak-to-peak value for each measuring block of one second was averaged to find the values presented. Further, a frequency analysis of the different air injection methods was performed.

The logging program updated every second in order to write to file, this lead to a small time gaps between each measuring block. Due to the 'write to file' pauses in the logging program, a missing data point problem occurred in the spectral analysis. Common spectral analysis methods require a constant time step, Δt, which was not constant in this case. The larger Δt which occured every second can be evaluated as loss of data points. The loss of data points is therefore a loss of information of the physical process.

There are different solutions to a data loss problem. A non-ideal solution to the problem is truncation of the time signal in the missing data area. Truncation of a time series before applying Fast Fourier Transform (FFT) algorithms will in general result in non-physical and spurious distortion, which often is seen in the low frequency band. When the original frequency is not known, these spurious results cannot be identified, hence the frequency spectra is not fully trustworthy. The Rheingans frequency is not constant and the low frequency band is the main focus. Truncation of the time signal is therefore not an acceptable solution.

To avoid truncation, an option is to perform a FFT on each block with constant time step, and thereby average the results. As the blocks are short in time, it will result in a far from satisfactory frequency resolution, especially for investigating the low frequency band. A significant level of white noise will also be introduced by using this method.

Other non-ideal methods to cure the problem could be to add zeroes or extrapolate the data for the missing time steps. Both methods will eliminate the time scale problem, but will introduce errors.

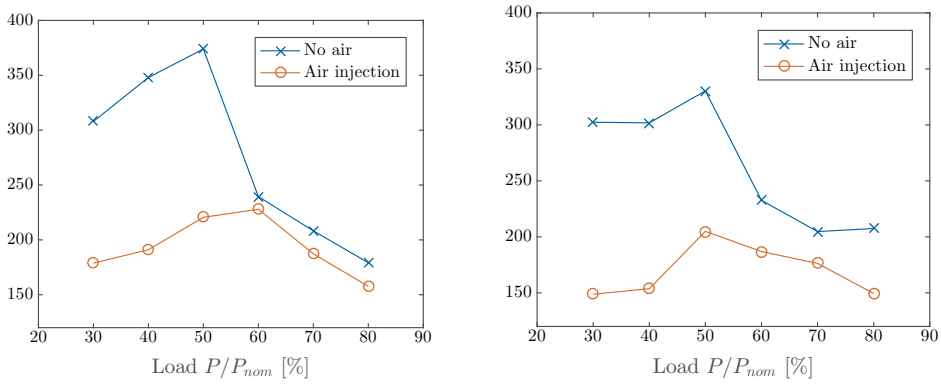

(a) Option A

(b) Option B

Figure 3: Peak-to-peak values with and without air injection

The missing data point problem is well known within geophysics from satellite transmissions. The measured signal transmitted is often disrupted by the satellite passing through a transmission shadow. The countermeasure developed is known as the least-square spectral analysis [14], commonly known as the Lomb-Scargle method, or Lomb normalized periodogram. The method weights data on a 'per point' basis instead of on a 'per time interval' basis as FFTs. This allows for a non-uniform time steps in the time series and avoiding truncation, zero insertion and extrapolation. However, computational costs are significantly increased from less than a second to more than an hour. Another aspect to be aware of is that the Nyquist frequency fn=fs/2 is not respected by the Lomb normalized periodogram. Hence, higher frequencies than the Nyquist frequency appear in the results. These are not to be trusted as these may be aliases. To avoid this, a low pass filter with cut-off frequency of half the logging frequency was used before applying the Lomb method. The highest frequency expected, the blade passing frequency, in the La Higuera turbine is 170 Hz which is well below the Nyquist frequency [15].

5. Results

Figure 3 shows the 99% confidence interval peak-to-peak values with and without air injection for each part load operational point investigated. A significant decrease in peak-to-peak values was found for 30-50% load with both methods of air injection. For higher loads, 60%-80%, a smaller decrease can be seen. The peak-to-peak amplitudes when air is injected are between 200 and 300 kPa for every load. For all measurements, a significant decrease in noise was noticed. Approximate measurements indicated the noise was reduced with 8-12 dB. This suggest a significant reduction of pressure pulsation amplitudes of higher frequency.

The spectral analysis for both options is shown in figure 4 and 5. The fundamental harmonic corresponds to the vortex rope, also known as the Rheingans frequency. The prominent peak is located between 2 and 4 Hz as expected. This frequency is somewhat lower than a third of the runner frequency as Rheingans found. This is due to design of the runner. The second harmonic is also clearly visible for loads above 50%. The vortex rope frequency also have a small shift towards a higher frequency when air is injected. For lower loads a significant decrease in amplitudes can be seen. However, for loads between 60% and 80%, the results are not consistent. For both options, sensor 1 shows a decrease in amplitudes for 80% load, while option A clearly

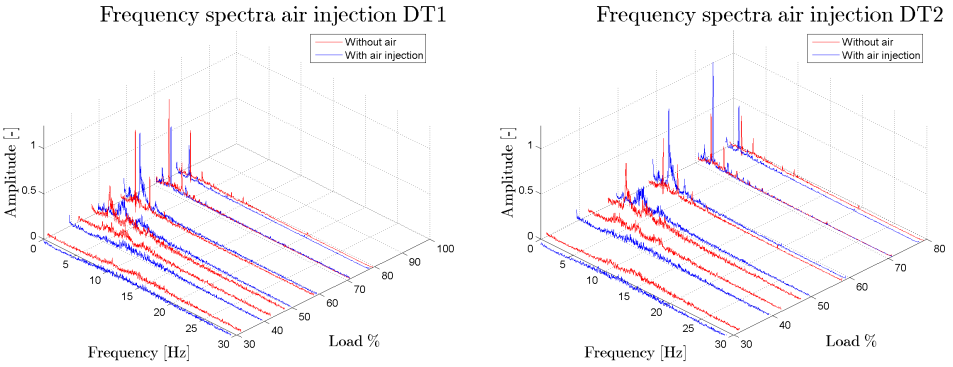

(a) Sensor 1 (b) Sensor 2

Figure 4: Option A

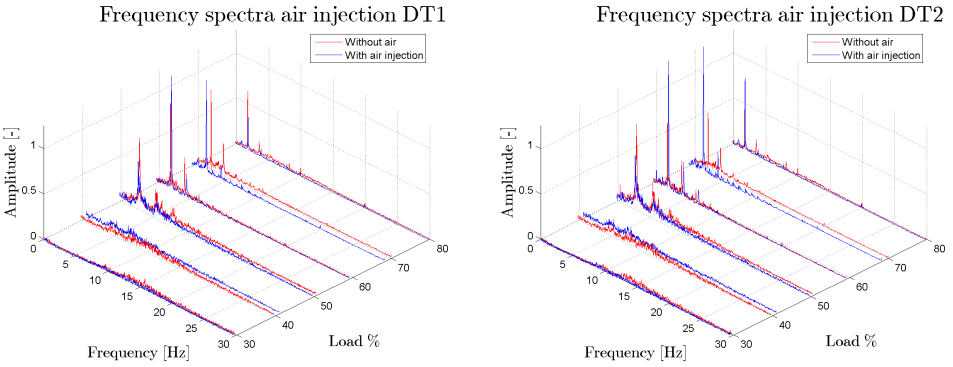

(a) Sensor 1 (b) Sensor 2

Figure 5: Option B

decreases the amplitudes for 60 and 70% load. Results from sensor 2 shows the initial amplitude of the dominant frequency is significantly lower than for sensor 1. The air injection also have a negative effect in this area, increasing the amplitudes with more than 100% in several cases. Option B has a smaller reduction in the dominant amplitude at sensor 1 and inflict a greater increase of the dominant frequency at sensor 2 than seen from option A.

The 10 Hz frequency is the runner speed and its second harmony is visible for 60% load and upwards.

Further investigation of pressure pulsations was carried out to explain the reduction in noise measured. Figure 6 shows that when air is injected the frequency amplitudes are reduced for frequencies above 300 Hz. For lower frequencies, the frequency amplitudes are higher when air is injected compared to operation without air injection. This matches well with decreased sound volume within the hearing range. The peak-to-peak values are a sum of all frequencies. An increase in frequency amplitudes for some frequencies and a decrease in freqeuncy amplitudes for many frequencies will give an overall reduction in peak-to-peak amplitudes. This will explain

why an increase in Rheingans frequency was measured when air was injected, but a significant decrease in peak-to-peak values was observed.

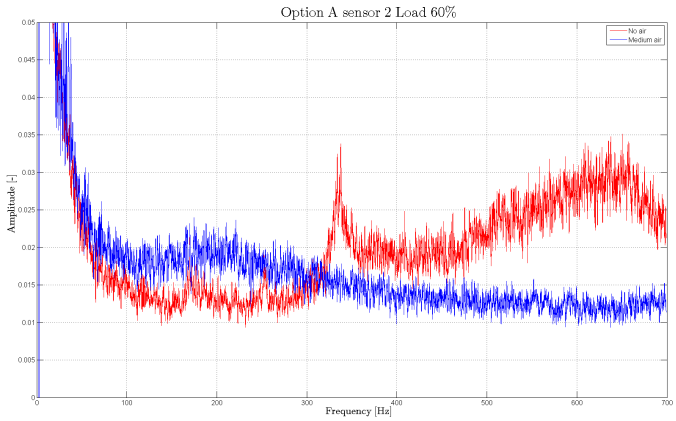

Figure 6: Frequency plot for 60% load

6. Conclusion

The paper presents an investigation of methods of reducing pressure pulsations amplitudes in Francis turbines with air injection. On site experimental investigations were performed to evaluate the performance of air injection as a method of reducing pressure pulsations amplitudes. For this specific turbine, the pressure pulsations were recorded with two sensors in the draft tube. A significant decrease in average peak-to-peak values were found for all loads. At lower loads, 30-50% of BEP, air injection significantly reduced the peak-to-peak amplitudes with up to 60%. The frequency analysis showed that air injection has a positive effect on amplitudes for frequencies higher than approximately 300 Hz. For frequencies lower than 20 Hz, the dominant frequency increased with more than 100% in several cases at sensor 2. At sensor 1, a decrease was found for option A, while option B still increased the dominant frequency amplitude for 60 and 70% load. The results is favorable towards option A, air injection through the upper cover. Measurement of noise level showed a reduction of 8-12% when air was injected.

Air injection reduced the peak-to-peak values, but did not decrease the amplitudes of the low frequency pressure pulsations. The dominant frequency increased significantly in some cases. The increase of the dominant frequency may in a worst-case scenario lead to mechanical failure. Therefore, it is recommended to investigate the air injection control for each turbine in order to identify dangerous operating regimes.

References

[1] Nicolet A, Arpe J and Avellan F 2004 *Proceedings of the 22nd IAHR Symposium on Hydraulic Machinery and Systems* (Stockholm, Sweden)
[2] Rheingans W 1940 *Trans. ASME* **62** 171–184
[3] Baya A, Muntean S, Câmpian V, Cuzmoş A, Diaconescu M and Bălan G 2010 *IOP Conference Series: Earth and Environmental Science* vol 12 (IOP Publishing) p 012007
[4] Grein H 1982 *Escher Wyss News.* **55** 37–42
[5] Casanova García F and Mantilla Viveros C A 2010 *Revista Facultad de Ingeniería Universidad de Antioquia* 90–98

[6] Susan-Resiga R, Vu T C, Muntean S, Ciocan G D and Nennemann B 2006 *Proceedings of the 23rd IAHR Symposium on Hydraulic Machinery and Systems* pp 17–21
[7] Kjeldsen M, Olsen K, Nielsen T and Dahlhaug O 2006 *Meeting of WG on Cavitation and Dynamic Problems in Hydraulic Machinery and Systems, Barcelona*
[8] Thicke R 1981 *Water Power & Dam Construct.* **33** 31–37
[9] Poll H G, Zanutto J C and Ponge-Ferreira W 2006 *Shock and Vibration* **13** 409–427
[10] García F C and Viveros C A M 2010 *Revista Facultad de Ingeniería Universidad de Antioquia* 90–98
[11] Fraser R, Désy N, Demers É, Deschênes C, Fau J and Hamel S 2011 *Proceedings of Waterpower XIV*
[12] Swain M 2008 *Electrical India* **48** 68
[13] Muntean S, Susan-Resiga R F, Câmpian V C, Dumbravă C and Cuzmoş A 2013 *Proc. of the 6th Int. Conference on Energy and Environment (CIEM), Bucharest*
[14] Lomb N R 1976 *Astrophysics and space science* **39** 447–462
[15] Van Dongen H, Olofsen E, Van Hartevelt J and Kruyt E 1999 *Biological Rhythm Research* **30** 149–177

Part III

Appendix

Appendix A

Deduction of the thermodynamic method

This chapter is an deduction of the thermodynamic method for efficiency measurements based on Kjølle [34] and the IEC 60041 [64].

A.1 Efficiency measurement

Efficiency is the ratio of the work done or energy developed by a machine, to the energy supplied to it. In the world of hydro power, the energy supplied is the water from the upper reservoir and the output is electricity to the grid. The higher efficiency, the more money is earned. The efficiency is an important input when it comes to optimizing power production and investments to refurbish power plants. To find the efficiency, efficiency measurements have to be performed. Efficiency measurements will also give information about the condition of a turbine. A drop in efficiency indicates degradations in the turbine or the waterways.

The efficiency for a turbine can be expressed as following:

$$\eta = \frac{P}{P_h} = \frac{P}{Q\Delta p} \tag{A.1}$$

where P is the produced power and P_h is the hydraulic power inserted. P_h is can be expressed as $Q\Delta p$ which is the volume flow multiplied by the pressure difference from inlet to outlet.

The total efficiency is a product of part efficiencies as shown in equation A.2.

$$\eta_{tot} = \eta_{transformer} \cdot \eta_{generator} \cdot \eta_{turbine} \cdot \eta_{headloss}(\cdot\eta_{leakage}) \tag{A.2}$$

The efficiency of the generator and transformer can be found without knowing the actual flow rate, but the turbine efficiency and head loss is dependent on the flow rate.

From a mechanical engineering point of view, the turbine efficiency is of most interest. The turbine efficiency describes the efficiency of the transformation from hydraulic power to rotating mechanical power as shown in Equation A.3.

$$\eta = \frac{T\omega}{Q\Delta p} = \frac{T\omega}{\rho g Q H} \tag{A.3}$$

T is torque, ω is the rotational speed and Δp can be written as $\rho g H$ where H is the head in meter. However, torque can not be measured in a commercial power plant. To solve the equation it has to be changed to include measurable quantities. The equation is there changed to include the generator output and generator efficiency.

$$\eta = \frac{P_{gen}}{\eta_{gen}\rho g Q H} \tag{A.4}$$

The generator output can be measured and the generator efficiency is known. To make the efficiency comparable the flow and power has to be adjusted for head variations. By using the affinity equations, head and flow can be adjusted to the design parameters of the power plant.

$$Q_2 = Q_1\left(\frac{H_2}{H_1}\right)^{\frac{1}{2}} \tag{A.5}$$

$$P_2 = P_1\left(\frac{P_2}{P_1}\right)^{\frac{3}{2}} \tag{A.6}$$

For efficiency measurements at a prototype, the standard commonly used is the IEC 60041:1991 *Field acceptance tests to determine the hydraulic*

performance of hydraulic turbines, storage pumps and pump turbines [64]. Different methods and limits of use is thoroughly described in the standard. The thermodynamic method was for the measurements presented in this work and will therefore be further described.

A.1.1 The thermodynamic efficiency measurement method

Efficiency measurements with thermodynamic method results from the application of the principle of conservation of energy. The losses in the turbine is transformed to heat in flow. By measuring the temperature difference from inlet to outlet of the turbine, the flow losses can be found. From here the efficiency can be computed. The thermodynamic method separates from the other methods as it does not measure flow, but directly measures losses [34]. Neglecting the volumetric losses in the water, the efficiency can be expressed as

$$\eta = \frac{P_m}{P_h} = 1 - \frac{\Delta H_{loss}}{H} \tag{A.7}$$

where H is the head. Hence measuring the flow is not necessary. The losses can be written as in equation A.8.

$$\Delta H_{loss} = \frac{E_{loss}}{g} = \frac{c_p}{g}\Delta T \tag{A.8}$$

ΔT is the temperature difference from inlet to the outlet of the turbine. The method is recognized and has high accuracy above 100 m head [64]. For lower heads, the temperature difference becomes very small and uncertainty increases. To achieve good results high accuracy temperature sensors and favourable conditions are necessary.

The energy transfer through the turbine can be described by a enthalpy-entropy diagram as shown in Figure A.1. The ideal process is aa process without losses, known as an isentropic process. Shown as the process from '1-1' to 's' as the pressure is reduced through the turbine. However, a real process includes losses and the entropy increases and the process will end in point '2-1'.

From the diagram the efficiency of the process can be written as

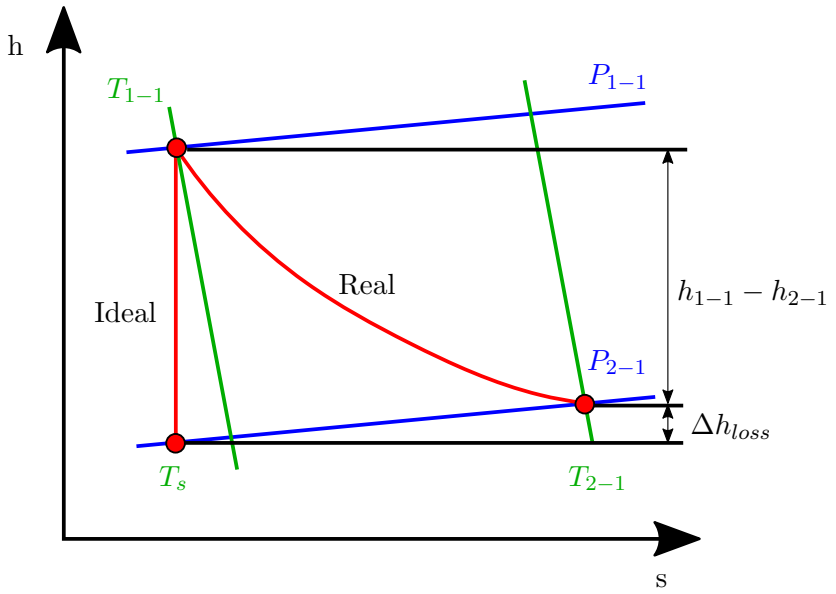

Figure A.1: Enthalpy-Entropy diagram. The green lines represents constant temperature and blue lines are constant pressure.

$$\eta = \frac{h_{1-1} - h_{2-1}}{h_{1-1} - h_s} \tag{A.9}$$

By using thermodynamic relations, the final equation can be derived.

$$\eta = \frac{E_m}{E_h} = \frac{\frac{1}{\bar{a}}(p_{1-1} - p_{2-1}) + \frac{1}{2}(c_{1-1}^2 - c_{2-1}^2) + g(z_{1-1} - z_{2-1}) + \bar{c_p}(T_{1-1} - T_{2-1})}{\frac{1}{\bar{\rho}}(p_1 - p_2) + \frac{1}{2}(c_1^2 - c_2^2) + g(z_1 - z_2)} \tag{A.10}$$

The density of water, ρ, the isotermic constant, a, and the specific heat capacity, c_p is calculated according to the IEC 60041 [64]. The reference indexes in numerator and denominator are different as the indexes in the numerator refers to exact measurement position of the temperature, while denominator are referring to centrelines at inlet and outlet. Adiabatic processes are assumed from centrelines to measurement points. A general overview of positions of the indexes are shown in Figure A.2.

The temperature of the water may be influenced by its external parameters. To take the external parameters into account, a corrective term δE_m is added to equation A.10.

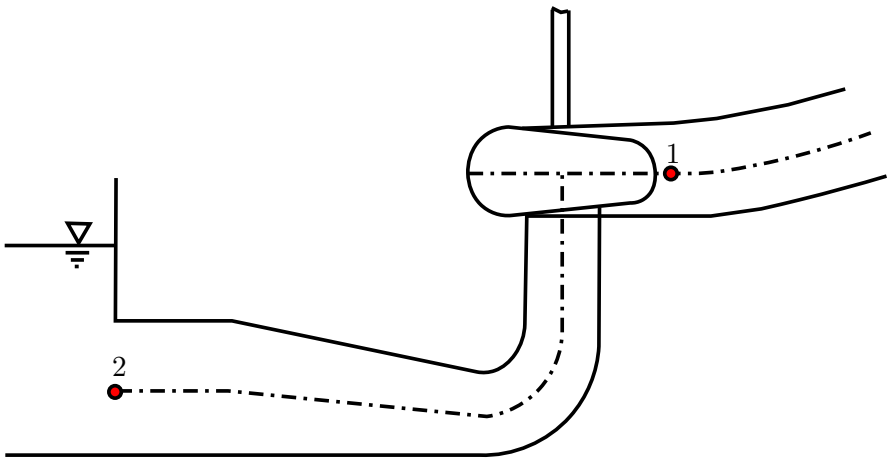

Figure A.2: Reference positions in the thermodynamic equation

$$\eta = \frac{\frac{1}{\bar{a}}(p_{1-1} - p_{2-1}) + \frac{1}{2}(c_{1-1}^2 - c_{2-1}^2) + g(z_{1-1} - z_{2-1}) + \bar{c_p}(T_{1-1} - T_{2-1}) + \delta E_m}{\frac{1}{\bar{\rho}}(p_1 - p_2) + \frac{1}{2}(c_1^2 - c_2^2) + g(z_1 - z_2)} \tag{A.11}$$

The following parameters should be taken into consideration for δE_m [64]:

- The travel time of the water between inlet and outlet cross section and possible errors due to temperature variations over the measurement.
- Heat exchange with the environment where pipes are exposed to surroundings.
- Heat exchange with air.

The leakage flow over the labyrinth seals is often a challenge as this is goes through a separate pipe before it is returned to the draft tube. The leakage flow and temperature may be measured separately and guided away from the draft tube during the measurements. The energy of the leakage water is added to the corrective term δE_m.

Appendix B

Leirfossene HPP

B.1 FFT

Part load of FRUCE at Leirfossen

The part load investigation includes four operational points at $0.47P_{nom}$, $056P_{nom}$, $0.66P_{nom}$ and $0.75P_n$. The results from the low frequency range from 1-15 Hz is presented first. As expected, the dominant frequency in this range is the RVR frequency which is related to the rotating vortex rope.

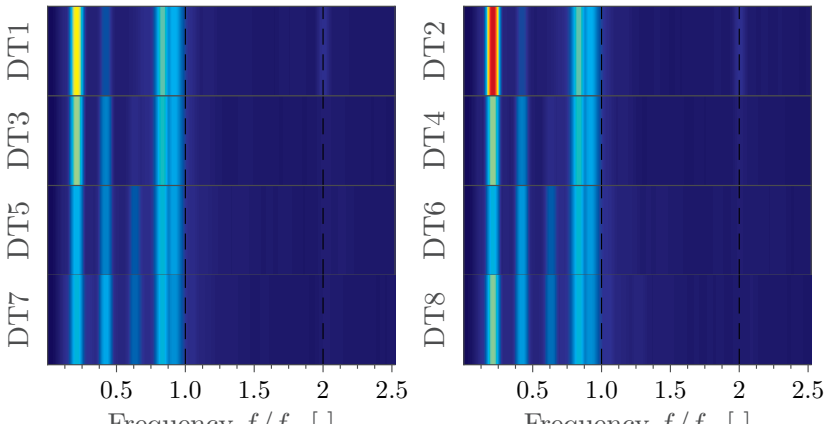

Figure B.1: Frequency spectrum for without FRUCE at $0.47P_n$

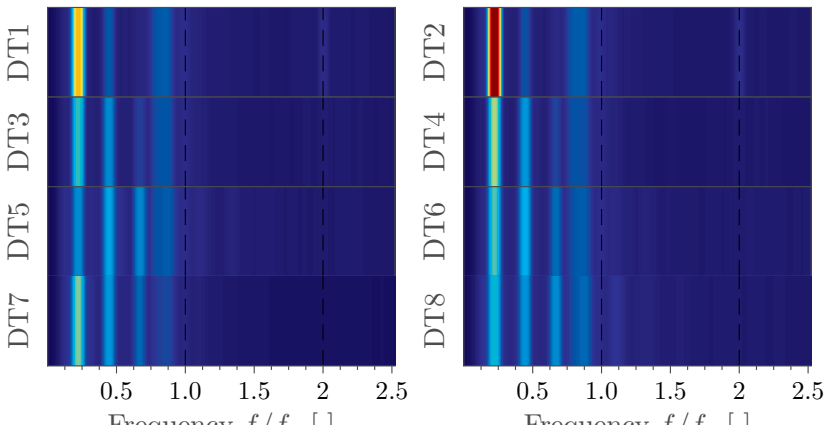

Figure B.2: Frequency spectrum for FRUCE 1 at $0.47P_n$

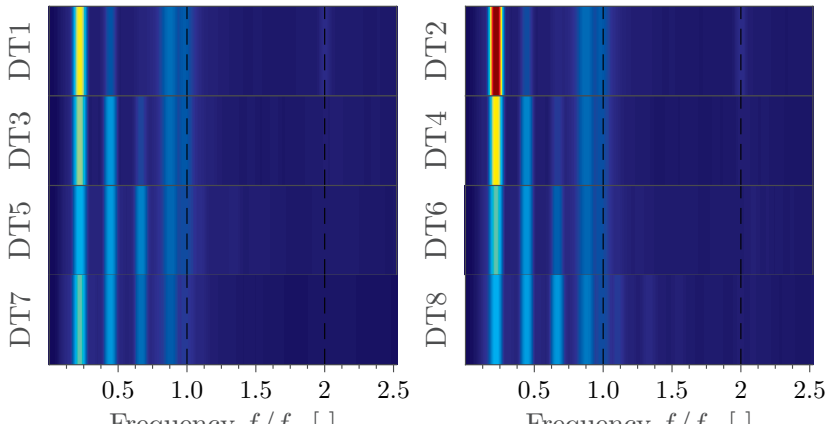

Figure B.3: Frequency spectrum for FRUCE 2 at $0.47P_n$

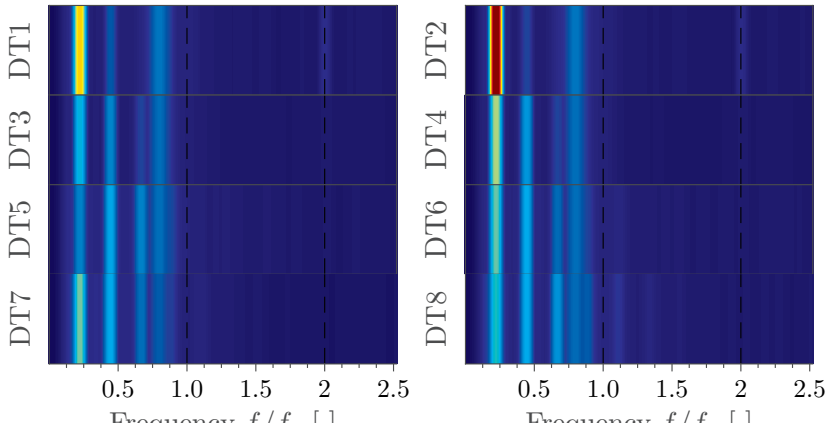

Figure B.4: Frequency spectrum for FRUCE 3 at $0.47P_n$

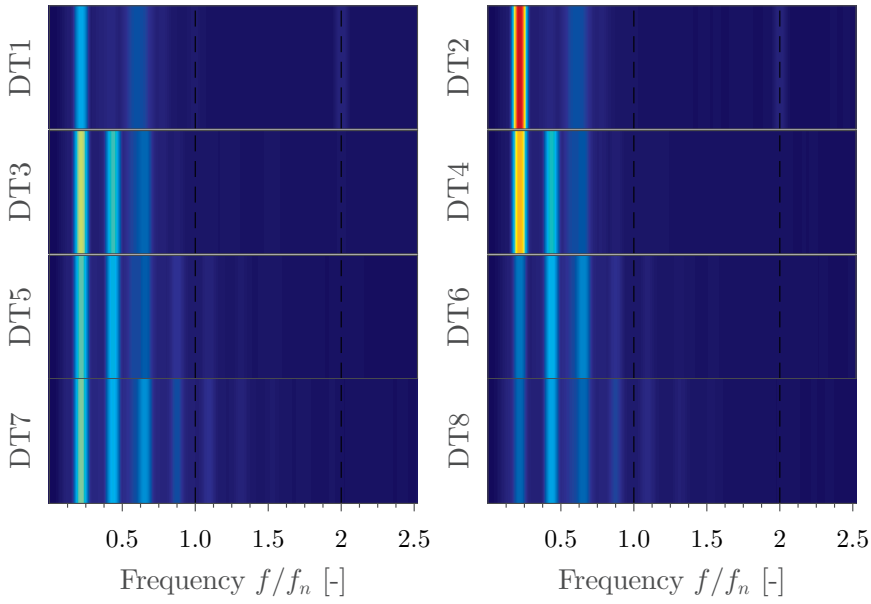

Figure B.5: Frequency spectrum for without FRUCE at $0.56P_n$

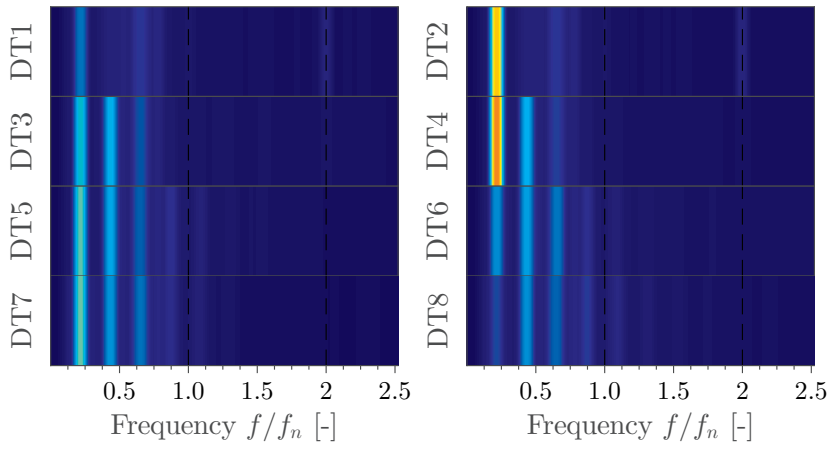

Figure B.6: Frequency spectrum for FRUCE 1 at $0.56P_n$

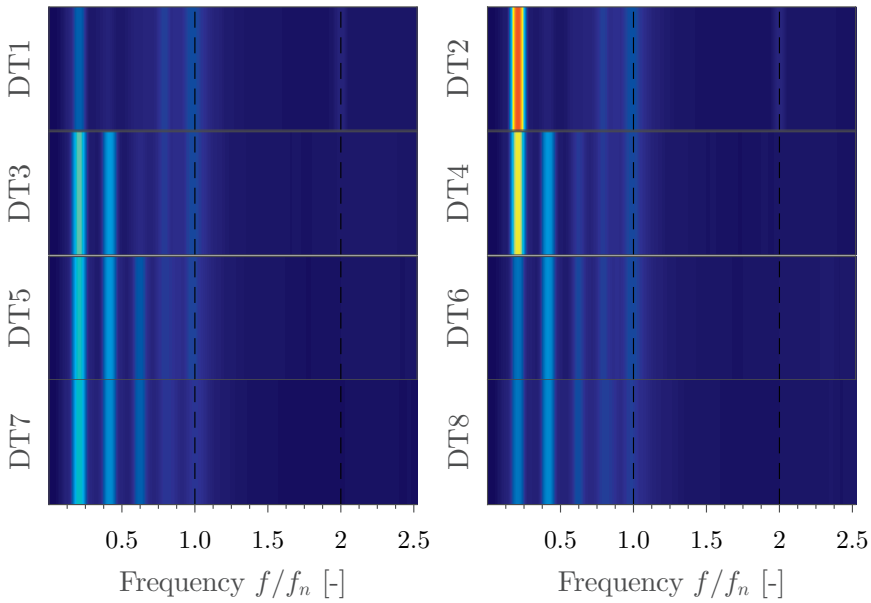

Figure B.7: Frequency spectrum for FRUCE 2 at $0.56P_n$

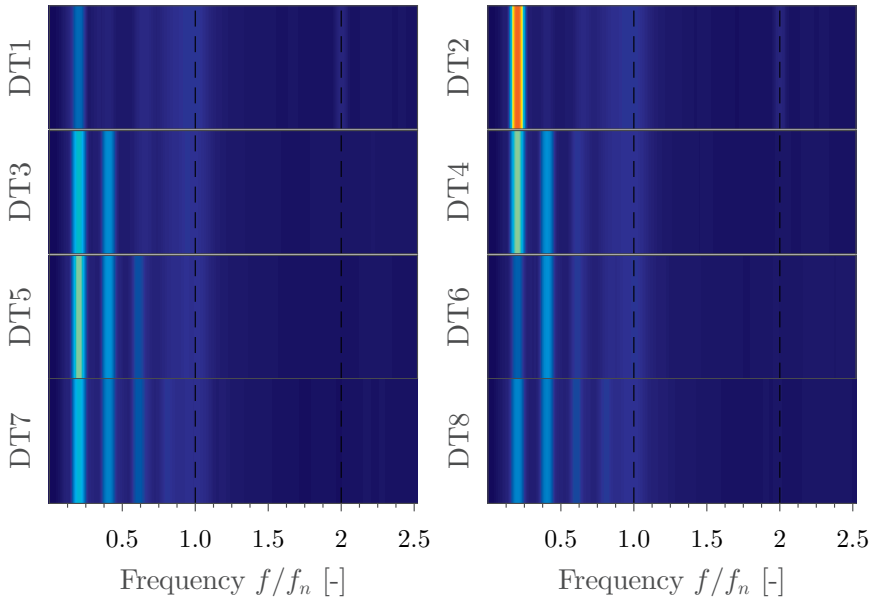

Figure B.8: Frequency spectrum for FRUCE 3 at $0.56P_n$

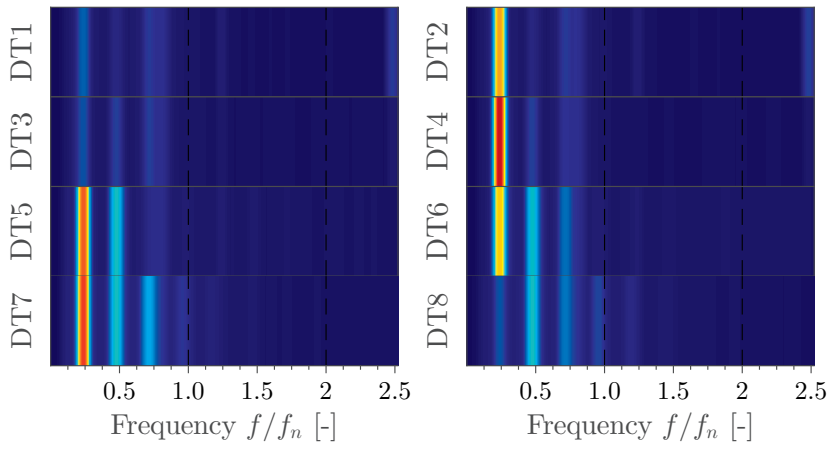

Figure B.9: Frequency spectrum without FRUCE at $0.66P_n$

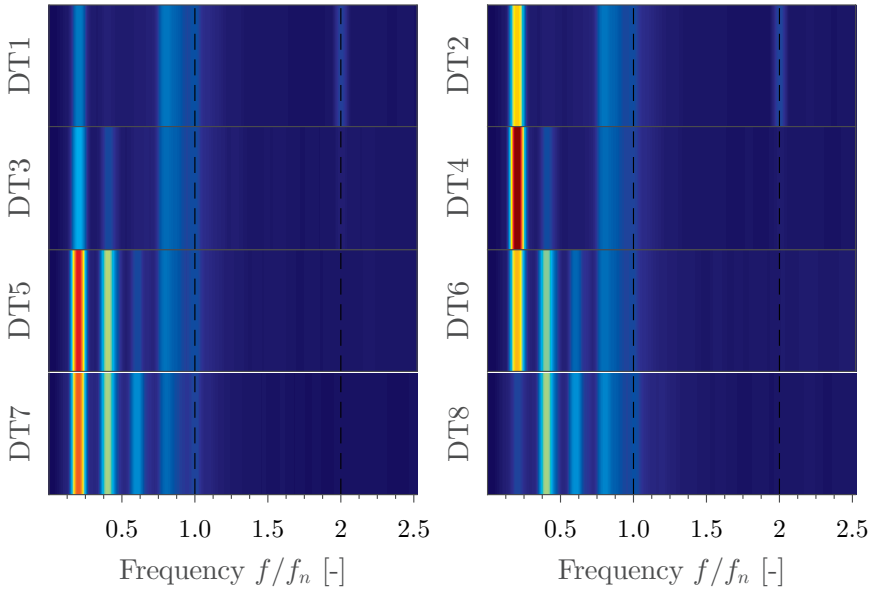

Figure B.10: Frequency spectrum for FRUCE 1 at $0.66P_n$

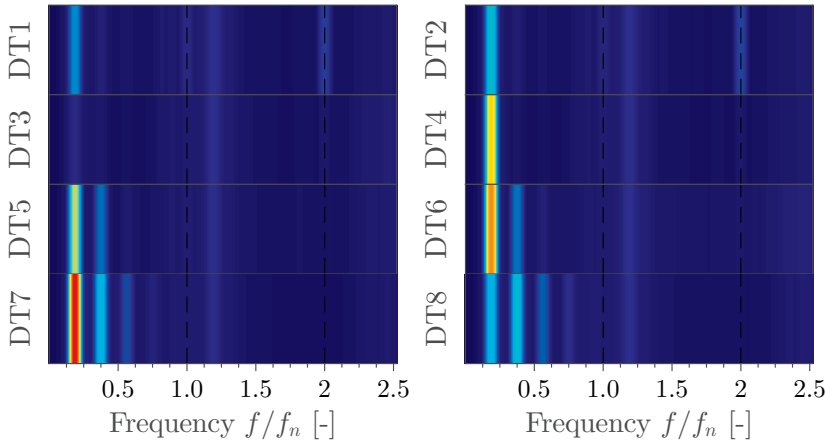

Figure B.11: Frequency spectrum for FRUCE 2 at $0.66P_n$

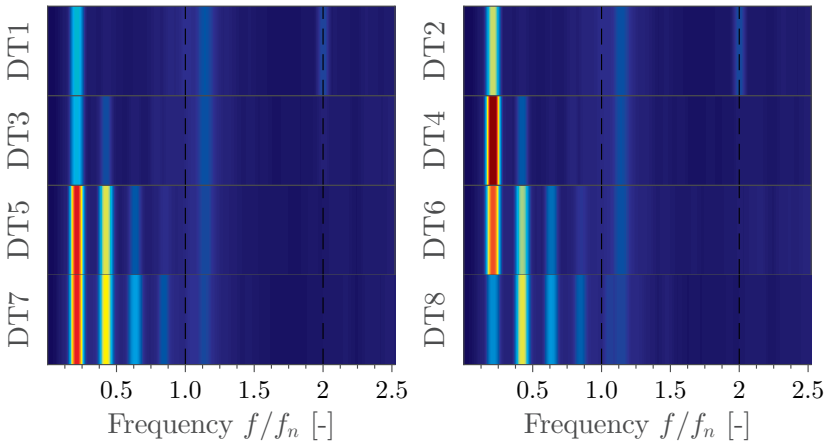

Figure B.12: Frequency spectrum for FRUCE 3 at $0.66P_n$

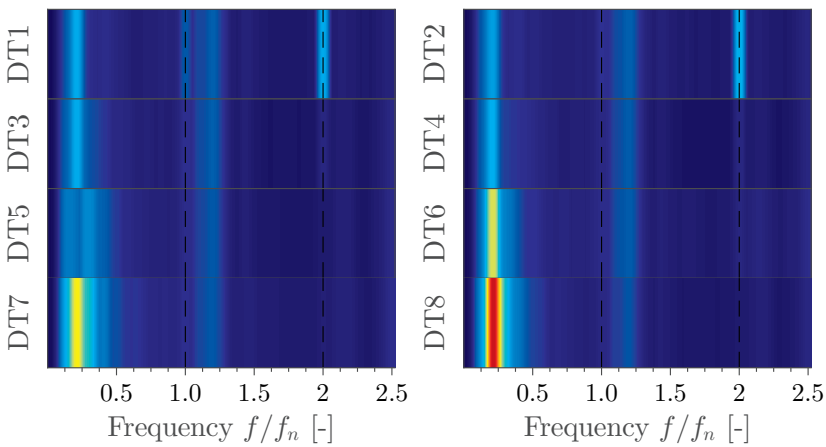

Figure B.13: Frequency spectrum without FRUCE at $0.75P_n$

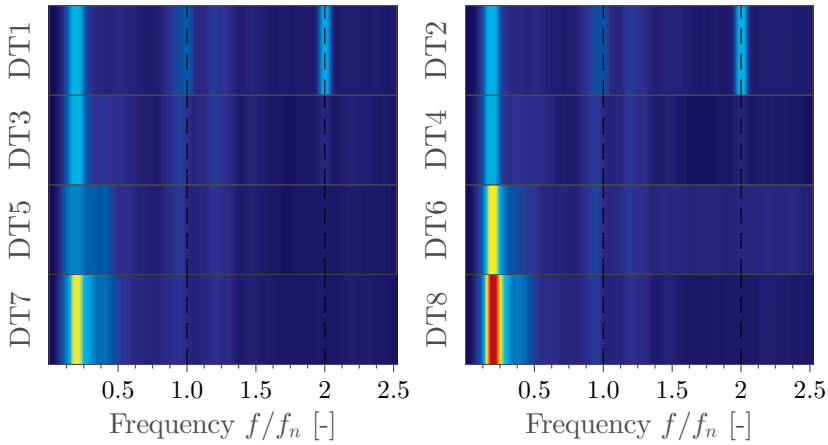

Figure B.14: Frequency spectrum for FRUCE 1 at $0.75P_n$

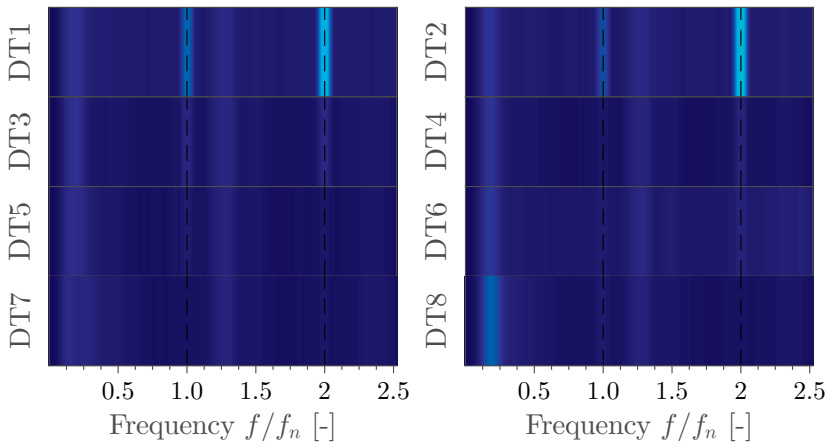

Figure B.15: Frequency spectrum for FRUCE 2 at $0.75P_n$

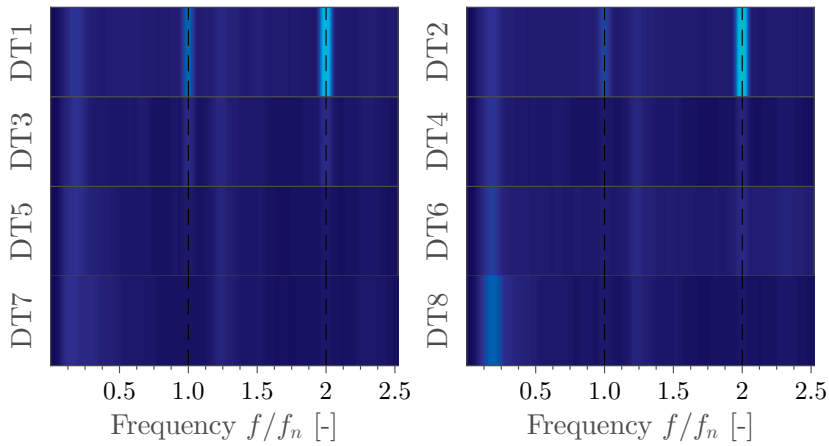

Figure B.16: Frequency spectrum for FRUCE 3 at $0.75P_n$